HYPERCOORDINATED ORGANOTIN(IV) COMPOUNDS CONTAINING κ²-*C,O*- AND κ²-*C,N*- CHELATING LIGANDS: SYNTHESIS, CHARACTERIZATION, AND POLYMERIZATION BEHAVIOUR

By

Julie Loungxay

Bachelor of Science (Honours) in Chemistry,

Ryerson University, Toronto, Canada, 2011

A thesis presented to Ryerson University in partial fulfillment of the

requirements for the degree of Master of Science

in the program of Molecular Science

Toronto, Ontario, Canada, 2019

Author's Declaration

I hereby declare that I am the sole author of this thesis. This is a true copy of the thesis, including any required final revisions, as accepted by my examiners.

I authorize Ryerson University to lend this thesis to other institutions or individuals for the purpose of scholarly research.

I further authorize Ryerson University to reproduce this thesis by photocopying or by other means, in total or in part, at the request of other institutions or individuals for the purpose of scholarly research.

I understand that my thesis may be made electronically available to the public.

HYPERCOORDINATED ORGANOTIN(IV) COMPOUNDS CONTAINING κ²-*C,O*- AND κ²-*C,N*- CHELATING LIGANDS: SYNTHESIS, CHARACTERIZATION, AND POLYMERIZATION BEHAVIOUR

Julie Loungxay MSc., Molecular Science, Ryerson University, 2019

Abstract

Rigid homopolystannanes and alternating polystannanes containing a benzyl methoxy ether (*C,O*) or benzyl dimethyl amine (*C,N*) ligand were prepared using either a direct approach, lithiation and transmetallation, or an alternative approach, either sequential chlorinations or brominations. X-ray crystallographic studies of **41** and **45** were conducted to find **41** in a distorted tetrahedral geometry with moderate hypercoordinate interaction (Sn-N: 2.917 Å) while **45** in a distorted trigonal bipyramidal with strong hypercoordinate interaction (Sn-N: 2.403 Å). Hydrogenation of **31** and **33** produced **42** and **43** in moderate-to-good yields. Dehydrocoupling polymerization produced modest molecular weight, rigid *C,O*- ($M_w = 3.03 \times 10^4$ Da, PDI: 1.4) and *C,N*- ($M_w = 3.10 \times 10^4$ Da, PDI: 1.82) homopolymers **56** and **57**. Finally, condensation polymerization was attempted to produce low molecular weight ($M_w = 1.30 \times 10^4$ Da, PDI: 2.0) *C,O*- alternating polymer **60** and oligomer **61** ($M_w = 0.92 \times 10^4$ Da, PDI: 2.71).

Acknowledgements

I would like to give many thanks to my supervisor Dr. Foucher. Firstly, he gave me the opportunity of allowing me to pursue this MSc, a dream of mine since I was a child. Throughout this experience, he has given his guidance, patience, and support, especially during my times of crisis. He has been nothing but understanding and has pushed me to work through tough times and personal problems, thank you; I feel extraordinarily grateful for all of your help throughout the years.

I would like to thank my committee members, Dr. Wylie, Dr. McWilliams, and Dr. Gossage for providing necessary feedback with this thesis. Thank you for Dr. Alan Lough for collecting the X-ray crystallography for this study.

Thanks to all my lab mates: Jeff, Joe, Gloria, Des, Rachel, David, Rachel, Kristy, Alex, Kathy, Tristan and my best friend Jeanette. I am especially grateful towards Jeff, he has always given me lots of guidance throughout my MSc and did much of the homopolymer work to finally push out the paper. Thank you everyone for great times with going to Blue Jay's games, board game nights, or any food excursions we had and for making my lab life an overall enjoyable experience, especially Joe and Jeanette. Working in the evening or night was always fun and relaxing with you guys around.

Additionally, a big thanks to Shawn, Rob, and Saif. They have helped me so much the last few years, teaching me how to deal with students and giving all the support needed to help me deal with my personal problems. Thank you again for helping me deal with my stress-related problems and staying with me to support me though it, I am so grateful.

Table of Contents

vi

List of Figures

List of Tables

List of Schemes

List of Abbreviations

Å	Angstrom
Br_2	Bromide
C_6D_6	Deuterated benzene
$CDCl_3$	Deuterated chloroform
Da	Daltons
DCM	Dichloromethane
DSC	Differential scanning calorimetry
Et_2O	Diethylether
eV	Electron volts
GPC	Gel permeation chromatography
HCl	Hydrochloric acid
Hex	Hexane
Hz	Hertz
kJ	Kilojoule
n-Bu	*n*-butyl
NMR	Nuclear Magnetic Resonance
Me	Methyl
M_w	Molecular weight
ppm	Parts per million
T_g	Glass transition temperature
THF-d_8	Deuterated tetrahydrofuran
σ	Sigma

List of Appendix Tables

List of Appendix Figures

1.0 Introduction

1.1 Hypercoordinate Compounds

Hypercoordinate compounds were first formally defined in 1969 by J. I. Musher and has since been used to describe datively bound hypercoordinate compounds from Groups 1, 2, 13-18.[1] Current research has focused on the synthesis of hypercoordinate species from Groups 15-18, including investigations of hypervalent iodine reagents and precatalysts.[2] These species can exceed the number of valence electrons dictated by the octet rule though an inter- or intra-molecular interaction from an electron-abundant atom (or donor atom, D) to a main group atom (M).[3] This forms a hypercoordinate or 3-center-4-electron bond, defined as a delocalization of bonding electrons along 3 atoms that lie in the same plane. This bond is characterized by the N-M-L notation, of which denotes the number of electrons associated with M (N), the main heteroatom, M, and the number of bound ligands to that heteroatom (L).[1]

Although there are many species that possess hypervalency, ranging from 3- to 8-coordinate, Group 14 compounds can only be 5- or 6- hypercoordinate (Figure 1). Previously, it was speculated that Group 14 elements utilize their unoccupied d-orbitals to accommodate additional electron density for the valence shell.[4] However, these orbitals are too diffuse and too high in energy to access; therefore, requiring the formation of the 3-center-4-electron bond.[4]

10-M-5
Trigonal
Bipyramidal

10-M-5
Square
Planar

12-M-6
Octahedral
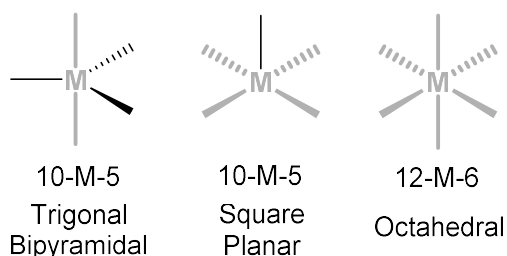
Figure 1: Geometries of 5- and 6-hypercoordinate compounds. The hypercoordinate bonds are highlighted in grey.

To form the 3-center-4-electron bond, the bound ligands in the apical positions must be more electronegative than the main heteroatom M and must participate in hypercoordinate bonding.[1] Resultantly, the strength of the hypercoordinate interaction M-D, is dependent on the main heteroatom itself and the other apical ligand. Halogens (X) are apicophilic ligands, very electronegative ligands, and if present, will partake in the hypercoordinate interaction.[1] Table 1 illustrates this and showcases the changes in calculated bond distances for various *s-cis* acrolein derivatives.
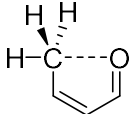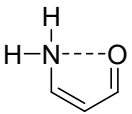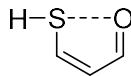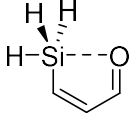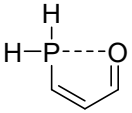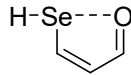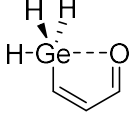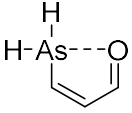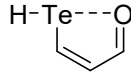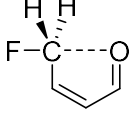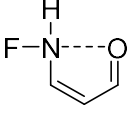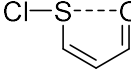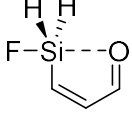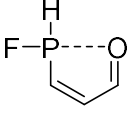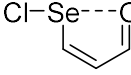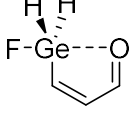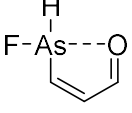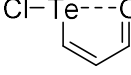
Group 14 Compound	M-D bond length (Å)[3]	Group 15 Compound	M-D bond length (Å)[3]	Group 16 Compound	M-D bond length (Å)[3]
H-C----O	2.963	H-N----O	2.763	H-S----O	2.980
H-Si---O	2.976	H-P----O	3.050	H-Se---O	2.935
H-Ge---O	2.975	H-As---O	3.012	H-Te---O	2.845
F-C----O	2.823	F-N----O	2.736	Cl-S----O	2.395
F-Si---O	2.620	F-P----O	2.593	Cl-Se---O	2.307
F-Ge---O	2.584	F-As---O	2.552	Cl-Te---O	2.296

Table 1: MP2/LanL2DZ calculated M-O distances of various acrolein derivatives.[3]

For Group 14 and 15 derivatives, the bond lengths initially increase, due the change to heavier heteroatoms, before the hypercoordinate bonds become stronger and shorten. The Lewis acidity of the heteroatoms pulls more electron density from the donor ligand to stabilize it. By incorporation of electronegative atoms, the 3c-4e bond is formed and withdraws even more electron density, which causes a greater shortening of bond distances. As the main heteroatom changes to heavier elements in its group, there is an increase in stabilization by the donation of a lone pair to the non-bonding orbital of the hypercoordinate or dative interaction. As stated previously, the more electronegative X is, the stronger the hypercoordinate M-D interaction will be. The donor lone pair also contributes to the antibonding σ orbital of the M-X bond, which causes M-X to elongate and M-D to shorten. Ultimately, the shorter the bond length, the stronger the hypercoordinate M-D interaction as seen in Table 1. For Group 14 hypercoordinate compounds, a simple MO diagram for the hypercoordinate bond is shown in Figure 2.
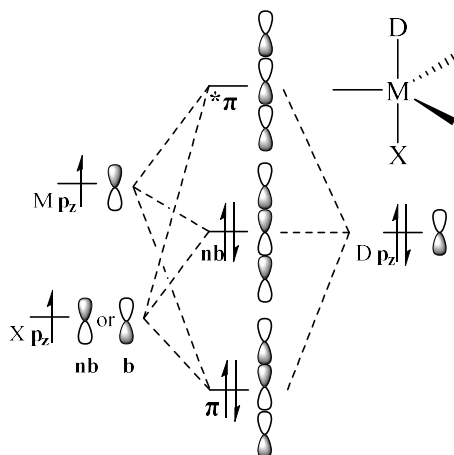
Figure 2: Typical MO bonding for hypercoordinate bond in a 5-coordinate compound.

For 5-hypercoordinate species, a pair of unshared electrons are replaced by a ligand causing a shift of geometry to either square pyramidal or more commonly, trigonal bipyramidal.[1] In the trigonal bipyramidal geometry, there are 3 sp^3 bonds in the equatorial positions while the

hypercoordinate bond resides in the linear apical plane. The bond lengths of the hypercoordinate bonds are weaker and longer than the equatorial bonds, but may be strengthened depending on the basicity of the donor atom.[1] While in the square planar geometry, there is a sp^3 bond in the apical position while the basal bonds are involved in the hypercoordinate bonding. The basal bonds are also longer and weaker than the apical bond. Between these two geometries, the energy difference between them is very small, which may result in a Berry pseudorotation or a turnstile rotation.[1] A trigonal bipyramidal compound may transition to a square pyramidal geometry to allow for rotation of the apical and equatorial positions. As for 6-hypercoordinate species, the octahedral geometry may accommodate up to 3 equivalent hypercoordinate bonds. The 4 equatorial bonds are typically longer than the apical bonds, however as compared to 5-hypercoordinate species, the hypercoordinate bonds are stronger than the apical bond of the trigonal bipyramidal geometry and would have shorter bond lengths.[1,4]

1.2 Group 14 Hypercoordinate Compounds

Ascending Group 14, intermolecular hypercoordinate compounds have been stabilized with N-, O-, S-, and P- donors. Group 14 elements in a 4^+ oxidation state are Lewis acidic and increase in acidity moving down the period (Si < Ge << Sn < Pb).[4] Thus the compounds become more unstable with an increasing number of bound ligands and/or the more electronegative X is. However as previously stated, the dative interaction decreases Lewis acidity and stabilizes the heteroatom. For the purposes of this investigation, we will exclusively look at N- and O-hypercoordinate organotin species.

1.3 κ^2-_C,N_-Chelated Organotin Compounds

One of the first _C,N_-chelating organotin compounds was synthesized in 1976 by the van Koten group.[5] They synthesized (2-Me$_2$NCH$_2$C$_6$H$_4$)R$_2$SnBr (R = Me, Ph) and a double _C,N_-

chelated bis(2-Me$_2$NCH$_2$C$_6$H$_4$)MeSnBr species by reacting a lithiated or Cu-(2-Me$_2$NCH$_2$C$_6$H$_4$) ligand with an dialkyltin dibromide or trialkyltin bromide, respectively, in a facile one-step synthesis. Their research extended on to other *C,N*-chelating organotin ligands to form a library of either 5- or 6-hypercoordinate tin species as shown in Figure 3.[5a-d, 6] These hypercoordinate tin species were synthesized using the transmetallation method as stated previously. Compounds **1-3** each have a flexible CH$_2$ bridge bound to the tin. This allows for the possibility of an "on" and "off" rotation where the ligand may freely rotate and reduce any steric bulk by breaking any hypercoordinate interaction. Compounds **4-6** are more rigid, thus the hypercoordinate interaction restricts any free rotation.

R = R' = Me (**1**)
R = R' = Ph (**2**)
R = Me, R' = Ph (**3**)

R = R' = Me (**4**)
R = R' = Ph (**5**)
R = Me, R' = Ph (**6**)

R = R' = Me (**7**)
R = R' = Ph (**8**)
R = Me, R' = Ph (**9**)
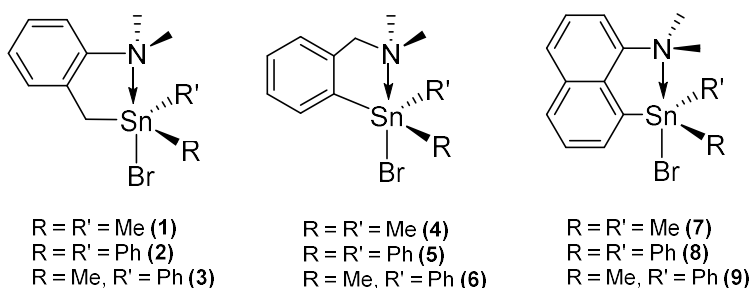
Figure 3: Select organotin compounds prepared by the van Koten Group.[5a-d, 6]

However, if the hypercoordinate interaction is broken and the amine rotates away from the tin center, a fluxional exchange may occur with the other substituted ligands.[6] Finally, compounds **7-9** are quite rigid due to the presence of a napthyl backbone which forces the N to be in close proximity with the tin center, facilitating the interaction. To confirm the hypervalency of these compounds, the distances between Sn-D substituents, in addition to chemical shifts in ^{119}Sn NMR spectroscopy can be evaluated. The ^{119}Sn NMR resonances show a characteristic large shift to a lower frequency when comparing hypercoordinate and unsubstituted tin analogues. Understandably, the donation of a lone pair from the donor group will decrease tin's Lewis acidity and shift the ^{119}Sn NMR resonance upfield. Comparing compounds **2** (^{119}Sn NMR δ: -122 ppm)[6]

and **5** (^{119}Sn NMR δ: -182 ppm)[6] to their unsubstituted analogue, SnPh$_3$Br (^{119}Sn NMR δ: -60 ppm)[7], a large chemical shift difference is observed.

The van Koten group carried out work on *C,N*-chelating hypercoordinate tin until 1991, after which the Holecek group continued to explore rigid *C,N*-chelating hypercoordinate tin species for next three decades. The compounds in Figure 4 were synthesized using the same transmetallation route established by van Koten. The organolithium was reacted with an alkyl or aryl tin mono-, di- or tri-halide species and recrystallized in boiling toluene to yield the respective species. In addition to greatly expanding known rigid *C,N*-chelated organotin library (compounds **12-23**), they synthesized novel double *C,N*-chelated and pincer *C,N*-chelated organotin species. The double *C,N*-chelated compounds **10** and **11** remain 5-coordinate and in trigonal bipyramidal geometry as the Sn-N1 interaction is clearly datively bound, with the other ligand rotated away from interacting with the Sn center. The standard covalent Sn-N radii is 2.154 Å and the van der Waals radii is 3.62 Å.[4] Thus N1 interacts with Sn very strongly (2.4752(17) Å) while pushing away Cl (2.5196(5) Å) and N2 (3.5174(19) Å) in **10**. For **11**, the additional chloride makes

R$_1$ = R$_2$ = *n*-Bu
R$_1$ = *n*-Bu, R$_2$ = Cl
R$_1$ = Ph, R$_2$ = Cl (**10**)
R$_1$ = R$_2$ = Cl (**11**)
R$_1$ = R$_2$ = Br
R$_1$ = R$_2$ = I

R$_1$ = R$_2$ = R$_3$ = Ph (**12**)
R$_1$ = R$_2$ = R$_3$ = *n*-Bu (**13**)
R$_1$ = Cl, R$_2$ = R$_3$ = *n*-Bu (**14**)
R$_1$ = Br, R$_2$ = R$_3$ = *n*-Bu (**15**)
R$_1$ = Cl, R$_2$ = R$_3$ = Ph (**16**)
R$_1$ = Br, R$_2$ = R$_3$ = Ph (**17**)
R$_1$ = R$_2$ = Cl, R$_3$ = *n*-Bu (**18**)
R$_1$ = R$_2$ = Cl, R$_3$ = Ph (**19**)
R$_1$ = R$_2$ = I, R$_3$ = Ph (**20**)
R$_1$ = R$_2$ = R$_3$ = Cl (**21**)
R$_1$ = R$_2$ = R$_3$ = Br (**22**)
R$_1$ = R$_2$ = R$_3$ = I (**23**)

R$_1$ = R$_2$ = R$_3$ = Ph
R$_1$ = Cl, R$_2$ = R$_3$ = Ph
R$_1$ = R$_2$ = Cl, R$_3$ = Ph
R$_1$ = Br, R$_2$ = R$_3$ = Ph
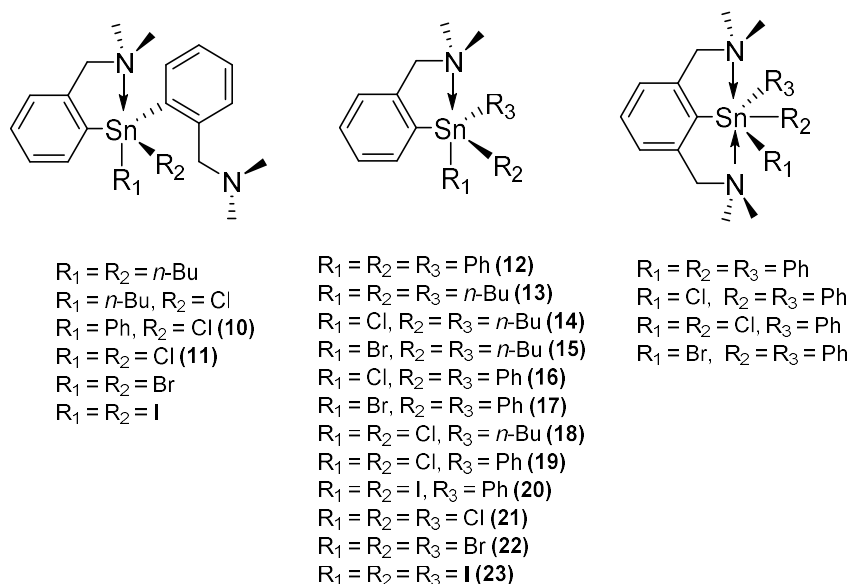
Figure 4: Organotin compounds prepared by the Holecek Group[8a-f] and the Ruzicka Group.[9]

Compounds	Sn-N bond length (Å)	^{119}Sn δ for compounds (ppm)	Unsubstituted tin analogues	^{119}Sn δ for unsubstituted analogues (ppm)
10	N1: 2.4752(17)[8d] N2: 3.5174(19)[8d]	-185*	SnPh$_3$Cl	-44[7,10,*]
11	N1: 2.5345(18)[8d] N2: 3.2736(19)[8d]	-252*	SnPh$_2$Cl$_2$	-32[10,‡]
12	2.917[this work]	-163[8b,8c,*]	SnPh$_4$	-137[7,*]
13	-	-50[8a, 8c,*]	SnPhBu$_3$	-41[10,§]
14	2.510(5)[8f]	-47[8a, 8c,*]	SnPhBu$_2$Cl	-
15	-	-40[8a, 8c,*]	SnPhBu$_2$Br	-
16	-	-176[8b,*]	SnPh$_3$Cl	-44[7,10,*]
17	2.511(12)[5b]	-180[8b,*]	SnPh$_3$Br	-60[7,10,*]
18	2.466(4)[8f]	-104[8a,*]	SnPhBuCl$_2$	-
19	2.444(5)[8d]	−170[8b, 8d,*]	SnPh$_2$Cl$_2$	-32[10,‡]
20	2.476(3)[9]	-337[9,*]	SnPh$_2$I$_2$	-
21	2.380(2)[8e]	-241[8b,*]	SnPhCl$_3$	-65[7,*]
22	2.402(3)[8e]	-408[8a, 8b,*]	SnPhBr$_3$	-
23	2.436(4)[8e]	−944[8e,†]	SnPhI$_3$	-

Table 2: Bond lengths and ^{119}Sn data of organotin compounds prepared by the Holecek Group[8a-f] and the Ruzicka Group.[9] Solvents used were CDCl$_3$ (*), Tol-d$_8$ (†), CH$_2$Cl$_2$ (‡), and C$_6$D$_6$ (§).

the tin center more Lewis acidic (Sn-Cl$_{R1}$ = Sn-Cl$_{R2}$ = 2.4390(3) Å) and pulls both N1 (2.5345(18) Å) and N2 (3.2736(19) Å) towards the Sn center. The rest of the rigid *C,N*-chelated organotin species in Table 2 also exhibit trigonal bipyramidal geometry and strong Sn-N interactions with the exception of **12**. Also as expected, compared to the unsubstituted analogues of compounds **10-13**, **16**, **17**, **19**, and **21**, a large upfield shift in the ^{119}Sn resonance is observed.

1.4 κ^2-*C,O*-Chelated Organotin Compounds

Prior to interest in the *C,N*-chelating derivatives, attention was focused on synthesizing *C,O*-chelated hypercoordinate tin species for their use in biological activity. These hypercoordinate tin species act as competition for binding sites of biological residues, as they are attracted to the tin center.[11]

In more recent times, there has been research on polymerizing flexible *C,O*-chelated monomers in hopes to utilizing their polymeric semiconducting properties.[12] To synthesize the rigid monodentate species, a transmetallation similar to the method used for the *C,N*-chelated analogue was employed, of which the lithiated ligand reacts with the respective tin halides. However to synthesize the flexible *C,O*-chelated tin species, sequential brominations are required. These compounds (**24**, **25**) possess a moderate Sn-O interaction. The standard covalent Sn-O radii is 2.122 Å and the van der Waals radii is 3.58 Å.[4] The Sn-O interaction is a weaker interaction than the Sn-N; of which understandably, N is a better Lewis base than O. This is reflected in Table 3, as all the bond lengths are longer than the Sn-N and the difference in ^{119}Sn NMR resonances is small.
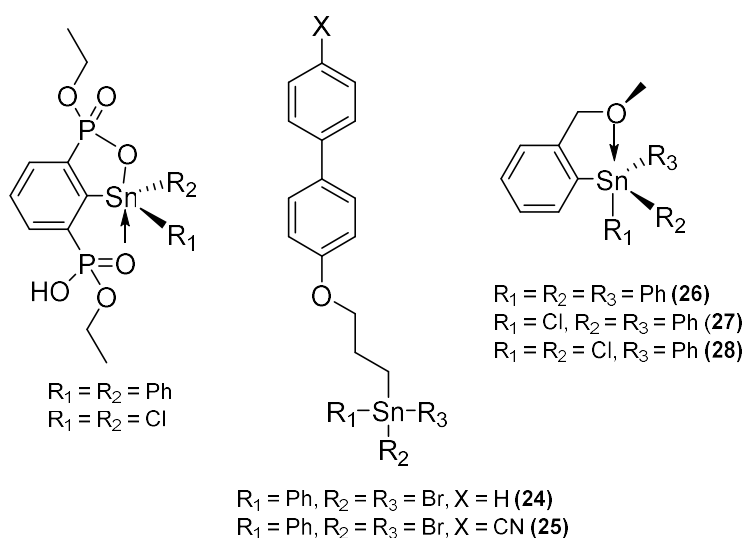
Figure 5: Examples of *C,O*-chelated organotin compounds.

Compounds	Sn-O bond length (Å)	^{119}Sn δ for compounds (ppm)	Unsubstituted analogues	^{119}Sn δ for unsubstituted analogues (ppm)
24	2.734(4)	-53[12]	SnPh$_2$Br$_2$	-
25	2.918(7)	-47[12]	SnPh$_2$Br$_2$	-
26	3.070	-114[11]	SnPh$_4$	-137[7]
27	2.767	-41[11]	SnPh$_3$Cl	-44[7]
28	2.898	-32[11]	SnPh$_2$Cl$_2$	-32[10]

Table 3: Bond lengths and ^{119}Sn data of organotin compounds **24-28**.

1.5 κ²-*C,O*- and κ²-*C,N*-Chelated Organotin Polymers

Polystannanes have been known since the 1990's and have garnered interest due to their inherent semiconducting properties. The tin backbone of polystannanes is comprised of covalently bound tin atoms with overlapping σ-orbitals, allowing for the delocalization of σ-electrons, rendering it intrinsically semiconductive. The electrons freely flow though the polymer backbone by occupying the lowest unoccupied molecular orbital (LUMO).[13] With a low or minimal energy barrier, the electrons can freely move into empty orbitals. Polystannanes are anticipated to have a semiconducting bandgap of 2.8 eV, considerably more conductive in the solid state compared to polysilanes (3.89 eV) and polygermanes (3.31 eV).[14] DFT calculations also reveal that polystannanes also have the lowest bond dissociation energy (146 kJ/mol) compared to polysilanes (222 kJ/mol) and polygermanes (188 kJ/mol).[15] Due to the relatively weak covalent bonds polystannanes possess, these compounds display low stability to water and light. Any moisture can readily break the polystannane chain by nucleophilic attack to form stannoxane products which is undesirable as the oxygens break any conjugation.[13] As for light, it is believed that an electron may be promoted to its antibonding orbital and cause homolytic cleavage. The broken, radicalized polymer chain then continues to completely degrade by either unzipping, to consecutively release oligomers or cyclics until complete degradation, or randomly broken by constant cleaving by other radicals.[13] However, with the incorporation of aryl substituents within the backbone of the polymer, the stability of solid-state polymers increases due to 6π orbital overlap.[13] To further increase the stability of these polymers, the incorporation of bulky, rigid donor-chelated ligands such as compounds **12-23** and **26-28** is envisioned. As previously stated, the hypercoordinate Sn-D interaction reduces the Lewis acidity of the compound, stabilizing it and the rigidity of the ligand

forces the interaction. Additionally, having a large sterically hindering group near the tin center may also protect the sensitive polymer backbone from any nucleophilic attack.

The first polystannanes were likely synthesized using Wurtz Coupling reactions in 1852. These are typical reductions where a diorganotin dichloride species reacts with sodium metal. This polymerization technique is a chain-growth mechanism where the formation of the polymer chain is random and typically forms high molecular weight homopolymers ranging between 10,000-1,000,000 Daltons.[13] Normally when synthesizing polystannanes, it is common to obtain cyclic oligomers as the polymer chain may attack itself during propogation or due to the light sensitivity of these polymers, degrade or terminate to form 5- or 6- membered rings. These stable cyclic oligomers are unwanted due to their lack of conducting properties, however for Wurtz coupling, these byproducts are minimally formed. Other methods of polymerization includes catalytic dehydrocoupling (chain-growth) and condensation (step-growth) polymerization. Metal-catalyzed dehydrocoupling utilizes a dihydride species and a common metal catalyst, such as Wilkinson's catalyst ($RhCl(PPh_3)_3$), to form high molecular weight polystannanes.[13] This is a controlled chain-growth type polymerization since the metal catalyst facilitates the propagation of the polymer and may be used to form homopolymers and random co-polymers. In the past, a zirconium catalyst ($Zp(Cp)_2Me_2$) was used, but often resulted in low molecular weight polymers of around 20,000 Daltons, in addition to the formation of cyclic oligomer. More recently, work by Caseri and coworkers has shown that a late transition metal catalyst, such as Wilkinson's catalyst, can be used for synthesizing cyclic-free polystannanes up to 200,000 Daltons.[13] Finally, condensation polymerization has been demonstrated for the formation of alternating co-polymers by reacting a dihydride tin monomer and a diamine tin monomer. This is a step-growth mechanism and may

form polystannanes up to 120,000 Daltons. This method is ideal to controlling the stability or solubility of the polymer by the incorporation of different dialkyl and diaryl groups.

1.6 Research Goals

Utilizing catalytic dehydrocoupling and condensation polymerization routes, this study is focused on synthesizing and characterizing rigid *C,N-* and *C,O*-chelated homo- and co-polystannanes (Figure 6). These polymers will be characterized by ^{1}H, ^{13}C, ^{119}Sn NMR spectroscopy, and where applicable by UV-vis spectroscopy, Differential Scanning Calorimetry (DSC) and elemental analysis.
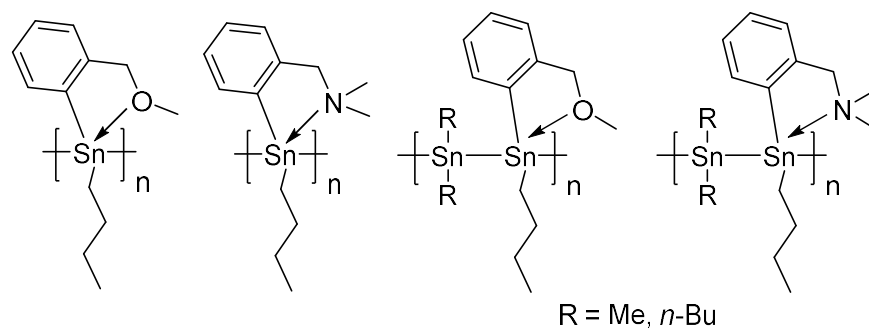
Figure 6: Target polystannanes of this study.

2.0 Results and Discussion

The work in this chapter was submitted as a manuscript to the Journal of Organometallic Chemistry in May of 2019. My contribution to this work included preparation of *C, N-* and *C, O-* monomers and the isolation of homo- and alternating new polystannanes bearing *C, N-* and *C, O-* groups. Jeff Pau completed additional characterization of these homopolymers, including GPC, DSC and ^{119}Sn NMR studies.

2.1 Synthesis of *C,O-* and *C,N-*chelated organotin monomers

2.1.1 Synthesis of *C,O-* and *C,N-*chelated organotin dichlorides

The benzyl methoxy ether **29** starting material was synthesized in high yields (~80%) as per literature procedure using a Williamson Ether synthesis.[16]
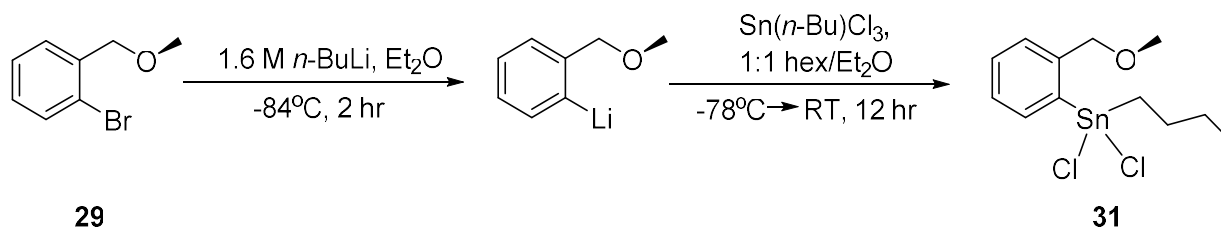
Scheme 1: Synthesis of compound **31**.

To synthesize the tin dichloride **31**, a one-step transmetallation between the lithiated benzyl methoxy ether ligand and (*n*-Bu)SnCl₃ was carried out (Scheme 1). While transmetallations of this nature are well known in literature, conditions leading to an optimal yield for this system were undertaken, as shown in Table 4. The literature procedure required a 2 hr, -78 °C lithiation with 1.6 M *n*-BuLi in hexanes, followed by a 3 hr, -78 °C transmetallation/coordination of the ligand to the tin species in 1:1 hex/Et₂O. This reaction was followed by a hot toluene extraction followed by layered hexanes recrystallization to isolate the pure product. Unfortunately, several attempts at following the literature procedure did not yield the desired product.

To remedy this, the lithiation step was allowed to proceed for a longer period of time (4 hr) to ensure that the ligand was completely lithiated. Under these conditions, the reaction yielded the target product (^{119}Sn (CDCl$_3$) δ: -60 ppm) as well as the undesired disubstituted product (^{119}Sn (CDCl$_3$) δ: -73 ppm) as seen in Figure 7. The lithiated ligand was quite reactive and may have degraded during the prolonged reaction time to form stannoxanes which results in a low yield after transmetallation. Additionally, changing the transmetallation reaction temperature from -78 °C to 0 °C was to ensure the reaction was proceeding and was not too cold. Slightly warmer conditions appeared to favour the formation of the di-substituted species **32**, as the temperature propagated the reactivity of the lithiated ligand and allowed for displacement of multiple chlorides.

31
^{119}Sn δ: -60 ppm

32
^{119}Sn δ: -73 ppm
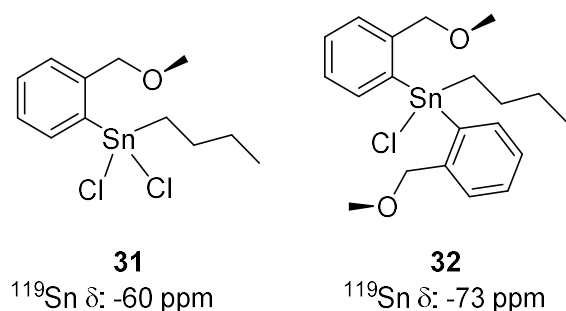
Figure 7: Compound **31** (left) and undesired di-substituted product **32** (right).

Trials	Reaction Conditions		Recovered Yields	^{119}Sn δ (CDCl$_3$)
	Lithiation	Transmetallation	(%)	(ppm)
1	-78 °C, 2 hr	-78 °C, 3 hr	-	-
2	-84 °C, 4 hr	0 °C → RT, 12 hr	16	-59, -73
3	-84 °C, 2 hr	0 °C → RT, 12 hr	35-42	-59, -73
4	-84 °C, 2 hr	-40 °C → RT, 12 hr	56-72	-59
5	-40 °C, 2 hr	-78 °C → RT, 12 hr	12	156, 5, -10, -60
6	-84 °C, 2 hr	-78 °C → RT, 12 hr	71	-60
7	-84 °C, 2 hr	-78 °C, 12 hr	94	-60

Table 4: Optimization for the synthesis of compound **31**.

Therefore, the conditions utilized in the third trial finally produced a moderate yield of **31** with few by-products. The yield was slightly improved by maintaining the transmetallation at -40 °C, which appears to have slowed down the rate of reaction and eliminated the presence of the di-substituted impurity. However, compared to the literature yield (81%[22]), the yield for this reaction was lower than expected. Attempts to repeat this reaction in Trial 5 with a higher lithiation temperature followed by a cooler transmetallation produced a mixture of ^{119}Sn tin resonances (^{119}Sn (CDCl$_3$) δ: 156, 5, -10, -60 ppm). These resonances correspond to the known tin species: (n-Bu)$_3$SnCl (^{119}Sn (CDCl$_3$) δ: 152.0 ppm[7]), (n-Bu)SnCl$_3$ (^{119}Sn (CDCl$_3$) δ: 6.1 ppm[7]), (n-Bu)$_4$Sn (^{119}Sn (CDCl$_3$) δ: -11.5 ppm[7]), and compound **31**. Instead of the transmetallation, a redistribution reaction of the (n-Bu)SnCl$_3$ starting material was occurring instead and the lithiation was simply not occurring. A change of the lithiation temperature to warmer conditions -40 °C did not alter the results and the redistribution products were still obtained. All subsequent trials were carried out using Ph$_3$SnCl to test the conditions instead of n-BuSnCl$_3$ due to differential costs of these reagents. The yielded products of the transmetallation consist primarily of stannoxanes (^{119}Sn (CDCl$_3$) δ: 86.0 ppm[7]) or unreacted starting material (^{119}Sn (CDCl$_3$) δ: -44.7 ppm[7]). Further adjustments to the procedure include the rate of addition (fast or dropwise), the addition of the lithiated species to the tin species, and changing the lithiation temperatures (-78 °C, -40 °C, -20 °C). However, the target [2-(MeOCH$_2$)C$_6$H$_4$]Ph$_3$Sn (**33**) species (^{119}Sn (CDCl$_3$) δ: 133 ppm) was still not obtained until the lithiated ligand was washed with additional dry hexanes. Before the transfer via double-tipped cannula for the transmetallation, the solution was allowed to settle and the top layer of hexanes was removed into another Schlenk flask. An additional 2 × 5 mL aliquots of dry hexanes was used to wash the settled precipitate, and this was used for the transmetallation. The only recovered product was the expected **33**, which was subsequently recrystallized in MeOH

in good yield (76%). With this success, compound **31** was attempted again in Trial 5 with the washing step incorporated prior to the transmetallation. In the initial attempt with this method (Trial 6), the lithiated solution accidentally warmed up to around 0 °C and the final yield was moderate (71%). However, if the solution was kept at -78 °C, a high yield was obtained (94%) with minimal work up.

The benzyl dimethyl amine **30** was synthesized (Scheme 2) in high yields (~90%) as per literature procedure.[17] Compound **34** was synthesized using a similar method as with the *C,O*-chelated organotin dichloride, utilizing a sequential lithiation and transmetallation in a one-pot synthesis.
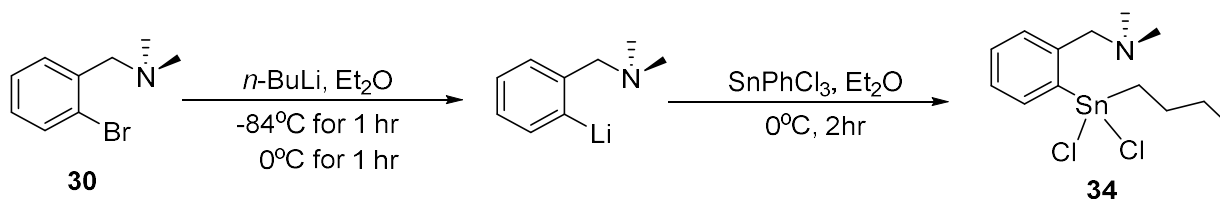
Scheme 2: Synthesis of compound **34**.

The literature synthesis proceeds as an overnight lithiation in Et$_2$O at RT followed by an overnight transmetallation at 0 °C. The product was extracted with hot hexanes in a 73 % yield. The conditions were optimized from a 2 d synthesis to a 1 d preparation. Attempts at following the literature procedure yielded a ^{119}Sn (CDCl$_3$) NMR resonance of δ: 3.13 ppm, which is likely the unreacted starting material (^{119}Sn (CDCl$_3$) δ: 6.1 ppm[7]). With the success of synthesizing the compound **31**, the conditions used for the third Trial in Table 4, were used as a starting point (Table 5). However, this did not yield the desired product. So again, Ph$_3$SnCl was used instead of (*n*-Bu)SnCl$_3$ to test the reaction conditions. Changes to the reaction conditions include rate of addition (fast or dropwise), addition of the tin species to the lithiated species, decanting off hexanes from the lithiated species before transmetallation, and changing the transmetallation reaction time to 3

hr. Attempts at this synthesis yielded stannoxanes (^{119}Sn (CDCl$_3$) δ: 86 ppm[7]), unreacted starting material (^{119}Sn (CDCl$_3$) δ: 44.7 ppm[7]), and an unknown product (^{119}Sn (CDCl$_3$) δ: -337 ppm). Finally, the product was successfully synthesized in Trial 3. The prolonged lithiation time may have completely degraded the species and transmetallation was proceeding. Using this procedure, compound **34** was synthesized successfully with moderate yields.

Trials	Reaction Conditions		Recovered Yields	^{119}Sn δ CDCl$_3$
	Lithiation	Transmetallation	(%)	(ppm)
1	-84ºC, Overnight	0 ºC → RT, Overnight	-	-3.13
2	-84 ºC, 2 hr	0 ºC → RT, 12 hr	-	86, 44, -337
3	-84 ºC, 2 hr	0 ºC, 2 hr	43-86	-105

Table 5: Optimization for synthesis of compound **34**.

2.1.2 Characterization of *C,O*- and *C,N*-chelated organotin dichlorides

Compounds **31** and **34** can be compared to other rigid, flexible, or asymmetrical *C,O*- and *C,N*-chelating organotin halides to gauge the relative hypercoordination interaction between the acceptor and donor parts of these molecules, Sn-D (D = O, N). In the ^{1}H NMR (CDCl$_3$) spectrum of **31**, the -CH$_3$ bound to the donor is shifted downfield due to the hypercoordinate interaction between Sn-D in comparison to a non-hypercoordinated species. The [2-(CH$_2$OCH$_3$)C$_6$H$_4$]Ph$_3$Sn (**33**) species -CH$_3$ resonance appears at 2.8 ppm[22], while for compound **31**, the resonance appears at 3.66 ppm. This difference is quite large since there is no hypercoordinate interaction present in **33**. However when compounds **31** and **34** are compared to the other butyltin halides, ([2-(MeDCH$_2$)C$_6$H$_4$](n-Bu)$_{n-3}$SnCl$_n$ (D = O, NMe)) of Table 6, the trend is as expected. Donation of the lone pair of electrons from oxygen to the tin shifts the adjacent -CH$_3$ protons downfield due to the hypercoordinate effect of the donor. Incorporating more chloride ligands would further strengthen the hypercoordination and deshield the -CH$_3$ protons.

16
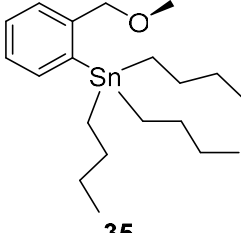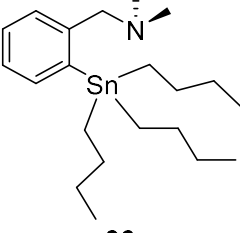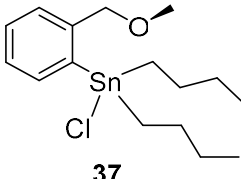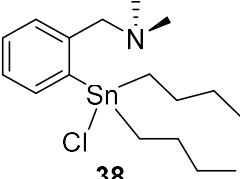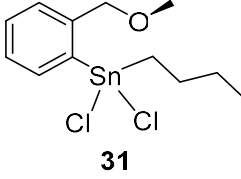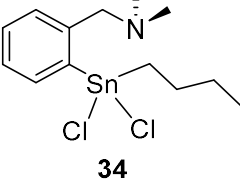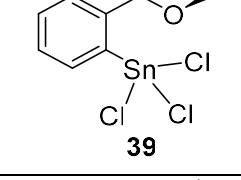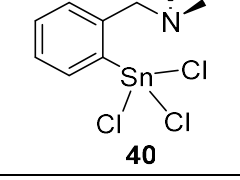
OMe Analogue NMR δ CDCl₃ (ppm)	^{1}H (-OCH₃)	^{119}Sn	NMe₂ Analogue NMR δ CDCl₃ (ppm)	^{1}H (-N(CH₃)₂)	^{119}Sn
35	3.40[22]	-40[22]	36	2.15[21]	-50[21]
37	3.60[22]	-91, -127[22]	38	2.30[21]	-51[21]
31	3.66	-59	34	2.39	-107
39	3.50	-184.3	40	2.61[21]	-241[21]

Table 6: Select ^{1}H and ^{119}Sn NMR (CDCl₃) resonances of [2-(MeDCH₂)C₆H₄](*n*-Bu)$_{n-3}$SnCl$_n$

(D = O, NMe)

The ^{119}Sn NMR spectroscopy reveals resonances that are further upfield from the range where diaryltin dichlorides typically appear, which is between 20-40 ppm.[23] These shifts are indicative of the hypercoordinate interaction, which shuttles electrons through the tin center, causing shielding and a upfield shift of the tin resonances. A substantial upfield shift in the ^{119}Sn resonances is typical observed with the increasing number of electron-withdrawing halogens at Sn.

2.1.3 Alternative Synthesis of *C,O-* and *C,N*-chelated organotin dichlorides

An alternative (indirect) route to prepare tin dichlorides was investigated to avoid the use of expensive tin trihalides. This may be achieved by using the triphenyl Sn analogue which may undergo sequential halogenations to achieve the dihalide. [2-$(CH_2N(CH_3)_2)C_6H_4$]Ph_3Sn (**41**) was previously been synthesized by the Holecek group[8b] in 2001 using lithatiation and transmetallation, while stepwise halogenations for tin species were first reported by the Molloy group.[24] Compound **40** was synthesized as per the methods used for compounds **31** and **34** (Scheme 3), however the yields obtained were often low (40-60%) compared to the reported literature (87 %).[8b]
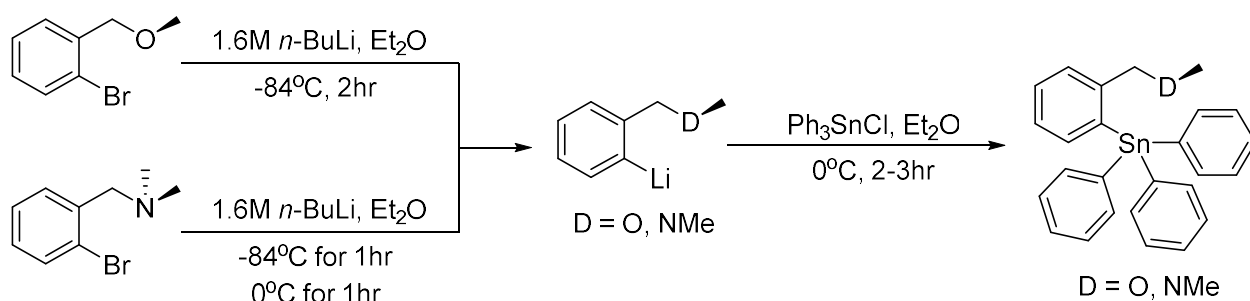
Scheme 3: Synthesis of compound **33** and **41**.

In this work, HCl and Br_2 were used as halogenation sources. HCl is an electronegative source of Cl and will attack the tin center by nucleophilic attack while the Br_2 is an electrophilic source of Br and will undergo a radical chain mechanism to displace the leaving group. Compounds **42**, **44**, and **45** were synthesized using stepwise chlorinations in great yields (97%) or brominations in low - moderate yields (**44:** 55 %, **45:** 38 %) as shown in Scheme 4.

Scheme 4: Synthesis of compounds **42**, **44**, & **45**.
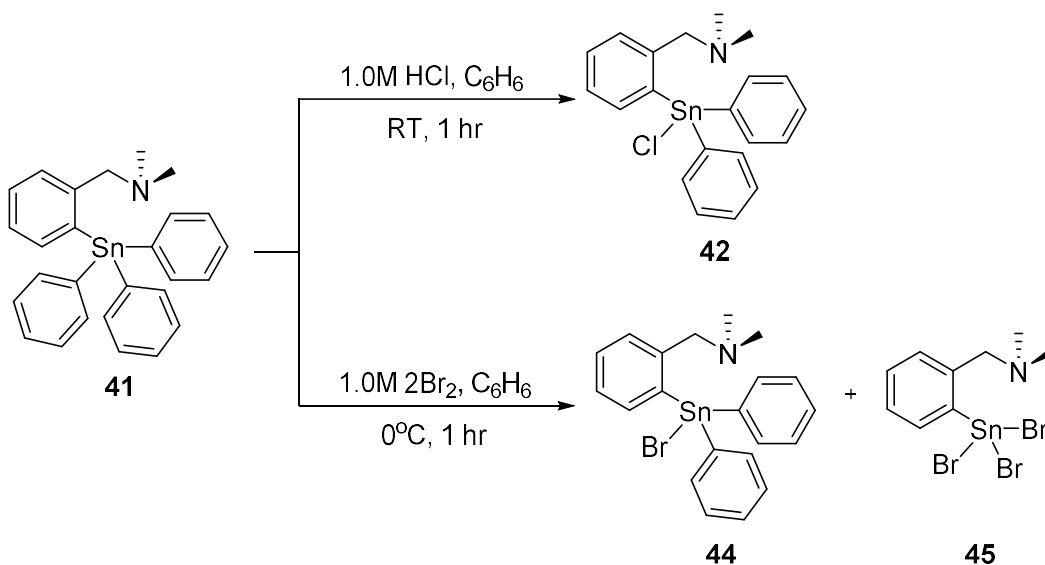
A second equivalence of HCl was added to **42** in hopes of synthesizing **43**, however, the reaction

did not proceed (Scheme 5). HCl in this instances is too weak halogenation source and was unable

to displace a second phenyl ligand.

Scheme 5: No reaction of **42** in a second chlorination.
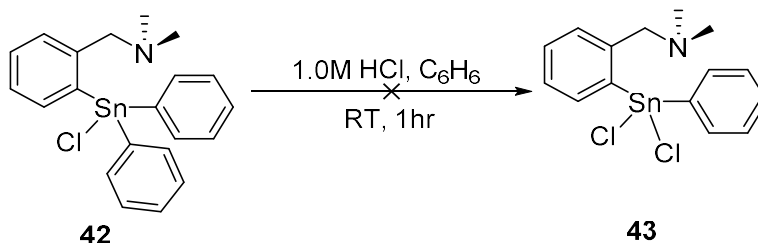
Conversely, the bromination of **41** produced a mixture of mono-(**44**) and tri-substituted

species (**45**). Changing the equivalence of Br₂ from 2 to 1 to the addition of a drop also brought

upon the same result. Bromine is an electrophilic source and producing radicals easily, which

pushes the reaction to be completely substituted as radicals are promoted to the antibonding σ

orbitals.

2.1.4 Characterization of Alternatively Synthesized *C,O*- and *C,N*-chelated Organotin Species

The ^{119}Sn NMR spectroscopy reveals resonances at -133 and -163 ppm for the *C,O*- (**32**) and *C,N*-chelated triphenyltin (**41**) analogues, respectively. These resonances are upfield compared to the unsubstituted analogue, tetraphenylstannane (^{119}Sn (CDCl$_3$) δ:-128 ppm[7]). Compound **41** has a slightly distorted trigonal bipyramidal geometry due to a small hypercoordinate interaction. This, as previously mentioned, shifts the ^{119}Sn resonance upfield. Compared to the *C,O*-chelated analogue, the slight upfield shift may indicate that the Sn-O interaction is not as strong as the Sn-N, and may be closer to a distorted tetrahedral geometry which is similar to the unsubstituted analogue.

The ^{119}Sn NMR resonance for monochloride compound **42** (^{119}Sn (CDCl$_3$) δ:-176 ppm) would normally be shifted to lower field, however even when the chloride facilitates the hypercoordinate Sn- N interaction, the ^{119}Sn resonances are not dramatically changed (mono—176.5 ppm, dichloro- -169.0 ppm[22]). Compared to the unsubstituted analogue, Ph$_3$SnCl (^{119}Sn (CDCl$_3$) δ:-44.7 ppm), there is the characteristic large upfield shift by 132 ppm. With the loss of even one sterically bulky ligand, a distinct hypercoordinate interaction is formed. This is also seen for the monobromotin **44** (^{119}Sn (CDCl$_3$) δ:-180.78 ppm) when compared to its unsubstituted analogue, Ph$_3$SnBr (^{119}Sn (CDCl$_3$) δ:-59.8 ppm[7]), with a difference of 120 ppm. Also, the addition of subsequent bromides by stepwise bromination pushes the ^{119}Sn resonance upfield rather than the expected downfield shift due to the effect of electron-withdrawing groups, as shown in Figure 8. These withdrawing effects help strengthen the hypercoordination bond causing more electron density to be pushed onto the tin and hence shift the ^{119}Sn resonance upfield.
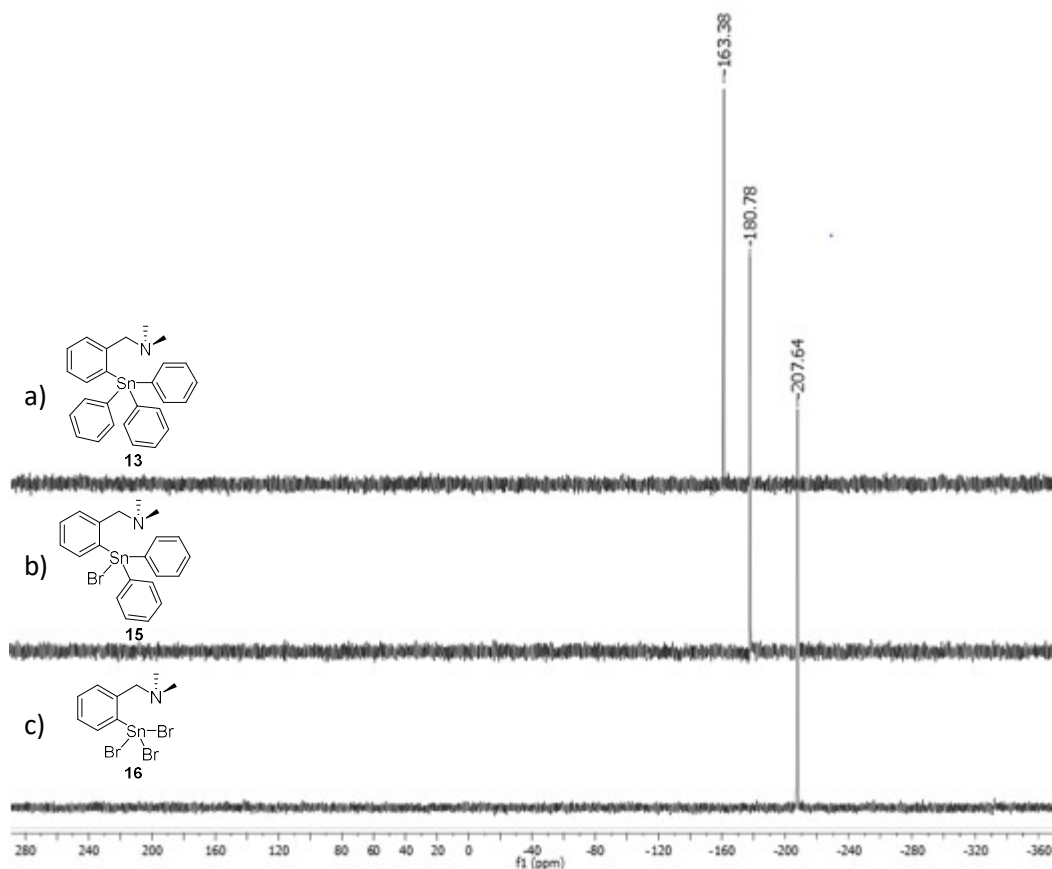
Figure 8: Sequential brominations shifts the [119]Sn (CDCl$_3$) resonance upfield.

The [119]Sn resonances of these compounds may be compared to other flexible and rigid structures in Table 7. Within the Foucher group, a rigid and a flexible symmetrical *C,N*-chelating oxazole tindibromide **47** display a significant Sn-N hypercoordinate interaction.[25] The incorporation of the oxazole group shifts the [119]Sn resonance upfield due to additional electron density in the oxazole ring and the hypercoordination interaction.

Conversely, changing the rigid moiety to a more flexible one shifts the [119]Sn resonances downfield. This is also seen in comparison to other flexible *C,O*-chelating organotin species. In 2007, the Pannell group synthesized flexible hypercoordinate *C,O*-chelated organotin species, (2-MeOC$_6$H$_4$)CH$_2$SnPh$_{n-3}$Cl$_n$.[11] Compared the rigid analogues (**48-50**), the opposite occurs; the observed trend [119]Sn resonances becomes deshielded.

21
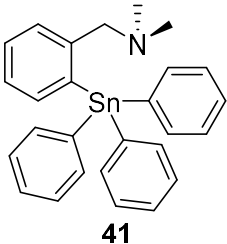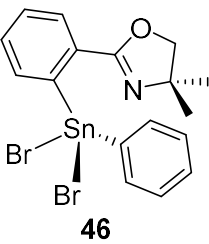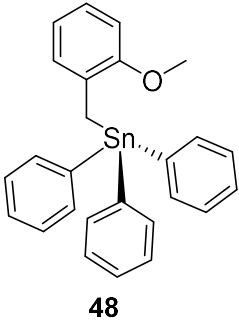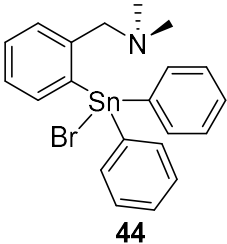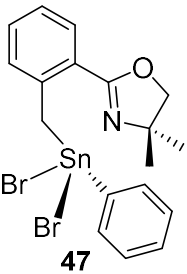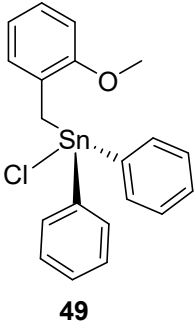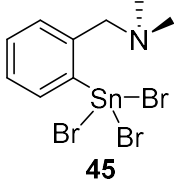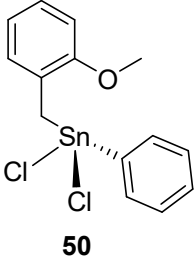
NMe$_2$ Analogue	^{119}Sn NMR δ (ppm)	Oxazole Analogue	^{119}Sn NMR δ (ppm)	OMe Analogue	^{119}Sn NMR δ (ppm)
41	-163	**46**	-290[25]	**48**	-114[11]
44	-176	**47**	-248[25]	**49**	-41[11]
45	-206			**50**	-32[11]

Table 7: Select ^{1}H and ^{119}Sn NMR (CDCl$_3$) resonances of rigid and flexible *C,O*- and *C,N*-chelating phenyltinhalides species.

2.1.5 Crystal Structures

The crystal structure of compound **41** was obtained by dissolving the crude product in hexanes and allowing the slow evaporation to form transparent rod-shaped crystals. The geometry is a distorted trigonal bipyramidal, with deviation of the dihedral bond angles. The Sn-N bond is much larger than the standard covalent bond length 2.154 Å (Table 8) and suggests a very weak hypervalent interaction. This is also supported by the moderate difference in the ^{119}Sn resonances by 26 ppm in comparison to the unsubstituted analogue at -137 ppm. Finally looking at the bond lengths around the tin center, only the apical bonds are elongated further from the tin center. The

steric bulk around the tin center is great and would prevent the hypervalent interaction to occur strongly.
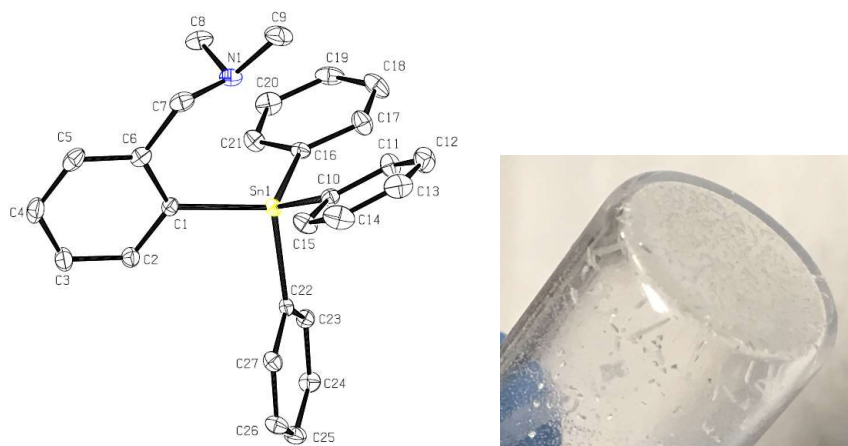
Figure 9: Molecular structure (left) and crystals (right) of compound **41**.

To exchange a phenyl ligand by stepwise halogenation is easily accomplished. C22 is most suitable as the leaving group since the Sn-C(22) bond donates extra electron density into the antibonding σ orbitals of C(23)-C(24) and C(27)-C(26) through negative hyperconjugation.[2] As compared to a rigid and flexible *C,N*-chelating oxazole tintriphenyl species, the rigid species (4,4-dimethyl-2-(2-(triphenylstannyl)phenyl)-4,5-dihydrooxazole) displays a strong Sn-N interaction (2.762(1) Å) while the flexible species (4,4-dimethyl-2-(2-((triphenylstannyl)methyl)phenyl)- 4,5-dihydrooxazole) is interacting weakly (two configurations, A: 3.176(4) Å, B: 3.234(4) Å). The rigid oxazole is a much more rigid structure than compound **41**, forcing the hypercoordinate interaction and changing the geometry to distorted trigonal bipyramidal. Compound **41** has a freely rotating donor ligand (-NMe$_2$), that does not facilitate the hypercoordinate bonding to take place. The ligand may rotate away from the tin center to accommodate the phenyl groups; hence elongating the Sn-N dative interaction. Conversely with the flexible oxazole species, there are even greater degrees of freedom due to the CH$_2$-Sn bond. The ligand itself is no longer forced to

participate in any hypercoordinate bonding; hence having the weak dative interaction. In comparison to monohalogenated species, the van Koten group synthesized a [2

Bond lengths, angles (Å, °)	
Sn-N	2.917
Sn(1)-C(16)	2.1331(18)
Sn(1)-C(10)	2.1422(18)
Sn(1)-C(1)	2.1523(18)
Sn(1)-C(22)	2.1661(18)
C(10)-Sn-C(1)	110.39(7)
C(16)-Sn-C(22)	102.35(7)

Table 8: Selected bond lengths and angles of **41**.

-$(CH_2N(CH_3)_2)C_6H_4]Ph_2SnBr$ (**44**) species in 1976[26]. The Sn-N dative bond was 2.511(12) Å, shorter than that of the triphenyl derivatives as expected. The Sn-C bond lengths also became slightly shorter due to the withdrawing nature of the bromides and the C-Sn-C angles increased to 121.2°, 122.0°, and 114.5° to accommodate the Sn-N dative bond by further distorting the trigonal bipyramidal geometry.

Previously, the van Koten group had synthesized the mono and tribromide species and reported resonances of ^{119}Sn (CDCl$_3$) δ: -180 ppm and ^{119}Sn (CDCl$_3$) δ: -414 ppm. However, the ^{119}Sn NMR consistently produced two resonances at ^{119}Sn (CDCl$_3$) δ: -180 ppm and ^{119}Sn (CDCl$_3$) δ: -206 ppm before purification. After purification, a translucent cubic crystal of the compound with a ^{119}Sn (CDCl$_3$) δ: -206 ppm resonance was grown by dissolving it in minimal DCM and layering with hexanes. However, the isolated crystal was determined to be tribromide species; of which the lack of the disubstituted species was unexpected. This is highly unusual since normally tribromides range around -400 ppm in ^{119}Sn NMR.
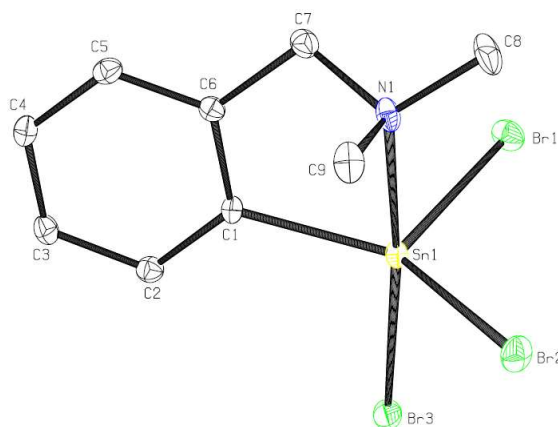
Figure 10: Molecular structure of compound **45**.

As a result of the large discrepancy in the ^{119}Sn NMR values (δ 200 ppm), an X-ray structure determination of the isolated crystals was undertaken. Despite the large difference in ^{119}Sn resonances, the obtained crystal structure of **45** have minimal differences between the bond lengths and angles as shown in Table 9. The donor nitrogen is not parallel to the phenyl of the ligand and deviates away from the plane of the phenyl by 34.33°. The dichloride derivative, also synthesized by the Holecek group, displays a slightly weaker Sn-N interaction by having a shorter Sn-N bond of 2.444(5) Å, though both bond lengths are typical for NMe$_2$ ligands.[8e] As expected, the more strongly withdrawing halogen and having an additional bromide would cause the hypercoordinate interaction to be stronger in compound **45**. Compound **45** displays a distorted trigonal bipyramidal geometry with $\tau_5 = 0.63$, distorted C-Sn-Br, Br(1)-Sn-Br(2) angles around 120° and the linear apical N(1)-Sn(1)-Br(3) bond. The Sn-N bond of 2.403 Å is indicative of a strong hypercoordinate interaction while elongating the apical bromide to 2.5772 Å. Around the tin center, the equatorial bromides are elongated. The electron withdrawing nature of these atoms may push electron density into the antibonding σ and hence elongate.

Bond lengths, angles (Å, °) this work		Holecek Group bond lengths and angles (Å, °)
Sn-N	2.403(2)	2.402(3)
Sn(1)-C(1)	2.127(3)	2.128(3)
Sn(1)-Br(1)	2.4829(4)	2.4826(4)
Sn(1)-Br(2)	2.4874(4)	2.4864(4)
Sn(1)-Br(3)	2.5772(4)	2.5760(4)
N(1)-Sn(1)-Br(3)	173.35(6)	173.29(7)
C(1)-Sn(1)-Br(1)	112.41(7)	112.26(9)
C(1)-Sn(1)-Br(2)	135.54(7)	135.66(9)
Br(1)-Sn(1)-Br(2)	108.642(13)	108.720(15)

Table 9: Comparison of selected bond lengths and angles of **45** for obtained and Holecek Group crystal structure.

2.1.6 Synthesis and Characterization of *C,O*- and *C,N*-chelated organotin dihydrides

To synthesize the dihydrides **51** and **52**, both a strong hydride source, LiAlH$_4$, and a weaker hydride source, NaBH$_4$, were used. The reaction is a simple hydrogenation, where the hydride will coordinate to the tin center and displace one of the chlorides. Both methods result in very similar yields, ranging from 50-80% yield.
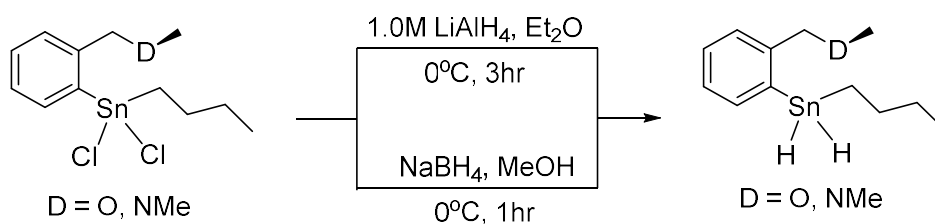
Scheme 6: Synthesis of [2-(MeOCH$_2$)C$_6$H$_4$]*n*-BuSnH$_2$, **51**, using either LiAlH$_4$ or NaBH$_4$.

In the ^{1}H NMR, there is the emergence of the hydride resonance at 5.67 ppm with the ^{119}Sn/^{117}Sn satellites at 7.82 ppm and 3.51 ppm. A characteristic property of hypercoordinated organotin hydrides is having a larger ^{119}Sn-^{1}H coupling over their unsubstituted analogues.[23] The ^{119}Sn coupling for **51** is 1764 Hz and is larger than of (*n*-Bu)$_2$SnH$_2$, 1675 Hz, suggesting a
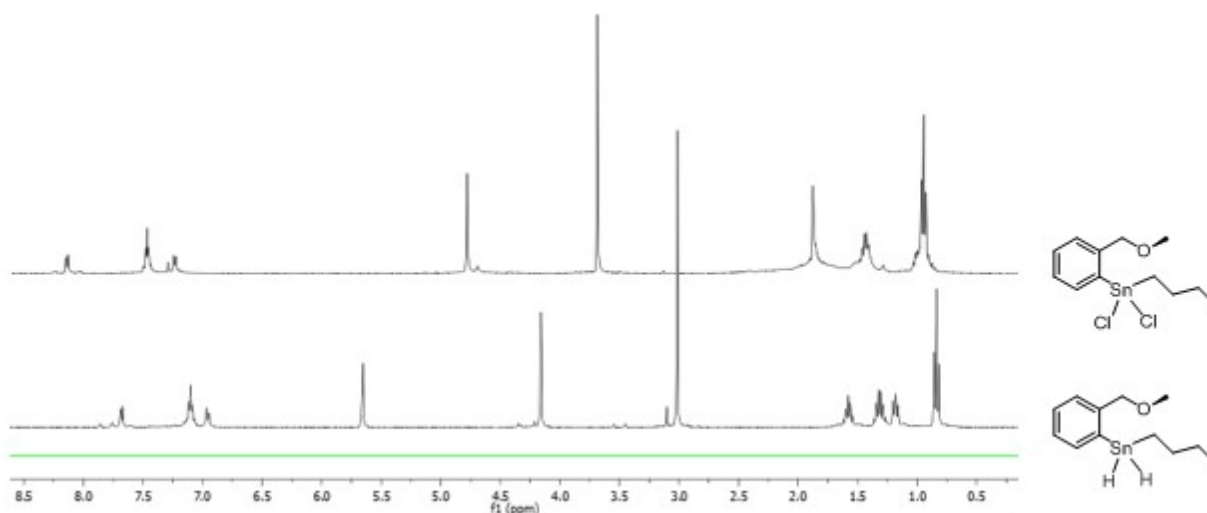
Figure 11: Comparison of ^{1}H NMR (C$_6$D$_6$) of tin dichloride **31** and tin dihydride **51**.

hypercoordinate interaction. Additionally, there is a drastic shift in the ^{119}Sn resonances from the unsubstituted analogue, Ph(n-Bu)SnH$_2$ (^{119}Sn (C$_6$D$_6$) δ: 105 ppm) to the dihydride (^{119}Sn (C$_6$D$_6$) δ: -210 ppm) due to changes from a low to a high shielding of the tin center (Figure 11). Finally, the ^{119}Sn-^{13}C couplings also show no significant shifts as expected, of which is consistent with DFT calculated trends.[23] For the *C,N*- analogue, the same general trend is also observed with a large shift in the ^{1}H NMR resonance, 5.66 ppm, and ^{119}Sn resonance, 217.5 ppm, respectively.

These results are comparable to the hypercoordinated tin monohydride (**55**) synthesized by the Ruzicka group in 2009[27] (Table 10). They synthesized [2-(CH$_2$N(CH$_3$)$_2$)C$_6$H$_4$]R$_2$SnH (R = *n*-Bu, *t*-Bu, Ph) using K(BEt$_3$)H·THF. The ^{1}H resonances of the *n*-butyltin hydrides would obviously be close, they are not electron withdrawing like the phenyl groups. More importantly, the addition of an extra hydride greatly shifts (~100 ppm) the ^{119}Sn NMR resonances upfield due to the extra electron density.
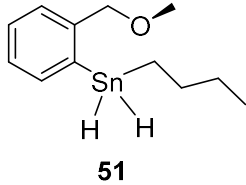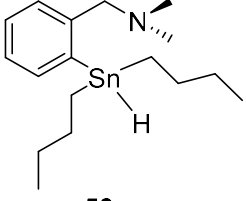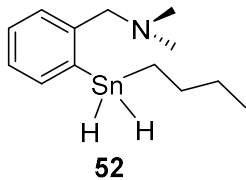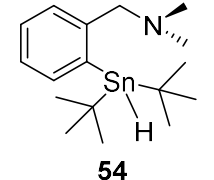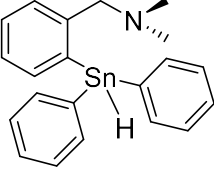
	^{1}H NMR δ (ppm)	^{119}Sn NMR δ (ppm)		^{1}H NMR δ (ppm)	^{119}Sn NMR δ (ppm)
51	5.67	-210.1	**53**	5.83	-113.2
52	5.66	-217.5	**54**	6.01	-90.0
			55	6.98	-180.9

Table 10: ^{1}H and ^{119}Sn NMR (C$_6$D$_6$) resonances of *C,O*- and *C,N*-chelating tin mono- and dihydride species.

2.2 Dehydrocoupling of *C,O*- and *C,N*-Monomers

Dehydrocoupling of hypercoordinated compounds **51** and **52** was attempted using Wilkinson's catalyst. The *C,O*- and *C,N*- dihydride butyl monomers were selected to ensure good solubility and processability of any resulting polymer. The polymerization followed conditions used for flexible polystannanes[28], where the reaction was carried out at room temperature in the absence of light in aluminum foil wrapped Schlenk flasks with 10 mL of degassed toluene containing 4 mol% of the Wilkinson's catalyst to which the monomer in the same solvent (6 mL) was slowly added and stirred for 4 h (Scheme 7).
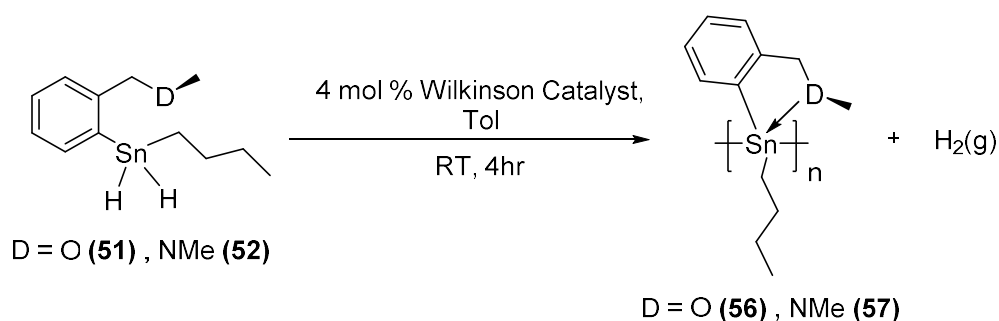
Scheme 7: Synthesis of rigid polystannanes **56** and **57**.

A lightly yellow coloured polymer **56** was recovered from the dehydrocoupling of **51** in good yield (65%), while a much darker yellow coloured polymer **57** was recovered from the polymerization **52** in poor yield (18%). After several attempts, modest molecular weights were obtained for both rigid polymers (**56**: $M_w = 3.03 \times 10^4$ Da, PDI = 1.4, **57**: $M_w = 3.10 \times 10^4$ Da, PDI 1.86). The degree of polymerization is approximately 100 monomer units each for **56** and **57**.

Analysis by ^{1}H and ^{13}C NMR spectroscopy confirmed the expected polymer structures. As for ^{119}Sn NMR spectroscopy, two different deuterated solvents (C_6D_6 and THF-d_8) were used to reveal structural details. Figure 12 compares the effect of each solvent for **56**, where two resonances (^{119}Sn δ: -49 and -199 ppm) appeared in C_6D_6, while in THF-d_8, only a single resonance (^{119}Sn δ: -44 ppm) was seen. THF-d_8 is a coordinating solvent and this may suggest that large excess of THF molecules were effectively displacing the Sn-O dative interaction of the chelating ligand, causing the complex to be in an "open" position. When the THF-d_8 was removed and redissolved in C_6D_6, (Figure 12 top) the sample did not return to its initial closed position, and no resonance at -199 ppm was detected. As for polymer **57** (Figure 13), conversely, only one resonance (^{119}Sn δ: -149 ppm) was observed in C_6D_6 while two resonances (^{119}Sn δ: -55 and -151 ppm) were seen in THF-d_8. Again, a partial redistribution from the upfield "closed" resonance to the "open" downfield resonance was seen. However unlike polymer **56**, when the THF-d_8 sample

was resuspended in C_6D_6 (Figure 13 top), all of the "open" structural isomers returned to the "closed" state. This is good evidence that the NMe$_2$ functionality of **57** is more strongly donating and coordinating to Sn than the OMe functionality of **56**. This also suggests that the ability of these rigid dihydride monomers to undergo dehydrocoupling maybe impacted by the strength of these dative interactions, which lead to very low yields in the case of **57**.
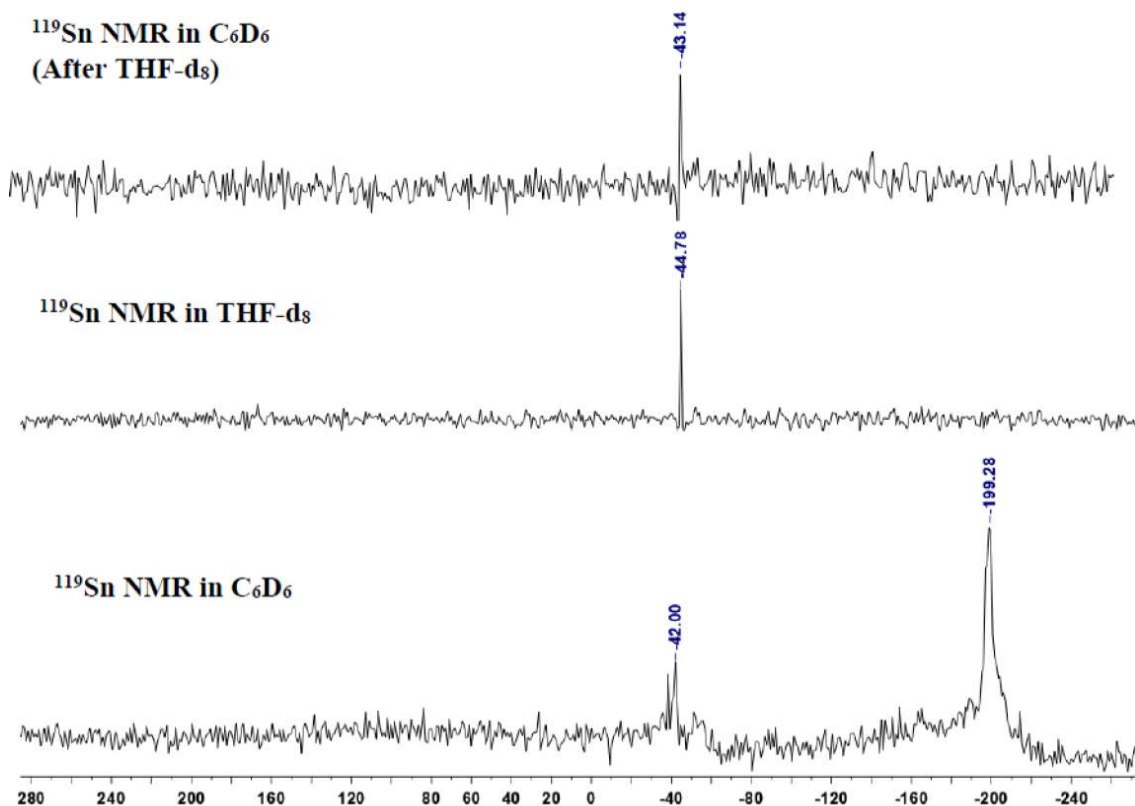
Figure 12: ^{119}Sn NMR of **56** in two different solvents: bottom C_6D_6, middle THF-d$_8$, and THF-d$_8$ sample dried and redispersed in C_6D_6.
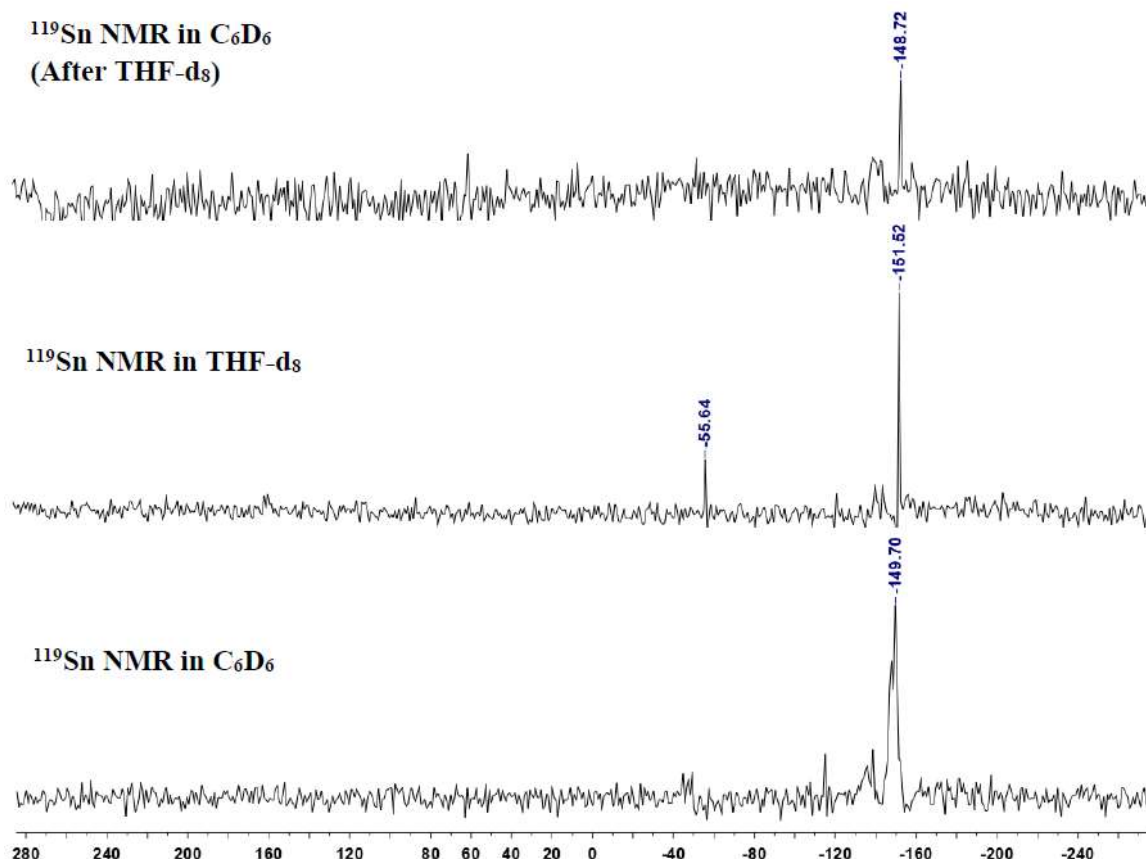
Figure 13: ^{119}Sn NMR of **57** in two different solvents: bottom C$_6$D$_6$, middle THF-d$_8$, and THF-d$_8$ sample dried and redispersed in C$_6$D$_6$.

2.2.1 Thermal Properties of 56 and 57

A DSC study of **56** and **57** revealed the two polymers to have amorphous character absent of any crystalline behaviour. The polymers showed no thermal behaviour changes when annealed prior to running or after multiple scans. Unfortunately, at these low molecular weights, polymer film properties were not evident.

2.3 Condensation Polymerization of *C,O-* and *C,N*-Monomers

Condensation polymerization of compounds **60** and **61** was utilized in hopes of adding additional flexibility and solubility to the rigid polymer chain. For this reason, dimethyl and di(*n*-butyl) tin monomers were used and prepared through transmetallation in high yields (86% and

92%) following literature procedure[15] as organotin amines **58** and **59**, respectively. The ligand is first lithiated to form $Li(NEt_2)_2$ before undergoing a transmetallation with R_2SnCl_2 to produce the respective tin amine. As for the polymerization[15], the hydride **51** was reacted in equivalence with either **58** or **59** in cold diethylether for 3 hrs at 0°C, to produce polymers **60** and **61**, respectively (Scheme 8).
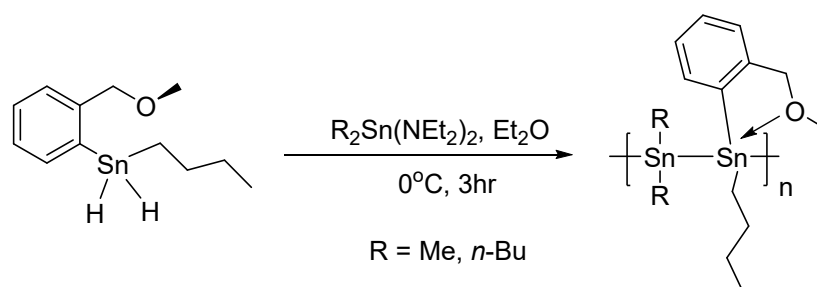
Scheme 8: General synthesis of alternating polymers, **60** and **61**.

After many attempts, two pale yellow coloured polymers **60** and **61** where recovered in good and poor yields (72% and 21%), respectively. A low molecular weight was obtained for polymer **60** with 1.30×10^4 Da, PDI: 2.0 and degree of polymerization of 21 while **61** was obtained as an oligomer with 0.92×10^4 Da, PDI: 2.71.
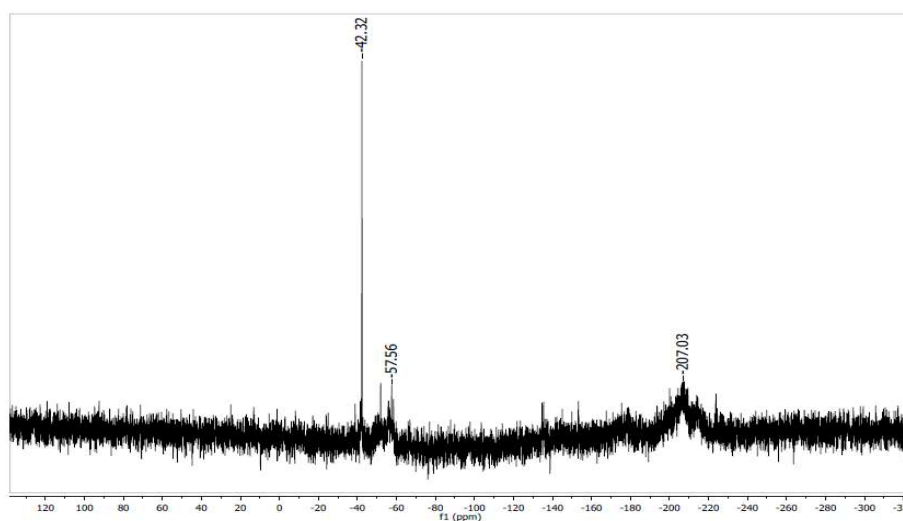
Figure 14: ^{119}Sn NMR of polymer **60**.

32

Analysis by ^{1}H and ^{119}Sn NMR spectroscopy confirmed polymer **60**. The ^{119}Sn NMR spectroscopy showcases two broad resonances (^{119}Sn δ: -57 and -207 ppm) and an unknown impurity at (^{119}Sn δ: -42 ppm). The obtained ^{119}Sn resonances for **60** match their respective unsubstituted analogue, shown in Table 11, where the diorganotin species corresponds to -57 ppm resonance and the *C,O*- chelating tin species corresponds to the -207 ppm resonance. In this case, it is likely that there is a hypercoordinate interaction, as the -207 ppm resonance falls within the range of the "closed" configuration.

As for oligomer **61**, the ^{1}H and ^{119}Sn NMR spectroscopy has evidence of impurities. It is possible that in the ^{119}Sn NMR of **61**, there was the presence of oligomers at -192 ppm and possible unreacted dihydride monomer at -226 ppm. Similar to **60**, it is possible that the 13 chain oligomer may also be in a "closed" configuration due to falling into the range of the "closed" configuration.

Alternating Polymer	^{119}Sn δ (ppm)	Unsubstitued Analogue	^{119}Sn δ (ppm)
60	-56, -209	–[Ph$_2$Sn-*alt*-SnMe$_2$]$_n$–	-60, -201[15]
61	-171, -202	–[Ph$_2$Sn-*alt*-Sn(*n*-Bu)$_2$]$_n$–	-178, -208[15]

Table 11: Comparison of ^{119}Sn resonances of alternating polymers and their unsubstituted analogues.

3.0 Conclusion

A series of new and known *C,O-* and *C,N-* rigid small molecule stannanes were prepared and characterized. Polymerization of *C,O-* and *C,N-* dihydrides **51** and **52** using Wilkinson's catalyst has led to the first examples of modest molecular weight rigidly hypercoordinated polystannanes **56** and **57** respectively. Condensation polymerization has resulted in a low molecular weight polymer **60** and oligomer **61.** Characterization by DSC of the amorphous polystannanes **56** and **57** display relatively low T_gs. The polymers appear to be indefinitely stable to both air and moisture. If higher molecular weights are obtained through improved catalyst selection and polymerization conditions, these rigid hypercoordinated polystannanes may be good candidates for polymeric wires.

4.0 Future Work

In this study, *C,O-* alternating and *C,O-* & *C,N-* homo-polymers were prepared from respective *C,O-* and *C,N- n-*butyltin dihydrides in an effort to produce polystannanes with increased stability to light and moisture due to rigid, bulky functional groups. Currently, investigation is required of the *C,N-* alternating polystannanes in addition to stability and thermal testing of these materials. The alternative route used to synthesize the hypercoordinate tin bromide species may also require further investigation.

5.0 Experimental

5.0.1 General Considerations

^{1}H NMR (400 MHz), ^{13}C NMR (100.6 MHz) and ^{119}Sn NMR (149.2 MHz) spectra were recorded on a Bruker Advance 400 MHz NMR spectrometer with a BBFO 5-mm direct probe. A ^{1}H pulse width of 30° was used, acquiring a spectral window of 8223 Hz (20 ppm) using a relaxation delay of 1s, acquisition time 3.98s, 32k points (16 scans). The ^{1}H 90° pulse width was 10.4 µs. A ^{13}C pulse width of 30° was used, acquiring a spectral window of 24038 Hz (239 ppm) using a relaxation delay of 2s, acquisition time 1.36s, 32k points (4096 scans). The ^{13}C 90º pulse width was 8.7 µs. A ^{119}Sn pulse width of 30º was used, 8.75 µs, acquiring a spectral window of 100000 Hz (670 ppm) using a relaxation delay of 1s, acquisition time 0.33s, 32k points (15360 scans) with inverse gated proton decoupling. All results were analyzed on MestReNova LITE 5.2.5 software. Chemical shifts were calculated using the chemical deuterated standards as a reference for ^{1}H and ^{13}C. The ^{119}Sn was referenced to SnMe$_4$ as an internal standard. All J coupling values are reported as absolute values. Time-of-flight mass spectrometry analyses were performed at the AIMS Mass Spectrometry Laboratory, University of Toronto using a JMS-T1000LC mass spectrometer (JEOL Inc., Peabody, MA) equipped with a Direct Analysis in Real Time (DART) ionization source (DART-SVP, Ionsense Inc., Saugus, MA). The DART source was operated with He gas and the temperature was adjusted in the range 100-400°C. Isotopic distributions for the observed ionic species were calculated using the Mass Center utility (JEOL) and were in good agreement with the measured mass spectra. Molecular weights of the polymers were determined by GPC using a Viscotek Triple Model 302 Detector system. GPC columns were calibrated versus polystyrene standards (American Polymer Standards). A flow rate of 1.0 mL/min. was used with ACS grade THF as the eluent. GPC samples were prepared using 3-10 mg of each polymer per mL THF, and

filtered using a 0.45 μm filter. All samples were run with and without UVA (conc. $\approx$ 0.001 M) for comparison. The X-ray diffraction data for compounds **41** and **45** were collected on a Bruker Kappa APEX-DUO diffractometer using monochromated Mo-Kα radiation (Bruker Triumph) and were measured using a combination of ϕ scans and ω scans. The data were processed using APEX2 and SAINT programs. Absorption corrections were carried out using SADAB. The structures were solved using SHELXT[75] and refined using SHELXL-2013[75] for full-matrix least-squares refinement that was based on F^2. For all structures, H atoms were included in calculated positions and allowed to refine in a riding-motion approximation with Uiso tied to the carrier atom. All reactions were carried out under a nitrogen atmosphere using Schlenk techniques unless otherwise described. LiAlH$_4$ (1.0 M in Et$_2$O), 1.0 M solution of HCl in Et$_2$O, anhydrous CaCl$_2$, anhydrous MgCl$_2$ and Wilkinson's catalyst were purchased commercially and used without further purification. Solvents were dried by standard procedures prior to use.

5.1 Synthesis of (2-(MeOCH₂)C₆H₄)Br (29):
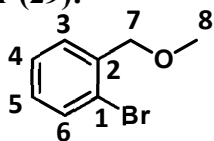
To a two-neck flask equipped with a condenser, 7.84 g (31.37 mmol) of 2-bromobenzyl bromide was added. An equivalent amount of sodium methoxide (1.695 g, 31.37 mmol) and 30 mL of dry MeOH was also added. The reaction was refluxed at 75 °C for 5 hr. The solution was cooled to room temperature and the solvent was removed under reduced pressure. A 50 mL solution of 1:1 hexane:Et₂O was added and extracted with H_2O (2 × 50 mL) and brine (2 × 50 mL). The solution was dried over $MgSO_4$ and volatile solvents removed under reduced pressure to yield 5.075 g (80.4 %) of a clear pale-yellow/colourless liquid. NMR data for this product agreed well with literature.[16]

¹H NMR (400 MHz, CDCl₃, δ): 7.54 (dd, $^4J_{1H-1H}$ = 0.9 Hz, $^3J_{1H-1H}$ = 7.9 Hz, 1H, H6), 7.46 (dd, $^4J_{1H-1H}$ = 0.7 Hz, $^3J_{1H-1H}$ = 7.6 Hz, 1H, H3), 7.32 (dt, $^4J_{1H-1H}$ = 0.8 Hz, $^3J_{1H-1H}$ = 7.4 Hz, 1H, H4), 7.11 (dt, $^4J_{1H-1H}$ = 1.6 Hz, $^3J_{1H-1H}$ = 7.9 Hz, 1H, H5), 4.54 (s, $^1J_{13C-1H}$ = 143.1 Hz, 2H, H7), 3.48 (s, $^1J_{13C-1H}$ = 141.2 Hz, 3H, H8) ppm; **¹³C NMR** (100 MHz, CDCl₃, δ): 137.64 (C1), 132.53 (C6), 128.98 (C3), 128.91 (C5), 127.41 (C4), 122.72 (C2), 73.91 (C7), 58.60 (C8) ppm.

5.2 Synthesis of (2-(CH₂N(CH₃)₂)C₆H₄)Br (30):
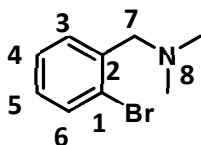
To a Schlenk flask, 15.00g (60.20 mmol) of 2-bromobenzyl bromide and 45 mL of dry DCM was added. A large excess of a 33% HNMe₂ in MeOH solution (60 mL, 1320.4 mmol) was added dropwise by syringe to the Schlenk flask. The reaction was heated to 45 °C and left to react for 7 hr. The product was extracted with 2M HCl (3 × 30 mL) and neutralized with a 20% NaOH solution. The basic product was extracted with DCM and a final extraction with distilled water carried out. The DCM was removed *in vacuo* and the isolated product recovered was a clear liquid (12.03 g, 93.6 %). NMR data for this product agreed well with literature.[17]

¹H NMR (400 MHz, CDCl₃, δ): 7.49 (dd, $^4J_{1H-1H}$ = 0.9 Hz, $^3J_{1H-1H}$ = 7.9 Hz, 1H, H6), 7.41 (dd, $^4J_{1H-1H}$ = 1.3 Hz, $^3J_{1H-1H}$ = 7.6 Hz, 1H, H3), 7.22 (dt, $^4J_{1H-1H}$ = 0.9 Hz, $^3J_{1H-1H}$ = 7.5 Hz, 1H, H4), 7.04 (dt, $^4J_{1H-1H}$ = 1.6 Hz, $^4J_{1H-1H}$ = 7.8 Hz, 1H, H5), 3.49 (s, $^1J_{13C-1H}$ = 133.5 Hz, 2H, H7), 2.27 (s, $^1J_{13C-1H}$ = 133.0 Hz, 6H, H8) ppm; **¹³C NMR** (100 MHz, CDCl₃, δ): 138.24 (C1), 132.71 (C6), 130.88 (C3), 128.37 (C4), 127.17 (C5), 124.68 (C2), 63.25 (C7), 45.53 (C8) ppm.

5.3 Synthesis of [2-(MeOCH₂)C₆H₄]*n*-BuSnCl₂ (31):
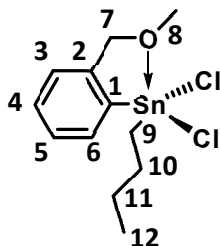
To a Schlenk flask, 1.25 g (6.21 mmol) 2-bromobenzyl methoxide and 30 mL of dry hexanes was added. The Schlenk flask was cooled down to -84 °C using an EtOAc/Liq. N_2 bath and maintained at this temperature for at least 5 min. To the cooled Schlenk flask, a solution of 1.6M *n*-BuLi in hexanes (3.88 mL, 6.21 mmol) was added slowly, dropwise, using a syringe. The temperature was maintained at -84 °C and left stirring for 2 hr. A white salt appeared during this time. While maintaining -84 °C, the residual reaction solvent was removed by double tip cannula and the organolithium solid was washed with 2 × 5 mL aliquots of dry hexane and decanted via cannula to remove impurities. In another Schlenk flask, 1.75 g (6.21 mmol) *n*-butyltintrichloride dissolved in a 15 mL solution of 1:1 hexane:Et_2O and cooled to 0 °C. The clean organolithium was resuspended in 10 mL of hexane and kept cool at -84 °C and then transferred to the tin solution via a cannula and the solution was stirred for 12 hr. The solvent was removed under reduced pressure. Toluene was added, and the solution filtered using a Schlenk filter funnel to remove any LiCl salts. The solvent was again removed under reduced pressure, and a minimal volume (3 mL) of toluene was added directly to the vicious oil. In a separate flask, hexane was heated until the solvent was boiling for a few minutes. The hot hexane was carefully layered on top of the toluene layer and become whitish in colour. The hexanes layer was carefully removed via pipet and transferred to a clean Schlenk flask. This process was repeated 3-5 times. The recovered hexane layers were dried

under reduced pressure to yield 1.56 g (68.6 %) of a clear, yellowish, or brownish gel. The NMR

data agreed well with literature data.[18]

¹H NMR (400 MHz, CDCl$_3$, δ): 8.12 (m, 1H, H6), 7.42 (m, 2H, H4-H5), 7.20 (m, 1H, H3), 4.75

(s, $^4J_{119/117Sn-1H}$ = 145.6 Hz, 2H, H7), 3.66(s, $^4J_{119/117Sn-1H}$ = 144.8 Hz, 3H, H8), 1.86 (m, 4H, H9-

H10), 1.41 (q, $^3J_{1H-1H}$ = 7.2 Hz, 2H, H11), 0.93 (t, $^3J_{1H-1H}$ = 7.3 Hz, 3H, H12) ppm; **¹¹⁹Sn NMR**

(149MHz, CDCl$_3$, δ): -59.53 ppm.

5.4 Synthesis of [2-(CH₂N(CH₃)₂)C₆H₄]n-BuSnCl₂ (34):
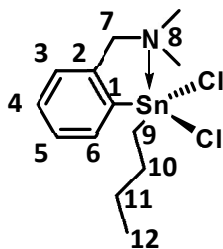
To a Schlenk flask, 0.50g (2.33 mmol) of (2-bromobenzyl) dimethylamine and 15 mL of dry Et₂O were added. The Schlenk flask was cooled down to -84 °C using an EtOAc/Liq. N₂ bath and maintained at that temperature for at least 5 min. To that Schlenk flask, a solution of 1.6M n-BuLi in hexanes (2.10 mL, 3.36 mmol) was added slowly, dropwise using a syringe. The temperature was maintained at -84 °C for 1 hr before warming up to 0 °C using an ice bath and left for 1 hr. In a second Schlenk flask, 0.66 g (2.33 mmol) n-butyltintrichloride was added and dissolved in 20 mL of dry Et₂O and cooled to 0 °C. The lithiated ligand was then transferred to the tin solution via a cannula and the solution was stirred for 2 hr at 0 °C. The solvent was removed under reduced pressure. Toluene was added, and the solution was filtered to remove any LiCl salts. The solvent was again removed under reduced pressure. Finally, hexane was added directly to the vicious oil and heated using a heat gun until the solvent was boiling for a few minutes. In a clean flask, the hot hexanes layer was poured out whilst decanting the oil layer and repeated 3-5 additional times. The collected solution was cooled to -20 °C overnight and the precipitate was collected and dried under reduced pressure to yield 0.77 g (86.5%) of a white crystalline solid. The NMR data agreed well with literature data.[19]

¹H NMR (400 MHz, CDCl₃, δ): 8.12 (dd, $^3J_{\text{1H-1H}}$ = 6.8 Hz, $^4J_{\text{1H-1H}}$ = 43.5 Hz, 1H, H6), 7.37 (m, 2H, H4-H5), 7.19 (d, 1H, H3), 3.71 (s, $^4J_{\text{119/117Sn-1H}}$ = 123.9 Hz, 2H, H7), 2.39 (s, $^4J_{\text{119/117Sn-1H}}$ = 136.7 Hz, 6H, H8), 1.89 (m, 2H, H9), 1.79 (m, 2H, H10), 1.44 (q, $^3J_{\text{1H-1H}}$ = 7.2 Hz, 2H, H11), 0.93

(t, $^3J_{1H-1H}$ = 7.3 Hz, 3H, H12) ppm; **^{13}C NMR** (100 MHz, CDCl$_3$, δ): 141.26 (C1, $^1J_{119/117Sn-13C}$ = 47.3 Hz), 139.49 (C2), 136.98 (C6, $^2J_{119/117Sn-13C}$ = 31.8 Hz), 131.01 (C5), 128.51 (C4, $^4J_{119/117Sn-13C}$ = 86.6 Hz), 127.55 (C3, $^3J_{119/117Sn-13C}$ = 72.4 Hz), 63.22 (C7, $^3J_{119/117Sn-13C}$ = 34.0 Hz), 45.06 (C8), 27.43 (C9, $^1J_{119/117Sn-13C}$ = 21.5 Hz), 27.00 (C10), 26.24 (C11), 13.75 (C12) ppm; **^{119}Sn NMR** (149 MHz, CDCl$_3$, δ): -107.99 ppm.

5.5 Synthesis of [2-(CH₂N(CH₃)₂)C₆H₄]Ph₃Sn (41):
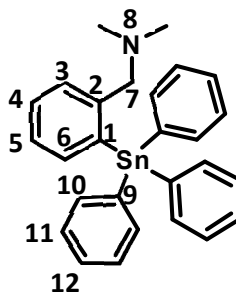
To a Schlenk flask, 0.51g (2.38mmol) of (2-bromobenzyl) dimethylamine and 15 mL of dry Et_2O was added. The Schlenk flask was cooled to -84 °C using an EtOAc/Liq. N_2 bath and was maintained at that temperature for at least 5 min. To that Schlenk flask, a solution of 1.6 M *n*-BuLi in hexanes (1.79 mL, 2.86 mmol) was added slowly, dropwise, using a syringe. The temperature was maintained at -84 °C for 1 hr before warming up to 0 °C using an ice bath and left for 1 hr. In another Schlenk flask, 0.92 g (2.38 mmol) *n*-butyltintrichloride and 20 mL of dry Et_2O was added and cooled to 0 °C. The lithiated ligand was then transferred to the tin solution via cannula and the solution stirred for 2 hr at 0 °C. The product was extracted with distilled H_2O. The organic layer was dried over $MgSO_4$, filtered, and solvents removed under reduced pressure to yield 0.66g (57.2%) of a white solid.

¹H NMR (400 MHz, CDCl₃, δ): 7.73-7.68 (m, 6H, H10), 7.65 (m, 1H, H6), 7.37 (m, 10H, H4, H11), 7.28 (m, 1H, H5), 7.23 (m, 1H, H3) ppm; **¹³C NMR** (100 MHz, CDCl₃, δ): 146.27 (C1), 142.02 (C9), 139.10 (C6), 138.45 (C2), 136.80 (C10), 128.98 (C4), 128.86.48 (C12), 128.67 (C3), 128.17 (C11), 127.02 (C5), 64.87 (C7), 45.81 (C8) ppm; **¹¹⁹Sn NMR** (149 MHz, CDCl₃, δ): -163.38 ppm.

5.6 Synthesis of [2-(CH₂N(CH₃)₂)C₆H₄]Ph₂SnCl (42):
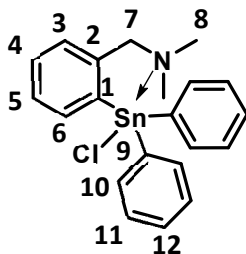
To a Schlenk flask, 0.10g (0.21mmol) of **41** and 10 mL of dry C_6D_6 were added. To that same flask, a dry solution of 1.0 M HCl in Et_2O (0.2 mL, 0.21 mmol) was added quickly and allowed to stir for 1 hr at room temperature. The solvent was removed under reduced pressure. The product was precipitated from 10 mL of hexane to yield 0.08g (97.6%) of a white crystalline solid.

¹H NMR (400 MHz, CDCl₃, δ): 8.55 (dt, $^4J_{1H-1H}$ = 6.7 Hz, $^3J_{1H-1H}$ = 35.1 Hz, 1H, H6), 7.76 (dt, $^4J_{1H-1H}$ = 5.6 Hz, $^3J_{1H-1H}$ = 31.5 Hz, 2H, H10), 7.53 (m, 1H, H5), 7.44 (m, 6H, H4, H11, H12), 7.23 (m, 1H, H3), 3.59 (s, 2H, H7), 1.93 (s, 6H, H8) ppm; **¹³C NMR** (100 MHz, CDCl₃, δ): 142.75 (C1), 141.49 (C9), 138.83 (C6), 137.48 (C2), 135.62 (C10, $^2J_{119/117Sn-13C}$ = 45.7 Hz), 130.12 (C4), 129.48 (C12), 128.92 (C11, $^3J_{119/117Sn-13C}$ = 68.6 Hz), 128.32 (C5), 127.21 (C3), 64.87 (C7), 45.81 (C8) ppm; **¹¹⁹Sn NMR** (149 MHz, CDCl₃, δ): -176.50 ppm.

5.7 Synthesis of [2-(CH₂N(CH₂)₂)C₆H₄]Ph₂SnBr (44) & [2-(CH₂N(CH₂)₂)C₆H₄]SnBr₃ (45):
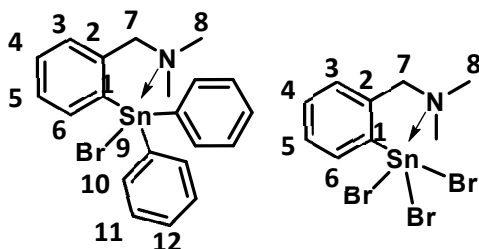
To a Schlenk flask covered in Al foil, 0.10 g (0.21 mmol) of **41** and 10 mL of dry C_6H_6 were added. To that same flask, Br_2 (0.2 mL, 0.21 mmol) was added and allowed to stir for 1 hr at room temperature. The solvent was removed under reduced pressure. The monobromide product (**44**) was precipitated from MeOH, decanted and solvents removed under reduced pressure to yield 0.055g (55.0%) of a white powder. The decanted MeOH was put under reduced pressure to remove solvents and yielded 0.038g (38.0%) of a white powder of **45**. The NMR data for these two compounds agreed with previously reported data.[20,21]

[2-(CH₂N(CH₃)₂)C₆H₄]Ph₂SnBr (44): **¹H NMR** (400 MHz, CDCl₃, δ): 8.60 (dt, $^4J_{1H-1H}$ = 6.1 Hz, $^3J_{1H-1H}$ = 35.8 Hz, 1H, H6), 7.75 (dt, $^4J_{1H-1H}$ = 7.1 Hz, $^3J_{1H-1H}$ = 31.5 Hz, 2H, H10), 7.53 (m, 1H, H5), 7.44 (m, 6H, H4, H11, H12), 7.28 (m, 1H, H3), 3.59 (s, 2H, H7), 1.91 (s, 6H, H8) ppm; **¹³C NMR** (100MHz, CDCl₃, δ): 142.57 (C1), 141.82 (C9), 139.54 (C6), 136.77 (C2), 135.47(C10, $^2J_{119/117Sn-13C}$ = 45.6 Hz), 130.16 (C4), 129.54 (C12), 128.92 (C11, $^3J_{119/117Sn-13C}$ = 68.3 Hz), 128.35 (C5), 127.19 (C3), 66.81 (C7), 45.83 (C8) ppm; **¹¹⁹Sn NMR** (149 MHz, CDCl₃, δ): -180.78 ppm.

[2-(CH₂N(CH₃)₂)C₆H₄]SnBr₃ (45): **¹H NMR** (400 MHz, CDCl₃, δ): 8.04 (d, $^3J_{1H-1H}$ = 7.6 Hz, 1H, H6), 7.58 (d, $^3J_{1H-1H}$ = 7.5 Hz, 1H, H3), 7.39 (t, $^3J_{1H-1H}$ = 7.0 Hz, 1H, H4), 7.25 (t, $^3J_{1H-1H}$ = 7.4 Hz, 1H, H5), 4.39 (s, 2H, H7), 2.79 (s, 6H, H8) ppm; **¹³C NMR** (100MHz, CDCl₃, δ): 133.62 (C6), 133.42 (C3), 131.68 (C4), 129.13 (C1), 128.76 (C5), 125.70 (C2), 59.44 (C7), 42.51 (C8) ppm; **¹¹⁹Sn NMR** (149MHz, CDCl₃, δ): -207.64 ppm.

5.8 Synthesis of [2-(MeOCH₂)C₆H₄]*n*-BuSnH₂ (51):
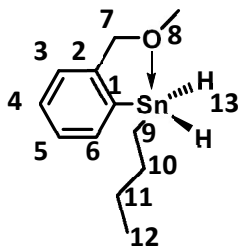
To a Schlenk flask, 0.50g (1.36 mmol) of **31** and 15 mL of dry Et₂O was added. In another Schlenk flask, an excess of NaBH₄ (0.51 g, 13.6 mmol) and 10 mL of dry Et₂O was added. Both flasks were chilled to 0 °C using an ice bath and the temperature was maintained for at least 10 min. Using a cannula, the hydride source was added to the tin solution and kept at 0 °C for 1 hr. Prior to the end of the 1 hr, distilled water was degassed and chilled for at least 30 min. The degassed water was added slowly to the tin hydride solution due to evolution of H₂ gas and the product was extracted (2 × 25mL). The organic layer was dried over MgSO₄ and filtered. Solvent was removed under reduced pressure to yield 0.34g (83.7 %) of a yellow liquid.

¹H NMR (400 MHz, CDCl₃, δ): 7.68 (m, 1H, H6), 7.10 (m, 2H, H4-H5), 6.96 (m, 1H, H3), 5.67 (s, $^1J_{119Sn-1H}$ = 1764.0 Hz, $^1J_{117Sn-1H}$ = 1685.6 Hz, 2H, H13), 4.15 (s, $^4J_{119/117Sn-1H}$ = 141.0 Hz, 2H, H7), 3.01 (s, $^3J_{119/117Sn-1H}$ = 141.2 Hz, 6H, H8), 1.58 (dt, $^3J_{1H-1H}$ = 2.0, 7.9 Hz, 2H, H10), 1.33 (sext, $^3J_{1H-1H}$ = 7.5, 2H, H11), 1.18 (tt, $^3J_{1H-1H}$ = 1.7, 8.1 Hz, 2H, H9), 0.84 (t, $^3J_{1H-1H}$ = 7.3 Hz, 3H, H12) ppm; **¹³C NMR** (100 MHz, CDCl₃, δ): 144.85 (C1), 138.89 (C6), 136.83 (C2), 128.33 (C4), 127.34 (C5), 127.00 (C3), 75.68 (C7), 56.69 (C8), 30.17 (C10), 26.75 (C11), 13.49 (C9), 9.84 (C12) ppm; **¹¹⁹Sn NMR** (149MHz, CDCl₃, δ): -210.10 ppm.

5.9 Synthesis of [2-(CH$_2$N(CH$_3$)$_2$)C$_6$H$_4$]n-BuSnH$_2$ (52):
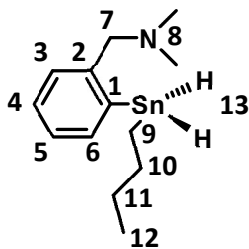
To a Schlenk flask, 0.41 g (1.08 mmol) of **34** and 15 mL of dry Et$_2$O was added. In another

Schlenk flask, an equivalent amount of 1.0 M LiAlH$_4$ (1.08 mL, 1.08 mol) and 10 mL of dry Et$_2$O

was added. Both flasks were chilled to 0 °C using an ice bath and the temperature was maintained

for at least 10 min. Using a cannula, the hydride source was added to the tin solution and kept at 0

°C for 3 hr. Prior to the end of the 3 hr, distilled water was degassed and chilled for at least 30 min.

The degassed water was added slowly to the tin hydride solution due to evolution of H$_2$ gas and

the product was extracted (2 × 25 mL). The organic layer was dried over MgSO$_4$ and filtered.

Solvent was removed under reduced pressure to yield 0.25 g (60.9 %) of a whitish or yellow semi-

solid liquid.

^{1}H NMR (400 MHz, CDCl$_3$, δ): 7.73 (m, 1H, H6), 7.11 (m, 2H, H4-H5), 6.93 (m, 1H, H3), 5.66

(s, 1H, H13), 3.13 (s, 2H, H7), 1.89 (s, 6H, H8), 1.65 (m, 2H, H9), 1.37 (m, 2H, H10), 1.09 (m,

2H, H11), 0.89 (m, 3H, H12) ppm; **^{13}C NMR** (100MHz, CDCl$_3$, δ): 144.96 (C6), 138.73 (C3),

65.05 (C7), 43.62 (C8), 30.48 (C9), 26.81 (C10), 13.57 (C11), 9.97 (C12) ppm; **^{119}Sn NMR** (149

MHz, CDCl$_3$, δ): -217.55 ppm.

5.10 Preparation of ([2-(MeOCH$_2$)C$_6$H$_4$]n-BuSn)$_n$ Polymer (56):
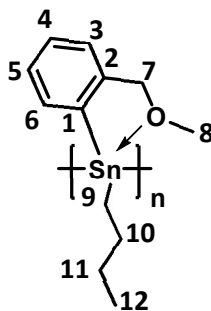
A solution containing RhCl(PPh$_3$)$_3$ (0.1620 g, 0.1751 mmol) in toluene (10 mL) was added to an Al foil-wrapped 50 mL Schlenk flask and stirred at RT for 20 min. Thereafter, **51** in 10 mL of toluene (1.310 g, 4.377 mmol) was added dropwise over 20 min to the catalyst solution. The reaction was allowed to stir at RT for 4 h. The toluene mixture was brought to dryness *in vacuo*. The crude solid was re-dissolved in 5 mL of THF and then added dropwise to a 100 mL foil-wrapped Schlenk flask containing a stirring solution of cold hexane (60 mL) for precipitation. A bright yellow precipitate formed immediately, and the mixture was stirred for additional 5 min and then allowed to settle. The top layer of the solution was then decanted. The residues were dried *in vacuo* to obtain a bright yellow solid. Yield 65.0% (0.842 g); M$_w$ = 30,300 Da, PDI = 1.32.

^{1}H NMR (400 MHz, C$_6$D$_6$, δ): 7.73-7.69 (bm, 2H, H4), 7.03–7.00 (bm, 2H, H5), 4.78–4.28 (bm, 2H, H2), 3.32-2.95 (bm, 3H, H1), 2.10– 1.45 (bm, 9H, H7-H10) ppm; **^{13}C{^{1}H} NMR** (100 MHz, C$_6$D$_6$, δ): 132.20 (C6), 131.35 (C3), 128.30-125.00 (C4 & C5), 76.79 (C2), 57.66 (C1), 29.26-26.76 (C7-C9), 13.75 (C10) ppm; **^{119}Sn{^{1}H} NMR** (149 MHz, C$_6$D$_6$, δ): -42, -199 ppm; Elemental analysis calcd (%): C 48.53, H 6.11; found: C 43.7, H 5.8.

5.11 Preparation of ([2-(Me₂NCH₂)C₆H₄]*n*-BuSn)ₙ Polymer (57):
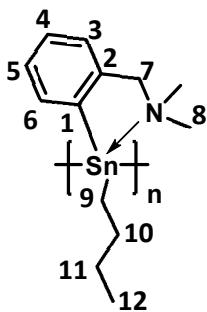
A solution containing RhCl(PPh₃)₃ (60.0 mg, 0.06409 mmol) in toluene (8 mL) was added to an Al foil-wrapped 50 mL Schlenk flask and stirred at RT for 20 min. Thereafter, **52** in 8 mL of toluene (0.500 g, 1.602 mmol) was added dropwise over 20 min to the catalyst solution. The reaction was allowed to stir at RT for 4 h. The mixture was then brought to dryness in *vacuo*. The crude product was re-dissolved in 5 mL of THF and added dropwise to a 100 mL foil-wrapped Schlenk flask containing a stirring solution of cold hexane (50 mL) for precipitation. A bright yellow precipitate formed immediately, and the mixture was stirred for additional 5 min and then allowed to settle. The top layer of the solution was then decanted. The residues were dried in vacuo to obtain a bright yellow solid. Yield 17.3% (0.0866 g); M_w = 21,800 Da, PDI = 1.41

5.12 Synthesis of $(CH_3)_2Sn(NEt_2)_2$ (58):
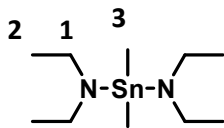
To a Schlenk flask, 0.94 mL (9.1 mmol) of $HNEt_2$ and 15 mL of dry Et_2O was added. A solution of 1.6 M n-BuLi in hexanes (5.69 mL, 9.1 mmol) was then added very slowly dropwise. The solution was stirred at 0 °C for 2 hr. In another Schlenk flask, 1.00 g (4.55 mmol) of Me_2SnCl_2 and 20 mL of dry Et_2O was added and chilled to 0 °C. The lithiated amine solution was transferred to the etheral solution containing the Me_2SnCl_2 via cannula and the solution stirred for 12 hr. The solution was filtered through a Schlenk filter funnel to remove LiCl and the solvent was removed under reduced pressure. A translucent yellow coloured liquid 1.44g (86.5 %) was recovered. The NMR data for this compound agreed with previously reported data.[15]

^{1}H NMR (400 MHz, $CDCl_3$, δ): 3.00 (q, $^3J_{1H-1H}$ = 7.0 Hz, $^3J_{117Sn-1H}$ = 37.7 Hz, $^3J_{119Sn-1H}$ = 51.7 Hz, 8H, H1), 1.066 (t, $^3J_{1H-1H}$ = 7.0 Hz, 12H, H2), 0.190 (s, $^1J_{119/117Sn-1H}$ = 58.5 Hz, 6H, H3)ppm; **^{13}C NMR** (100 MHz, $CDCl_3$, δ): 45.25 (C1), 17.10 (C2), -6.28 (C3, $J_{119Sn-13C}$ = 448.1 Hz, $J_{117Sn-13C}$ = 469.0 Hz) ppm; **^{119}Sn NMR** (149 MHz, $CDCl_3$, δ): 43.22 ppm.

5.13 Synthesis of (*n*-Bu)₂Sn(NEt₂)₂ (59):
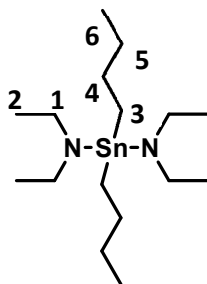
To a Schlenk flask, 0.34 mL (6.58 mmol) of HNEt₂ and 15 mL of dry Et₂O was added. A solution of 1.6 M *n*-BuLi in hexanes (4.11 mL, 6.58 mmol) was then added slowly, dropwise. The solution stirred at 0 °C for 2 hr. In another Schlenk flask, 1.00 g (3.29 mmol) of (*n*-Bu)₂SnCl₂ and 20 mL of dry Et₂O was added and chilled to 0°C. The lithiated amine solution was transferred to the (*n*-Bu)₂SnCl₂ solution via cannula and the solution was stirred for 12 hr. The solution was filtered through a Schlenk filter funnel to remove LiCl and the solvent was removed under reduced pressure to yield 1.44g (92.8%) of a translucent liquid with a clear, pale yellow, or brownish colouration. The NMR data for this compound agreed with previously reported data.[15]

¹H NMR (400 MHz, CDCl₃, δ): 3.05 (q, $^3J_{1H-1H}$ = 6.9 Hz, $^3J_{117Sn-1H}$ = 32.5 Hz, $^3J_{119Sn-1H}$ = 46.7 Hz, 8H, H1), 1.59 (m, 4H, H3), 1.34 (q, $^3J_{1H-1H}$ = 7.3 Hz, 4H, H4), 1.10 (t, $^3J_{1H-1H}$ = 7.0 Hz, 12H, H2), 1.03 (t, $^3J_{1H-1H}$ = 8.3 Hz, 4H, H5), 0.89 (t, $^3J_{1H-1H}$ = 7.3 Hz, 6H, H6) ppm; **¹³C NMR** (100MHz, CDCl₃, δ): 45.26 (C1, $^2J_{119Sn-13C}$ = 8.9 Hz), 28.13 (C3, $^1J_{119Sn-13C}$ = 19.3 Hz), 27.13 (C4, $^2J_{119Sn-13C}$ = 71.0 Hz) 17.08 (C2, $^3J_{119Sn-13C}$ = 12.7 Hz), 13.97 (C5), 13.43 (C6) ppm; **¹¹⁹Sn NMR** (149MHz, CDCl₃, δ): 19.51 ppm.

5.14 Synthesis of Poly([2-(MeOCH$_2$)C$_6$H$_4$]n-Bu]-alt-(CH$_3$)$_2$)Sn (60):
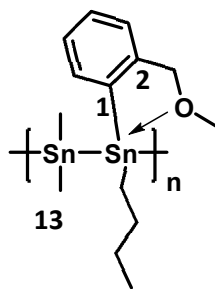
To a Schlenk flask, 0.31g (1.03 mmol) of **51** and 5 mL of dry Et$_2$O was added. In another Schlenk flask covered fully with Al foil, 0.41 g (1.03 mmol) of **58** and 10 mL of dry Et$_2$O was added. Both flasks were cooled to 0 °C and maintained at that temperature for at least 10 min. The hydride solution was transferred over to the amine solution via cannula and the solution was stirred at 0 °C for 3 hr. The solvent was removed at reduced pressure and yielded a bright yellow solid. The polymer was then dissolved in 5 mL of dry THF and added dropwise to a Schlenk flask stirring 50mL cold hexanes. The solution was decanted and re-purified once more. The remaining precipitate was dried with reduced pressure to yield 0.09 g (21%) of a pale-yellow powder.

^{1}H NMR (400 MHz, CDCl$_3$, δ): 7.56-6.58 (m, 4H, H3-H6), 4.58-3.51 (m, 2H, H7), 3.35-2.30 (m, 3H, H8), 2.08-1.14 (m, 6H, H6-12), 0.18 (m, 6H, H13) ppm; **^{13}C NMR** (100MHz, CDCl$_3$, δ): 67.44 (C1), 139.49 (C2), 136.98 (C6), 131.01 (C5), 128.51 (C4), 127.55 (C3), 63.22 (C7), 31.59 (C9), 29.84 (C10), 25.44 (C8), 22.68 (C11), 15.21 (C13), 13.97 (C12) ppm; **^{119}Sn NMR** (149MHz, CDCl$_3$, δ): -207.03, -57.56 ppm.

5.15 Attempted Synthesis of Poly([2-(MeOCH₂)C₆H₄]*n*-Bu]-alt-(*n*-Bu)₂)Sn (61):
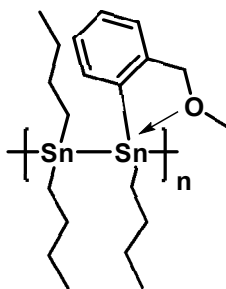
To a Schlenk flask, 0.112 g (0.374 mmol) of **51** and 5 mL of dry Et₂O was added. In another Schlenk flask covered fully with Al foil, 0.147g (0.374mmol) of **59** and 10 mL of dry Et₂O was added. Both flasks were cooled to 0 °C and maintained at that temperature for at least 10 min. The hydride solution was transferred over to the amine solution via cannula and the solution was stirred at 0 °C for 3 hr. The solvent was removed at reduced pressure and yielded a yellow gel. The polymer was then dissolved in 5 mL of dry THF and added dropwise to a Schlenk flask stirring 50 mL cold hexanes. The solution was decanted and the remaining precipitate was dried with reduced pressure. Purification was done twice, yielding 0.108 g (72%) of a pale yellow powder.

¹H NMR (400 MHz, CDCl₃, δ): 7.32-6.91 (m, 4H, H3-H6), 4.69-3.65 (m, 2H, H7), 3.39-2.49 (m, 3H, H8), 1.88-0.73(m, 29H, H9-16) ppm; **¹¹⁹Sn NMR** (149MHz, CDCl₃, δ): -171.36, -202.19 ppm.

Appendix
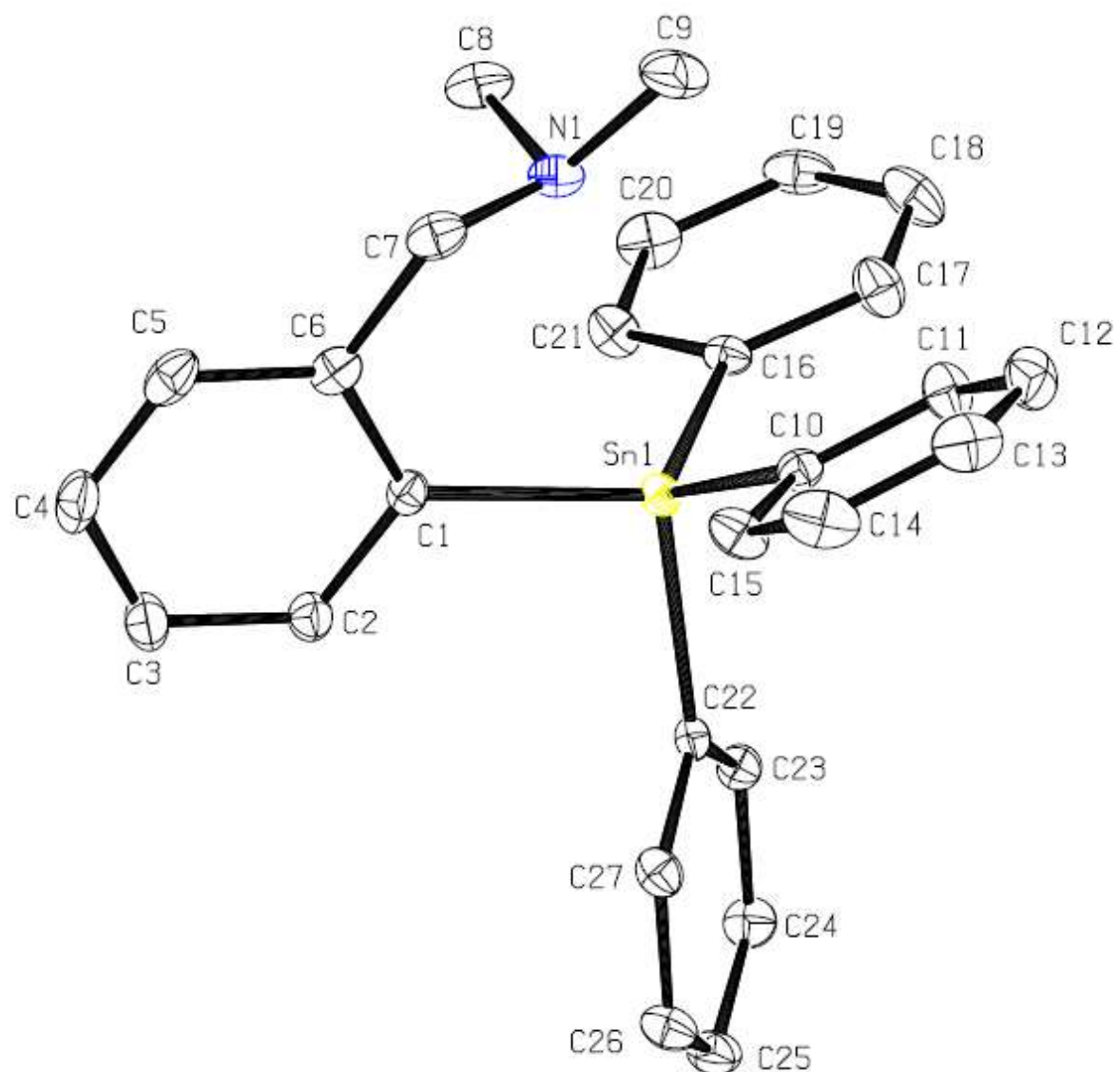
Table A 1: Crystal data and structure refinement for d1822_a.

Identification code	d1822_a
Empirical formula	C27 H27 N Sn
Formula weight	484.18
Temperature	150(2) K
Wavelength	0.71073 Å
Crystal system	Monoclinic
Space group	$P2_1/n$
Unit cell dimensions	a = 13.8303(8) Å $\quad$ $\square$ = 90°.
	b = 12.5018(7) Å $\quad$ $\square$ = 114.324(2)°.
	c = 14.2180(9) Å $\quad$ $\square$ = 90°.
Volume	2240.1(2) Å^3
Z	4
Density (calculated)	1.436 Mg/m^3
Absorption coefficient	1.153 mm^{-1}
F(000)	984
Crystal size	0.180 x 0.170 x 0.150 mm^3
Theta range for data collection	1.729 to 27.530°.
Index ranges	-17<=h<=17, -16<=k<=16, -18<=l<=18
Reflections collected	49939
Independent reflections	5165 [R(int) = 0.0350]
Completeness to theta = 25.242°	100.0 %
Absorption correction	Semi-empirical from equivalents
Max. and min. transmission	0.7456 and 0.7144
Refinement method	Full-matrix least-squares on F^2
Data / restraints / parameters	5165 / 0 / 264
Goodness-of-fit on F^2	1.063
Final R indices [I>2sigma(I)]	R1 = 0.0203, wR2 = 0.0408
R indices (all data)	R1 = 0.0336, wR2 = 0.0462
Extinction coefficient	n/a
Largest diff. peak and hole	0.754 and -0.395 e.Å^{-3}

Table A 2: Atomic coordinates (x 10^4) and equivalent isotropic displacement parameters (Å^{2}x 10^3) for d1822_a. U(eq) is defined as one third of the trace of the orthogonalized U^{ij} tensor.

	x	y	z	U(eq)
Sn(1)	3704(1)	3795(1)	6427(1)	20(1)
N(1)	4713(1)	1756(1)	7273(1)	28(1)
C(1)	4010(1)	2886(1)	5293(2)	22(1)
C(2)	3473(2)	3150(2)	4250(2)	27(1)
C(3)	3640(2)	2594(2)	3487(2)	36(1)
C(4)	4354(2)	1759(2)	3755(2)	38(1)
C(5)	4891(2)	1482(2)	4782(2)	35(1)
C(6)	4731(2)	2031(2)	5559(2)	27(1)
C(7)	5360(2)	1731(2)	6680(2)	33(1)
C(8)	3959(2)	866(2)	6982(2)	38(1)
C(9)	5382(2)	1707(2)	8378(2)	45(1)
C(10)	5162(1)	4357(1)	7608(2)	23(1)
C(11)	5340(2)	4492(2)	8638(2)	33(1)
C(12)	6307(2)	4850(2)	9367(2)	41(1)
C(13)	7121(2)	5079(2)	9079(2)	44(1)
C(14)	6968(2)	4946(2)	8070(2)	46(1)
C(15)	5996(2)	4597(2)	7340(2)	34(1)
C(16)	2551(1)	3113(2)	6885(1)	22(1)
C(17)	2518(2)	3288(2)	7837(2)	35(1)
C(18)	1747(2)	2810(2)	8087(2)	42(1)
C(19)	999(2)	2152(2)	7395(2)	37(1)
C(20)	1003(2)	1982(2)	6440(2)	38(1)
C(21)	1773(2)	2458(2)	6190(2)	31(1)
C(22)	2873(1)	5170(1)	5532(1)	20(1)
C(23)	1820(2)	5367(2)	5358(2)	24(1)
C(24)	1245(2)	6199(2)	4727(2)	29(1)
C(25)	1715(2)	6856(2)	4255(2)	31(1)
C(26)	2764(2)	6686(2)	4422(2)	32(1)
C(27)	3336(2)	5855(2)	5057(2)	26(1)

Table A 3: Bond lengths [Å] and angles [°] for d1822_a.

_____

Sn(1)-C(16)	2.1331(18)
Sn(1)-C(10)	2.1422(18)
Sn(1)-C(1)	2.1523(18)
Sn(1)-C(22)	2.1661(18)
N(1)-C(9)	1.459(3)
N(1)-C(7)	1.461(3)
N(1)-C(8)	1.463(3)
C(1)-C(2)	1.397(3)
C(1)-C(6)	1.403(3)
C(2)-C(3)	1.386(3)
C(2)-H(2A)	0.9500
C(3)-C(4)	1.379(3)
C(3)-H(3A)	0.9500
C(4)-C(5)	1.382(3)
C(4)-H(4A)	0.9500
C(5)-C(6)	1.394(3)
C(5)-H(5A)	0.9500
C(6)-C(7)	1.515(3)
C(7)-H(7A)	0.9900
C(7)-H(7B)	0.9900
C(8)-H(8A)	0.9800
C(8)-H(8B)	0.9800
C(8)-H(8C)	0.9800
C(9)-H(9A)	0.9800
C(9)-H(9B)	0.9800
C(9)-H(9C)	0.9800
C(10)-C(15)	1.387(3)
C(10)-C(11)	1.391(3)
C(11)-C(12)	1.387(3)
C(11)-H(11A)	0.9500
C(12)-C(13)	1.377(3)
C(12)-H(12A)	0.9500
C(13)-C(14)	1.371(4)

C(13)-H(13A)	0.9500
C(14)-C(15)	1.388(3)
C(14)-H(14A)	0.9500
C(15)-H(15A)	0.9500
C(16)-C(21)	1.388(3)
C(16)-C(17)	1.391(3)
C(17)-C(18)	1.389(3)
C(17)-H(17A)	0.9500
C(18)-C(19)	1.369(3)
C(18)-H(18A)	0.9500
C(19)-C(20)	1.377(3)
C(19)-H(19A)	0.9500
C(20)-C(21)	1.388(3)
C(20)-H(20A)	0.9500
C(21)-H(21A)	0.9500
C(22)-C(23)	1.395(3)
C(22)-C(27)	1.399(3)
C(23)-C(24)	1.390(3)
C(23)-H(23A)	0.9500
C(24)-C(25)	1.381(3)
C(24)-H(24A)	0.9500
C(25)-C(26)	1.386(3)
C(25)-H(25A)	0.9500
C(26)-C(27)	1.391(3)
C(26)-H(26A)	0.9500
C(27)-H(27B)	0.9500
C(16)-Sn(1)-C(10)	118.23(7)
C(16)-Sn(1)-C(1)	114.83(7)
C(10)-Sn(1)-C(1)	110.39(7)
C(16)-Sn(1)-C(22)	102.35(7)
C(10)-Sn(1)-C(22)	107.49(7)
C(1)-Sn(1)-C(22)	101.49(7)
C(9)-N(1)-C(7)	110.66(17)
C(9)-N(1)-C(8)	109.56(17)
C(7)-N(1)-C(8)	110.79(17)

C(2)-C(1)-C(6)	118.27(17)
C(2)-C(1)-Sn(1)	119.21(13)
C(6)-C(1)-Sn(1)	122.52(14)
C(3)-C(2)-C(1)	121.69(19)
C(3)-C(2)-H(2A)	119.2
C(1)-C(2)-H(2A)	119.2
C(4)-C(3)-C(2)	119.7(2)
C(4)-C(3)-H(3A)	120.2
C(2)-C(3)-H(3A)	120.2
C(3)-C(4)-C(5)	119.6(2)
C(3)-C(4)-H(4A)	120.2
C(5)-C(4)-H(4A)	120.2
C(4)-C(5)-C(6)	121.50(19)
C(4)-C(5)-H(5A)	119.3
C(6)-C(5)-H(5A)	119.3
C(5)-C(6)-C(1)	119.30(19)
C(5)-C(6)-C(7)	120.11(18)
C(1)-C(6)-C(7)	120.55(18)
N(1)-C(7)-C(6)	112.30(16)
N(1)-C(7)-H(7A)	109.1
C(6)-C(7)-H(7A)	109.1
N(1)-C(7)-H(7B)	109.1
C(6)-C(7)-H(7B)	109.1
H(7A)-C(7)-H(7B)	107.9
N(1)-C(8)-H(8A)	109.5
N(1)-C(8)-H(8B)	109.5
H(8A)-C(8)-H(8B)	109.5
N(1)-C(8)-H(8C)	109.5
H(8A)-C(8)-H(8C)	109.5
H(8B)-C(8)-H(8C)	109.5
N(1)-C(9)-H(9A)	109.5
N(1)-C(9)-H(9B)	109.5
H(9A)-C(9)-H(9B)	109.5
N(1)-C(9)-H(9C)	109.5
H(9A)-C(9)-H(9C)	109.5
H(9B)-C(9)-H(9C)	109.5

C(15)-C(10)-C(11)	117.14(18)
C(15)-C(10)-Sn(1)	118.42(15)
C(11)-C(10)-Sn(1)	124.44(14)
C(12)-C(11)-C(10)	121.6(2)
C(12)-C(11)-H(11A)	119.2
C(10)-C(11)-H(11A)	119.2
C(13)-C(12)-C(11)	120.0(2)
C(13)-C(12)-H(12A)	120.0
C(11)-C(12)-H(12A)	120.0
C(14)-C(13)-C(12)	119.6(2)
C(14)-C(13)-H(13A)	120.2
C(12)-C(13)-H(13A)	120.2
C(13)-C(14)-C(15)	120.3(2)
C(13)-C(14)-H(14A)	119.9
C(15)-C(14)-H(14A)	119.9
C(10)-C(15)-C(14)	121.5(2)
C(10)-C(15)-H(15A)	119.3
C(14)-C(15)-H(15A)	119.3
C(21)-C(16)-C(17)	117.29(18)
C(21)-C(16)-Sn(1)	118.47(14)
C(17)-C(16)-Sn(1)	124.23(15)
C(18)-C(17)-C(16)	121.1(2)
C(18)-C(17)-H(17A)	119.4
C(16)-C(17)-H(17A)	119.4
C(19)-C(18)-C(17)	120.5(2)
C(19)-C(18)-H(18A)	119.7
C(17)-C(18)-H(18A)	119.7
C(18)-C(19)-C(20)	119.5(2)
C(18)-C(19)-H(19A)	120.3
C(20)-C(19)-H(19A)	120.3
C(19)-C(20)-C(21)	120.1(2)
C(19)-C(20)-H(20A)	120.0
C(21)-C(20)-H(20A)	120.0
C(16)-C(21)-C(20)	121.5(2)
C(16)-C(21)-H(21A)	119.2
C(20)-C(21)-H(21A)	119.2

C(23)-C(22)-C(27)	117.28(17)
C(23)-C(22)-Sn(1)	120.48(13)
C(27)-C(22)-Sn(1)	122.13(13)
C(24)-C(23)-C(22)	121.65(18)
C(24)-C(23)-H(23A)	119.2
C(22)-C(23)-H(23A)	119.2
C(25)-C(24)-C(23)	120.01(18)
C(25)-C(24)-H(24A)	120.0
C(23)-C(24)-H(24A)	120.0
C(24)-C(25)-C(26)	119.66(19)
C(24)-C(25)-H(25A)	120.2
C(26)-C(25)-H(25A)	120.2
C(25)-C(26)-C(27)	120.05(19)
C(25)-C(26)-H(26A)	120.0
C(27)-C(26)-H(26A)	120.0
C(26)-C(27)-C(22)	121.35(18)
C(26)-C(27)-H(27B)	119.3
C(22)-C(27)-H(27B)	119.3

Symmetry transformations used to generate equivalent atoms:

Table A 4: Anisotropic displacement parameters $(\text{Å}^2\text{x } 10^3)$ for d1822_a. The anisotropic displacement factor exponent takes the form: $-2\square^2[\, h^2\, a^{*2}U^{11} + ... + 2\, h\, k\, a^*\, b^*\, U^{12}\,]$

	U^{11}	U^{22}	U^{33}	U^{23}	U^{13}	U^{12}
Sn(1)	18(1)	23(1)	19(1)	0(1)	8(1)	1(1)
N(1)	25(1)	27(1)	31(1)	8(1)	9(1)	2(1)
C(1)	22(1)	21(1)	26(1)	-2(1)	14(1)	-2(1)
C(2)	30(1)	27(1)	27(1)	-2(1)	14(1)	0(1)
C(3)	47(1)	37(1)	29(1)	-8(1)	20(1)	-5(1)
C(4)	49(1)	33(1)	44(1)	-13(1)	32(1)	-6(1)
C(5)	33(1)	25(1)	56(2)	-4(1)	27(1)	2(1)
C(6)	23(1)	24(1)	38(1)	0(1)	16(1)	-1(1)
C(7)	25(1)	28(1)	45(1)	6(1)	14(1)	6(1)
C(8)	35(1)	29(1)	51(2)	11(1)	18(1)	0(1)
C(9)	45(1)	45(1)	35(1)	16(1)	6(1)	6(1)
C(10)	20(1)	21(1)	25(1)	2(1)	7(1)	2(1)
C(11)	26(1)	44(1)	28(1)	-3(1)	10(1)	1(1)
C(12)	38(1)	47(1)	28(1)	-6(1)	3(1)	1(1)
C(13)	28(1)	42(1)	44(2)	3(1)	-3(1)	-9(1)
C(14)	27(1)	55(2)	52(2)	12(1)	11(1)	-12(1)
C(15)	29(1)	44(1)	29(1)	7(1)	11(1)	-4(1)
C(16)	19(1)	24(1)	25(1)	7(1)	11(1)	4(1)
C(17)	32(1)	47(1)	30(1)	-3(1)	16(1)	-7(1)
C(18)	38(1)	63(2)	32(1)	9(1)	22(1)	0(1)
C(19)	26(1)	39(1)	48(1)	20(1)	19(1)	5(1)
C(20)	25(1)	38(1)	47(1)	2(1)	12(1)	-7(1)
C(21)	26(1)	38(1)	28(1)	1(1)	12(1)	-3(1)
C(22)	22(1)	23(1)	16(1)	-3(1)	7(1)	-1(1)
C(23)	25(1)	24(1)	26(1)	-1(1)	13(1)	-2(1)
C(24)	23(1)	32(1)	34(1)	2(1)	12(1)	4(1)
C(25)	32(1)	31(1)	28(1)	9(1)	11(1)	7(1)
C(26)	35(1)	36(1)	30(1)	9(1)	17(1)	0(1)
C(27)	23(1)	34(1)	25(1)	1(1)	12(1)	1(1)

Table A 5: Hydrogen coordinates (x 10^4) and isotropic displacement parameters ($Å^2$x 10^3) for d1822_a.

	x	y	z	U(eq)
H(2A)	2981	3726	4059	33
H(3A)	3264	2787	2783	43
H(4A)	4476	1376	3237	46
H(5A)	5380	904	4962	42
H(7A)	5655	1003	6716	39
H(7B)	5961	2233	6993	39
H(8A)	3527	904	7382	58
H(8B)	4348	187	7127	58
H(8C)	3498	911	6244	58
H(9A)	5902	2290	8568	68
H(9B)	5754	1019	8544	68
H(9C)	4940	1779	8764	68
H(11A)	4785	4336	8846	40
H(12A)	6409	4937	10065	49
H(13A)	7784	5327	9576	53
H(14A)	7530	5095	7869	55
H(15A)	5898	4520	6642	41
H(17A)	3031	3742	8326	42
H(18A)	1740	2940	8742	50
H(19A)	481	1817	7573	44
H(20A)	478	1538	5951	45
H(21A)	1767	2333	5529	37
H(23A)	1487	4921	5678	29
H(24A)	529	6316	4620	35
H(25A)	1322	7421	3818	37
H(26A)	3092	7139	4102	39
H(27B)	4056	5749	5170	32

Table A 6: Torsion angles [°] for d1822_a.

C(6)-C(1)-C(2)-C(3)	-0.3(3)
Sn(1)-C(1)-C(2)-C(3)	179.88(15)
C(1)-C(2)-C(3)-C(4)	-0.1(3)
C(2)-C(3)-C(4)-C(5)	0.4(3)
C(3)-C(4)-C(5)-C(6)	-0.3(3)
C(4)-C(5)-C(6)-C(1)	-0.1(3)
C(4)-C(5)-C(6)-C(7)	-177.92(19)
C(2)-C(1)-C(6)-C(5)	0.4(3)
Sn(1)-C(1)-C(6)-C(5)	-179.76(14)
C(2)-C(1)-C(6)-C(7)	178.17(17)
Sn(1)-C(1)-C(6)-C(7)	-2.0(2)
C(9)-N(1)-C(7)-C(6)	-166.95(18)
C(8)-N(1)-C(7)-C(6)	71.3(2)
C(5)-C(6)-C(7)-N(1)	-139.97(19)
C(1)-C(6)-C(7)-N(1)	42.3(3)
C(15)-C(10)-C(11)-C(12)	-0.1(3)
Sn(1)-C(10)-C(11)-C(12)	179.35(16)
C(10)-C(11)-C(12)-C(13)	-0.1(4)
C(11)-C(12)-C(13)-C(14)	-0.3(4)
C(12)-C(13)-C(14)-C(15)	0.8(4)
C(11)-C(10)-C(15)-C(14)	0.6(3)
Sn(1)-C(10)-C(15)-C(14)	-178.84(18)
C(13)-C(14)-C(15)-C(10)	-1.0(4)
C(21)-C(16)-C(17)-C(18)	1.1(3)
Sn(1)-C(16)-C(17)-C(18)	-179.48(17)
C(16)-C(17)-C(18)-C(19)	-0.1(4)
C(17)-C(18)-C(19)-C(20)	-1.1(3)
C(18)-C(19)-C(20)-C(21)	1.2(3)
C(17)-C(16)-C(21)-C(20)	-1.1(3)
Sn(1)-C(16)-C(21)-C(20)	179.51(16)
C(19)-C(20)-C(21)-C(16)	-0.1(3)
C(27)-C(22)-C(23)-C(24)	0.8(3)
Sn(1)-C(22)-C(23)-C(24)	-175.42(15)

C(22)-C(23)-C(24)-C(25)	0.0(3)
C(23)-C(24)-C(25)-C(26)	-0.6(3)
C(24)-C(25)-C(26)-C(27)	0.4(3)
C(25)-C(26)-C(27)-C(22)	0.5(3)
C(23)-C(22)-C(27)-C(26)	-1.1(3)
Sn(1)-C(22)-C(27)-C(26)	175.13(15)

Symmetry transformations used to generate equivalent atoms:
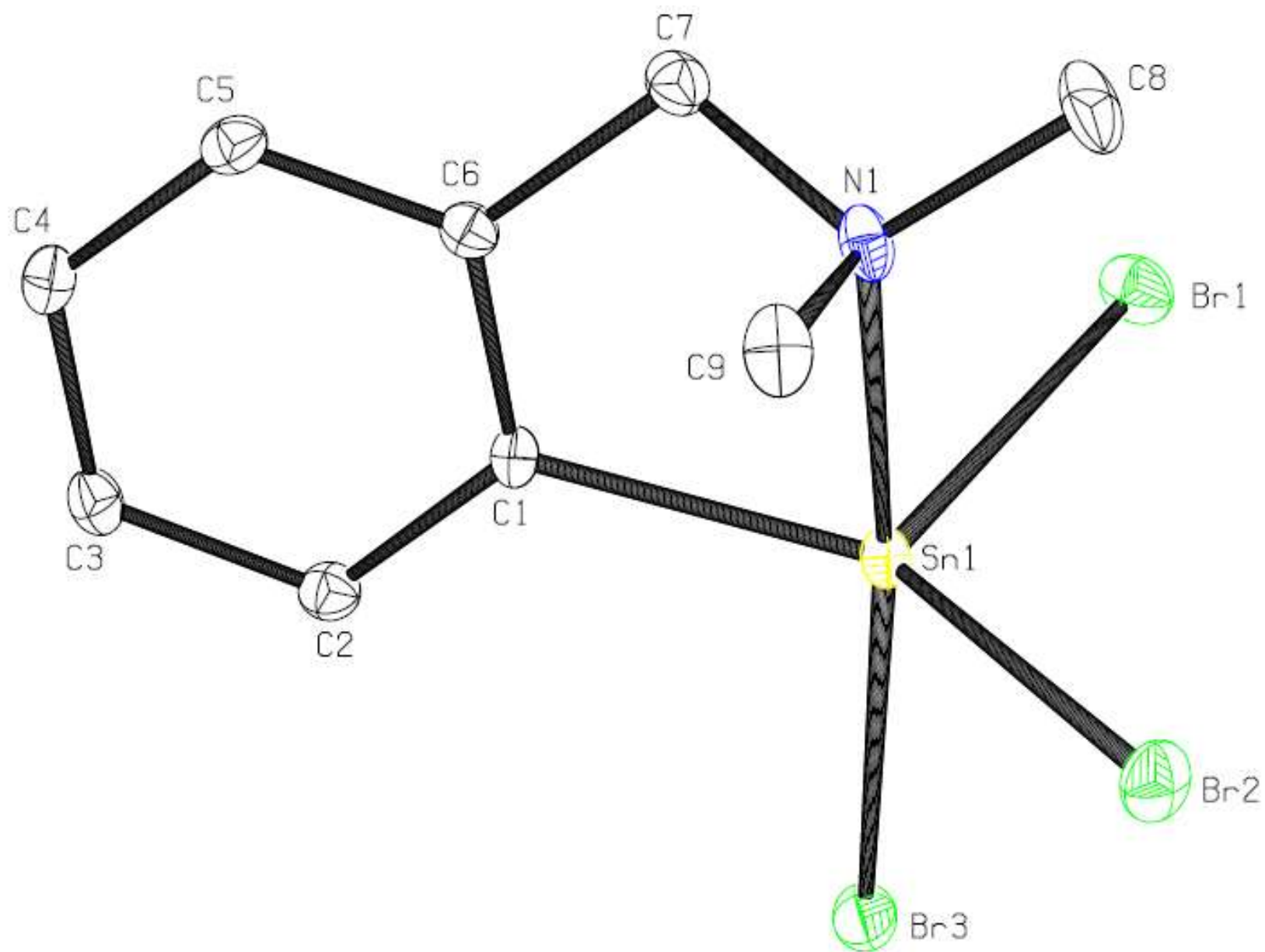
Table A 7: Crystal data and structure refinement for d1821_a.

Identification code	d1821_a
Empirical formula	C9 H12 Br3 N Sn
Formula weight	492.62
Temperature	150(2) K
Wavelength	0.71073 Å
Crystal system	Monoclinic
Space group	$P2_1/n$
Unit cell dimensions	a = 6.8067(3) Å $\quad\square= 90°$.
	b = 15.7680(9) Å $\quad\square= 102.371(2)°$.
	c = 12.6365(7) Å $\quad\square = 90°$.
Volume	1324.76(12) $Å^3$
Z	4
Density (calculated)	2.470 Mg/m^3
Absorption coefficient	10.943 mm^{-1}
F(000)	912
Crystal size	0.170 x 0.150 x 0.130 mm^3
Theta range for data collection	2.095 to 27.550°.
Index ranges	-8<=h<=8, -20<=k<=20, -16<=l<=16
Reflections collected	23815
Independent reflections	3057 [R(int) = 0.0350]
Completeness to theta = 25.242°	100.0 %
Absorption correction	Semi-empirical from equivalents
Max. and min. transmission	0.7456 and 0.5687
Refinement method	Full-matrix least-squares on F^2
Data / restraints / parameters	3057 / 0 / 129
Goodness-of-fit on F^2	1.030
Final R indices [I>2sigma(I)]	R1 = 0.0202, wR2 = 0.0362
R indices (all data)	R1 = 0.0312, wR2 = 0.0388
Extinction coefficient	n/a
Largest diff. peak and hole	0.672 and -0.503 $e.Å^{-3}$

Table A 8: Atomic coordinates (x 10^4) and equivalent isotropic displacement parameters ($Å^2$x 10^3) for d1821_a. U(eq) is defined as one third of the trace of the orthogonalized U^{ij} tensor.

	x	y	z	U(eq)
Sn(1)	5691(1)	2587(1)	2772(1)	17(1)
Br(1)	3533(1)	2156(1)	1012(1)	26(1)
Br(2)	9201(1)	2127(1)	2812(1)	30(1)
Br(3)	5022(1)	1280(1)	3870(1)	26(1)
N(1)	6465(4)	3882(2)	1948(2)	22(1)
C(1)	4314(4)	3530(2)	3574(2)	16(1)
C(2)	3655(4)	3409(2)	4529(2)	19(1)
C(3)	2722(4)	4072(2)	4951(2)	21(1)
C(4)	2449(4)	4843(2)	4420(2)	21(1)
C(5)	3095(4)	4962(2)	3464(2)	21(1)
C(6)	4012(4)	4305(2)	3023(2)	17(1)
C(7)	4649(4)	4399(2)	1954(2)	23(1)
C(8)	6865(6)	3827(2)	843(3)	35(1)
C(9)	8237(5)	4280(2)	2675(3)	30(1)

Table A 9: Bond lengths [Å] and angles [°] for d1821_a.

_____

Sn(1)-C(1)	2.127(3)
Sn(1)-N(1)	2.403(2)
Sn(1)-Br(1)	2.4829(4)
Sn(1)-Br(2)	2.4874(4)
Sn(1)-Br(3)	2.5772(4)
N(1)-C(7)	1.481(4)
N(1)-C(8)	1.481(4)
N(1)-C(9)	1.489(4)
C(1)-C(2)	1.388(4)
C(1)-C(6)	1.400(4)
C(2)-C(3)	1.387(4)
C(2)-H(2A)	0.9500
C(3)-C(4)	1.383(4)
C(3)-H(3A)	0.9500
C(4)-C(5)	1.384(4)
C(4)-H(4A)	0.9500
C(5)-C(6)	1.386(4)
C(5)-H(5A)	0.9500
C(6)-C(7)	1.512(4)
C(7)-H(7A)	0.9900
C(7)-H(7B)	0.9900
C(8)-H(8A)	0.9800
C(8)-H(8B)	0.9800
C(8)-H(8C)	0.9800
C(9)-H(9A)	0.9800
C(9)-H(9B)	0.9800
C(9)-H(9C)	0.9800
C(1)-Sn(1)-N(1)	76.81(9)
C(1)-Sn(1)-Br(1)	112.41(7)
N(1)-Sn(1)-Br(1)	89.22(6)
C(1)-Sn(1)-Br(2)	135.54(7)
N(1)-Sn(1)-Br(2)	87.57(6)

Br(1)-Sn(1)-Br(2)	108.642(13)
C(1)-Sn(1)-Br(3)	98.96(7)
N(1)-Sn(1)-Br(3)	173.35(6)
Br(1)-Sn(1)-Br(3)	97.182(12)
Br(2)-Sn(1)-Br(3)	92.068(12)
C(7)-N(1)-C(8)	111.0(2)
C(7)-N(1)-C(9)	109.4(2)
C(8)-N(1)-C(9)	108.5(2)
C(7)-N(1)-Sn(1)	101.82(15)
C(8)-N(1)-Sn(1)	117.43(18)
C(9)-N(1)-Sn(1)	108.34(18)
C(2)-C(1)-C(6)	120.8(2)
C(2)-C(1)-Sn(1)	125.2(2)
C(6)-C(1)-Sn(1)	113.98(19)
C(3)-C(2)-C(1)	119.4(3)
C(3)-C(2)-H(2A)	120.3
C(1)-C(2)-H(2A)	120.3
C(4)-C(3)-C(2)	120.0(3)
C(4)-C(3)-H(3A)	120.0
C(2)-C(3)-H(3A)	120.0
C(3)-C(4)-C(5)	120.5(3)
C(3)-C(4)-H(4A)	119.7
C(5)-C(4)-H(4A)	119.7
C(4)-C(5)-C(6)	120.3(3)
C(4)-C(5)-H(5A)	119.9
C(6)-C(5)-H(5A)	119.9
C(5)-C(6)-C(1)	118.9(3)
C(5)-C(6)-C(7)	121.7(2)
C(1)-C(6)-C(7)	119.3(2)
N(1)-C(7)-C(6)	110.5(2)
N(1)-C(7)-H(7A)	109.6
C(6)-C(7)-H(7A)	109.6
N(1)-C(7)-H(7B)	109.6
C(6)-C(7)-H(7B)	109.6
H(7A)-C(7)-H(7B)	108.1
N(1)-C(8)-H(8A)	109.5

N(1)-C(8)-H(8B)	109.5
H(8A)-C(8)-H(8B)	109.5
N(1)-C(8)-H(8C)	109.5
H(8A)-C(8)-H(8C)	109.5
H(8B)-C(8)-H(8C)	109.5
N(1)-C(9)-H(9A)	109.5
N(1)-C(9)-H(9B)	109.5
H(9A)-C(9)-H(9B)	109.5
N(1)-C(9)-H(9C)	109.5
H(9A)-C(9)-H(9C)	109.5
H(9B)-C(9)-H(9C)	109.5

Symmetry transformations used to generate equivalent atoms:

Table A 10: Anisotropic displacement parameters ($\text{Å}^2\text{x } 10^3$) for d1821_a. The anisotropic displacement factor exponent takes the form: $-2\pi^2[\,h^2\,a^{*2}U^{11} + ... + 2\,h\,k\,a^*\,b^*\,U^{12}\,]$

	U^{11}	U^{22}	U^{33}	U^{23}	U^{13}	U^{12}
Sn(1)	17(1)	17(1)	16(1)	-3(1)	5(1)	-1(1)
Br(1)	29(1)	26(1)	21(1)	-3(1)	-1(1)	-6(1)
Br(2)	19(1)	37(1)	36(1)	-4(1)	8(1)	3(1)
Br(3)	37(1)	19(1)	25(1)	1(1)	11(1)	0(1)
N(1)	26(1)	24(1)	20(1)	-4(1)	13(1)	-7(1)
C(1)	16(1)	17(1)	18(2)	-3(1)	6(1)	0(1)
C(2)	20(1)	18(1)	20(2)	1(1)	4(1)	-1(1)
C(3)	20(2)	26(2)	18(2)	-2(1)	7(1)	-1(1)
C(4)	20(2)	20(1)	23(2)	-6(1)	6(1)	1(1)
C(5)	21(2)	17(1)	24(2)	0(1)	1(1)	0(1)
C(6)	16(1)	18(1)	16(2)	-1(1)	2(1)	-2(1)
C(7)	31(2)	20(2)	20(2)	1(1)	7(1)	-2(1)
C(8)	56(2)	32(2)	26(2)	-4(1)	26(2)	-10(2)
C(9)	30(2)	28(2)	36(2)	-8(1)	15(2)	-11(1)

Table A 11: Hydrogen coordinates (x 10^4) and isotropic displacement parameters ($Å^2$x 10 ^{3}) for d1821_a.

	x	y	z	U(eq)
H(2A)	3840	2878	4890	23
H(3A)	2271	3995	5606	25
H(4A)	1814	5296	4713	25
H(5A)	2909	5496	3108	25
H(7A)	3541	4214	1357	28
H(7B)	4938	5002	1834	28
H(8A)	7158	4394	600	53
H(8B)	5681	3596	346	53
H(8C)	8022	3455	852	53
H(9A)	8400	4862	2434	45
H(9B)	9448	3951	2651	45
H(9C)	8028	4290	3419	45

Table A 12: Torsion angles [°] for d1821_a.

C(6)-C(1)-C(2)-C(3)	-1.3(4)
Sn(1)-C(1)-C(2)-C(3)	-178.0(2)
C(1)-C(2)-C(3)-C(4)	0.2(4)
C(2)-C(3)-C(4)-C(5)	0.2(4)
C(3)-C(4)-C(5)-C(6)	0.5(4)
C(4)-C(5)-C(6)-C(1)	-1.5(4)
C(4)-C(5)-C(6)-C(7)	177.1(3)
C(2)-C(1)-C(6)-C(5)	2.0(4)
Sn(1)-C(1)-C(6)-C(5)	179.0(2)
C(2)-C(1)-C(6)-C(7)	-176.7(3)
Sn(1)-C(1)-C(6)-C(7)	0.3(3)
C(8)-N(1)-C(7)-C(6)	168.5(2)
C(9)-N(1)-C(7)-C(6)	-71.8(3)
Sn(1)-N(1)-C(7)-C(6)	42.7(2)
C(5)-C(6)-C(7)-N(1)	148.1(3)
C(1)-C(6)-C(7)-N(1)	-33.2(3)

Symmetry transformations used to generate equivalent atoms:
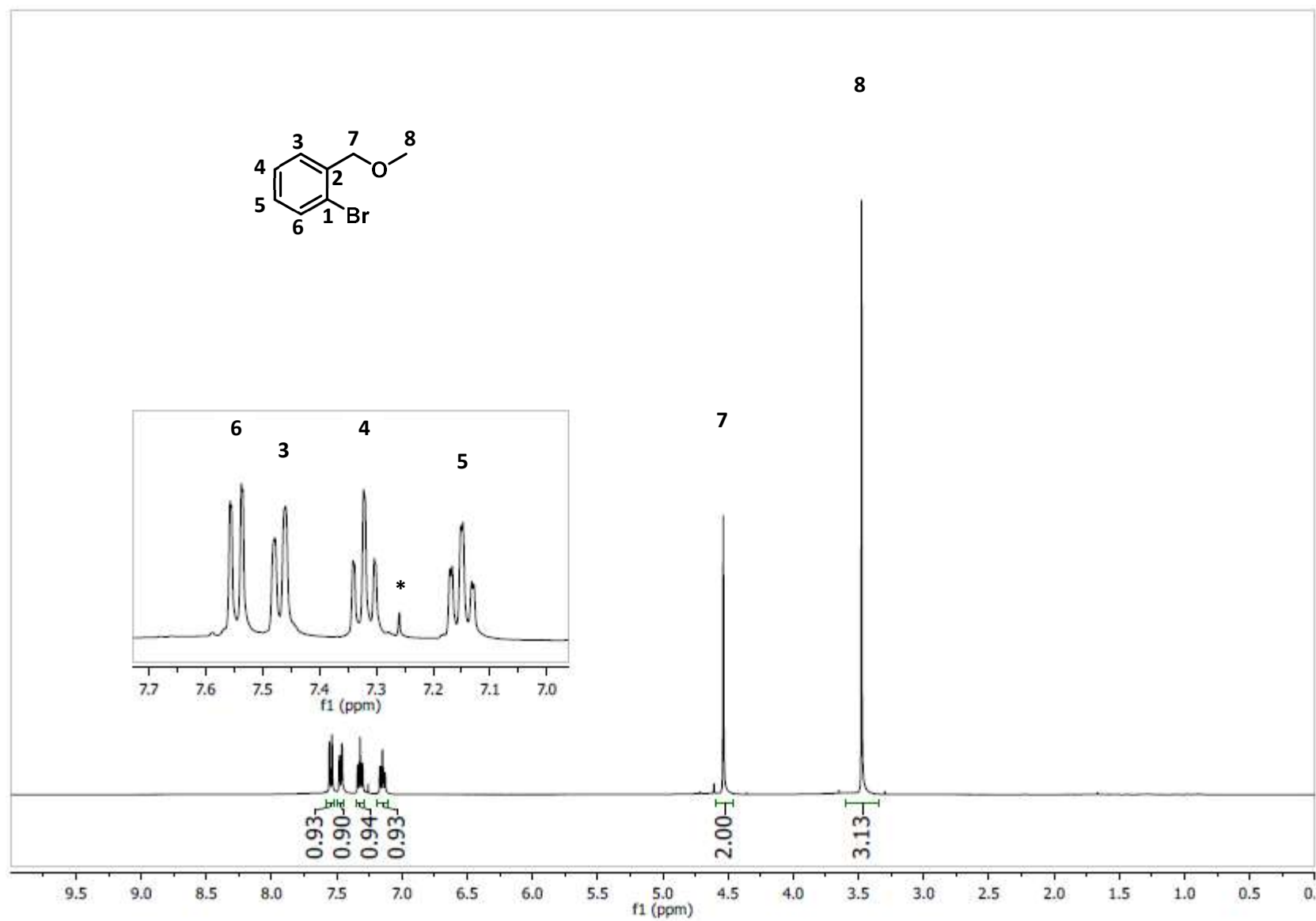
Figure A 1: ^1H NMR ($CDCl_3$) spectrum of $(2\text{-}(CH_2OCH_3)C_6H_4)Br$.
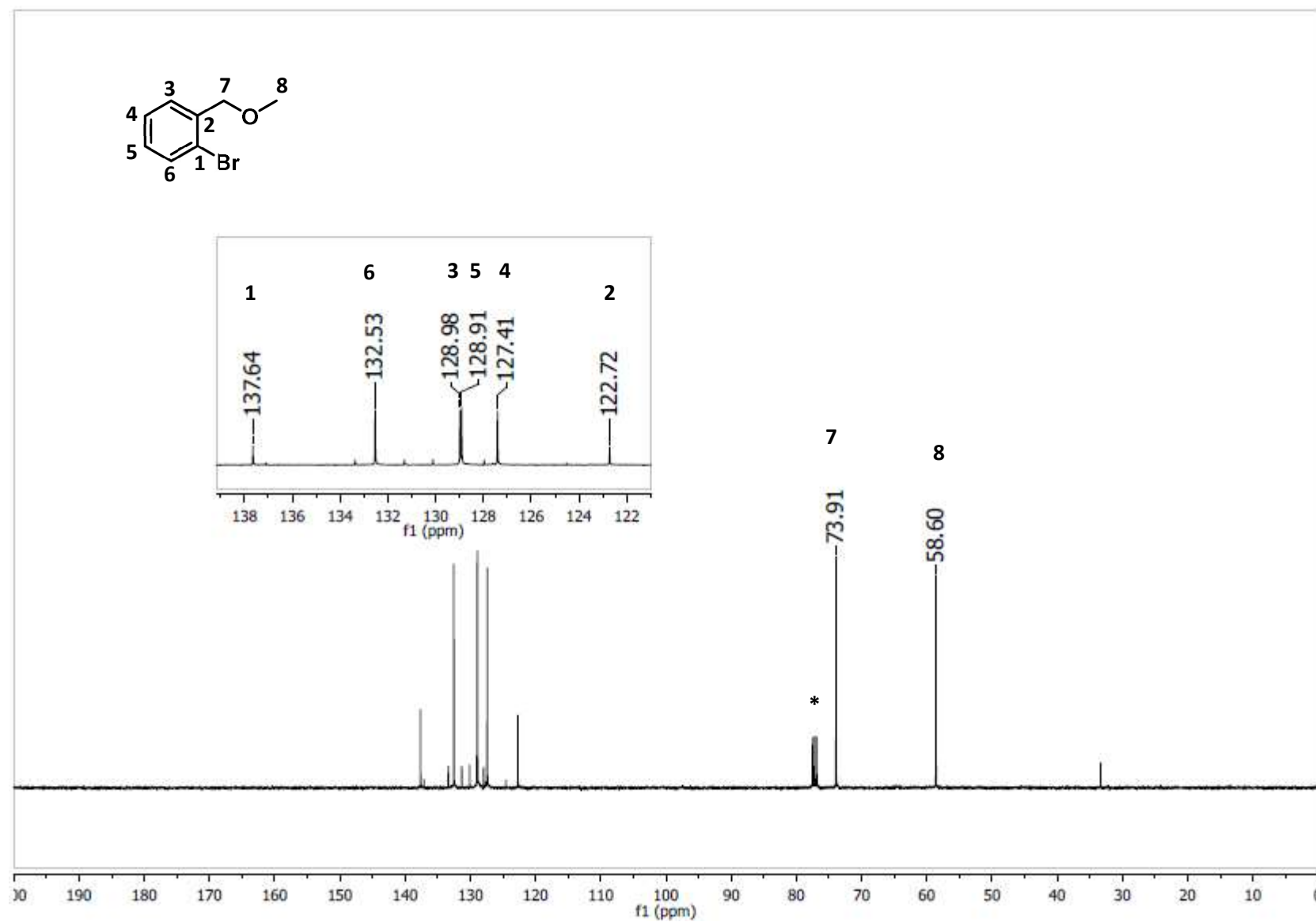
Figure A 2: ^{13}C NMR (CDCl$_3$) spectrum of (2-(CH$_2$OCH$_3$)C$_6$H$_4$)Br.
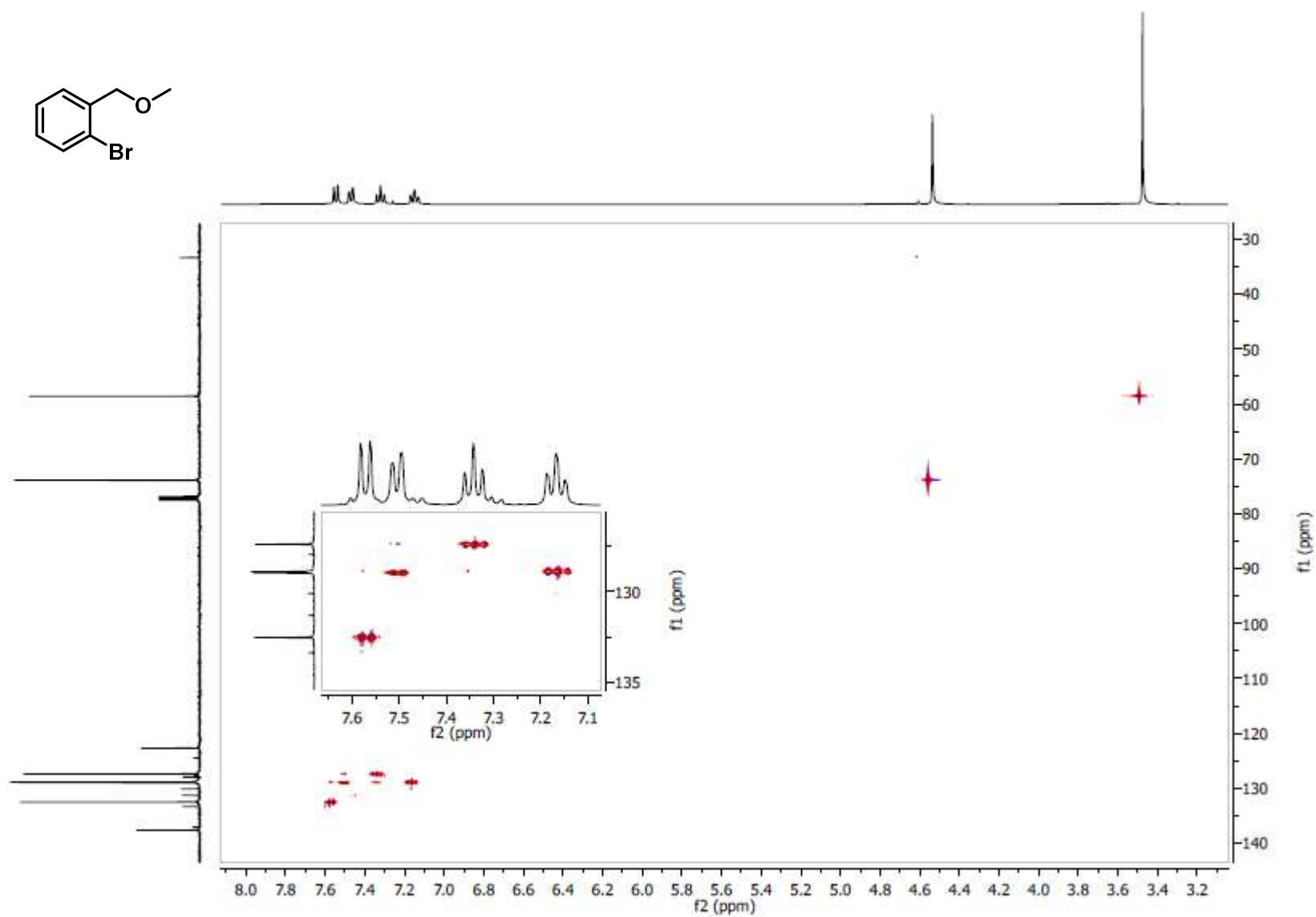
Figure A 3: 2D HSQC NMR (CDCl$_3$) spectrum of (2-(CH$_2$OCH$_3$)C$_6$H$_4$)Br.
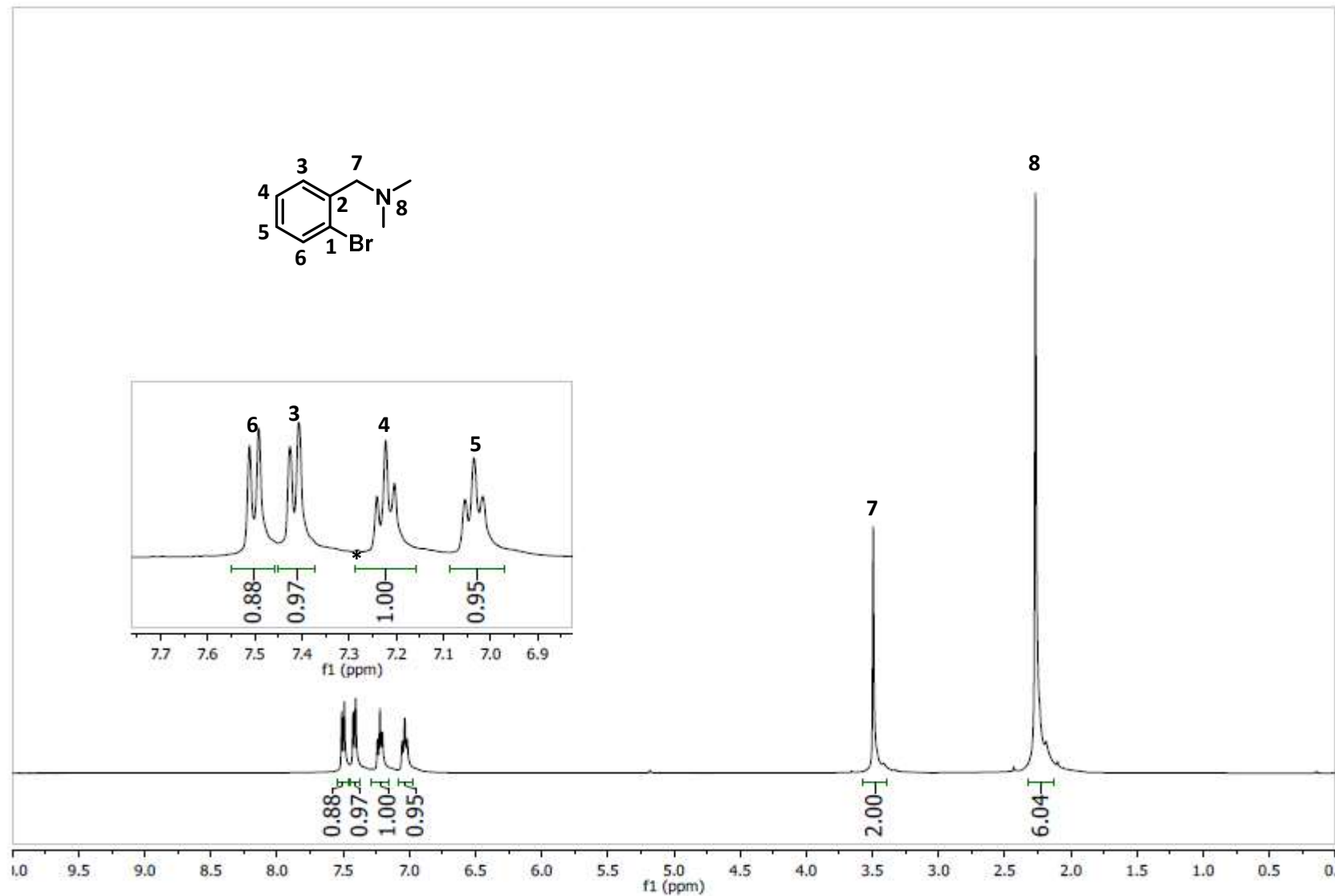
Figure A 4: ^{1}H NMR (CDCl$_3$) spectrum of (2-(CH$_2$N(CH$_3$)$_2$)C$_6$H$_4$)Br.
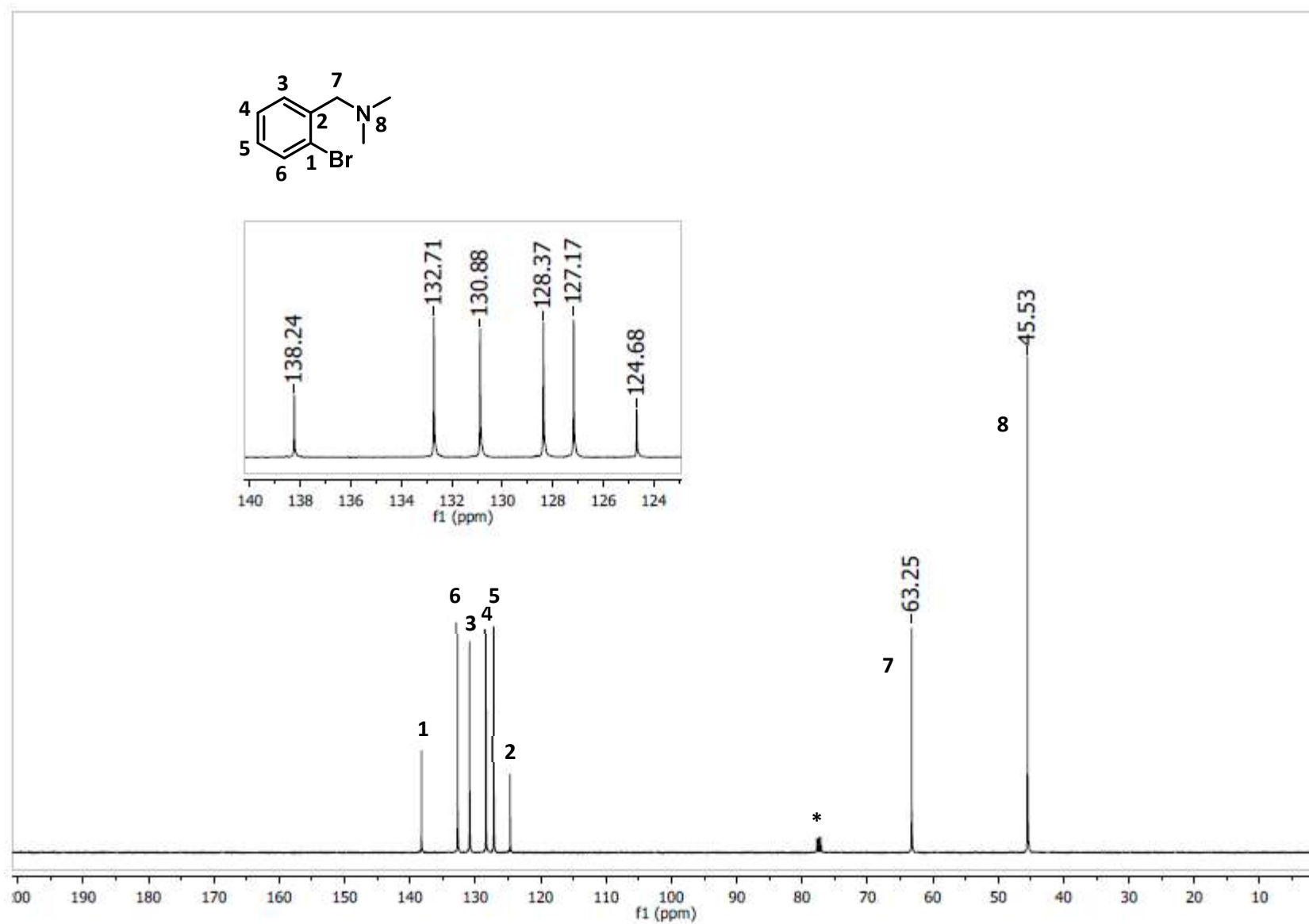
Figure A 5: ^{13}C NMR (CDCl$_3$) spectrum of (2-(CH$_2$N(CH$_3$)$_2$)C$_6$H$_4$)Br.
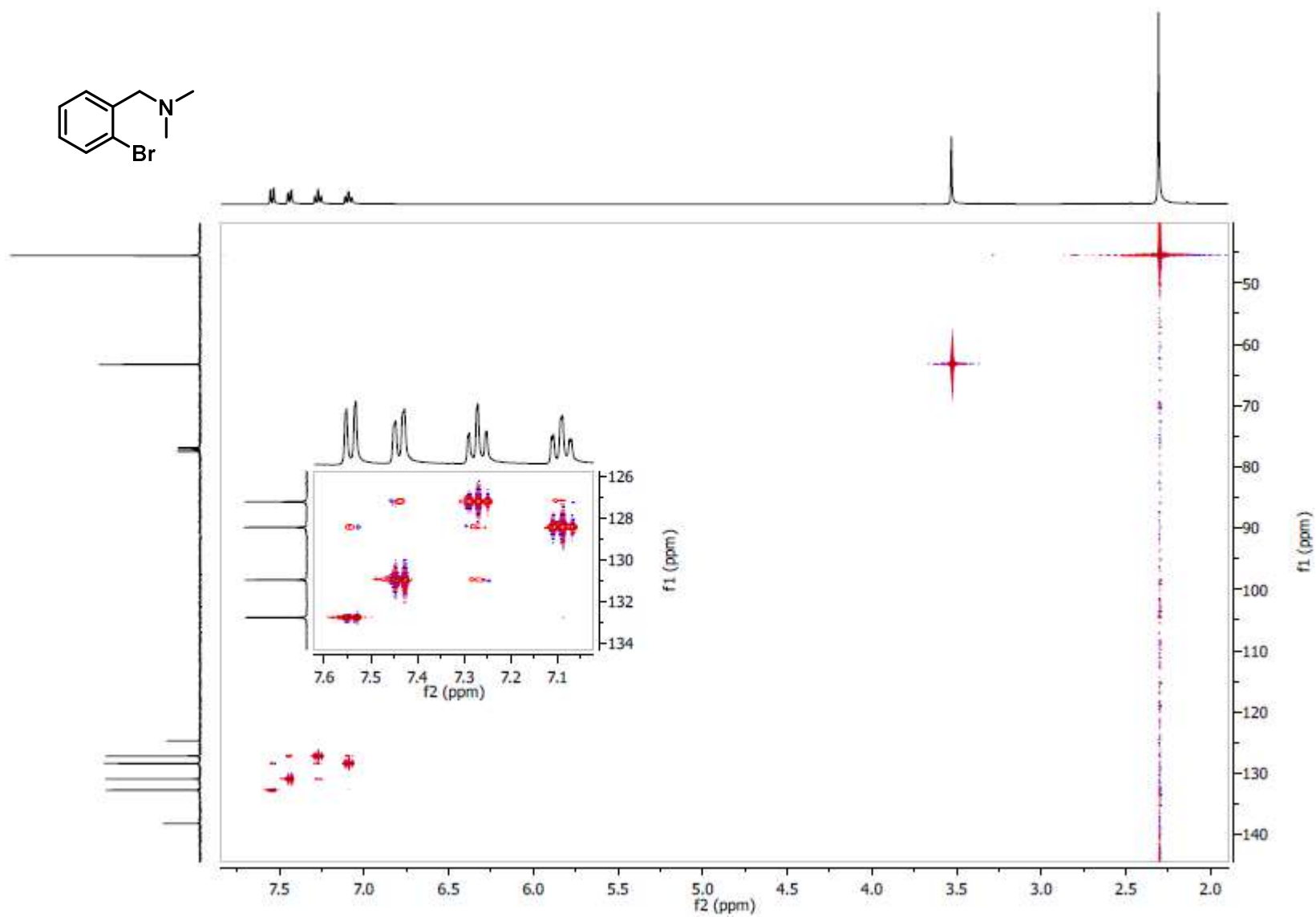
Figure A 6: 2D HSQC NMR (CDCl₃) spectrum of (2-(CH₂N(CH₃)₂)C₆H₄)Br.
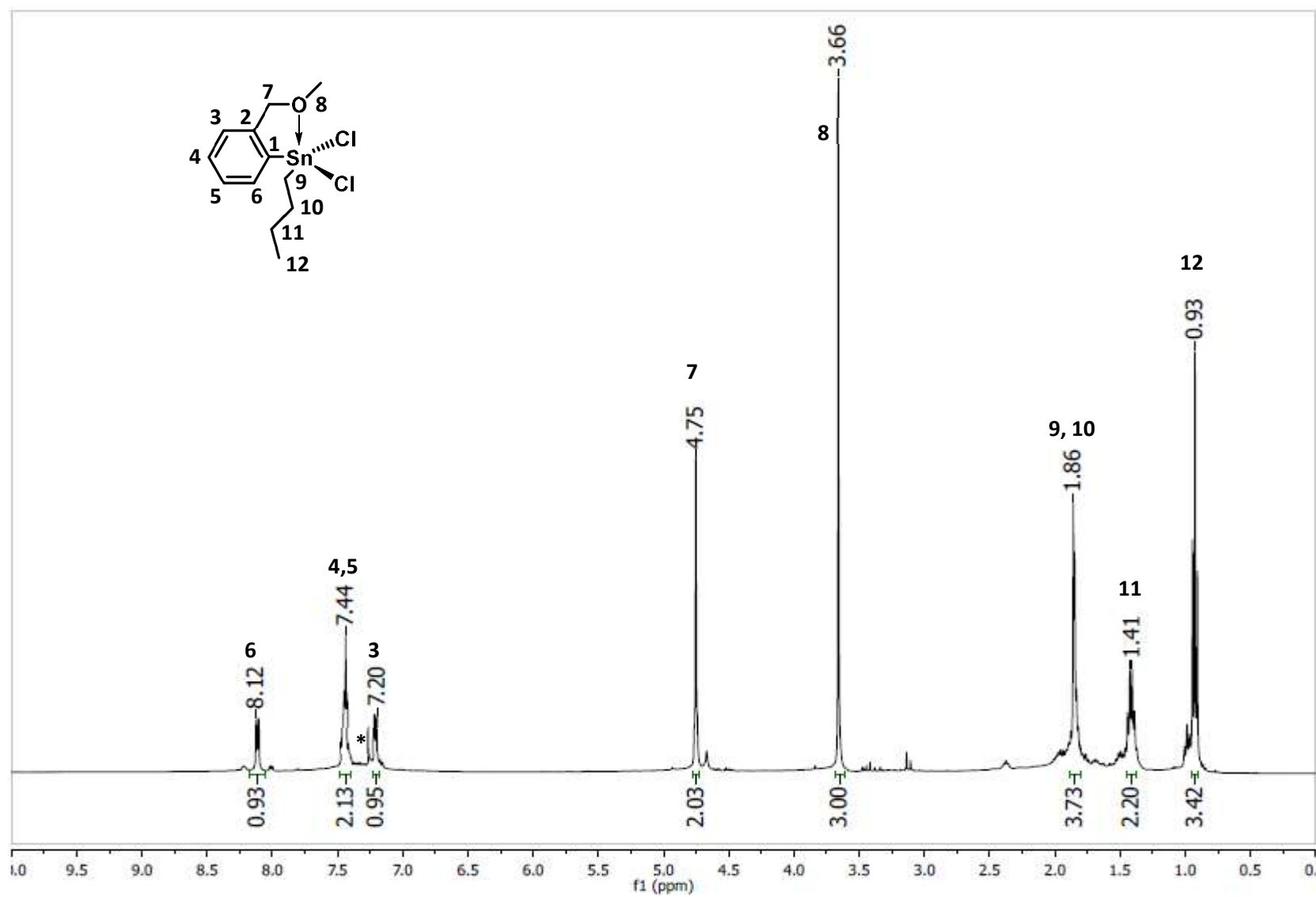
Figure A 7: ^1H NMR (CDCl$_3$) spectrum of [2-(CH$_2$OCH$_3$)C$_6$H$_4$](n-Bu)SnCl$_2$.
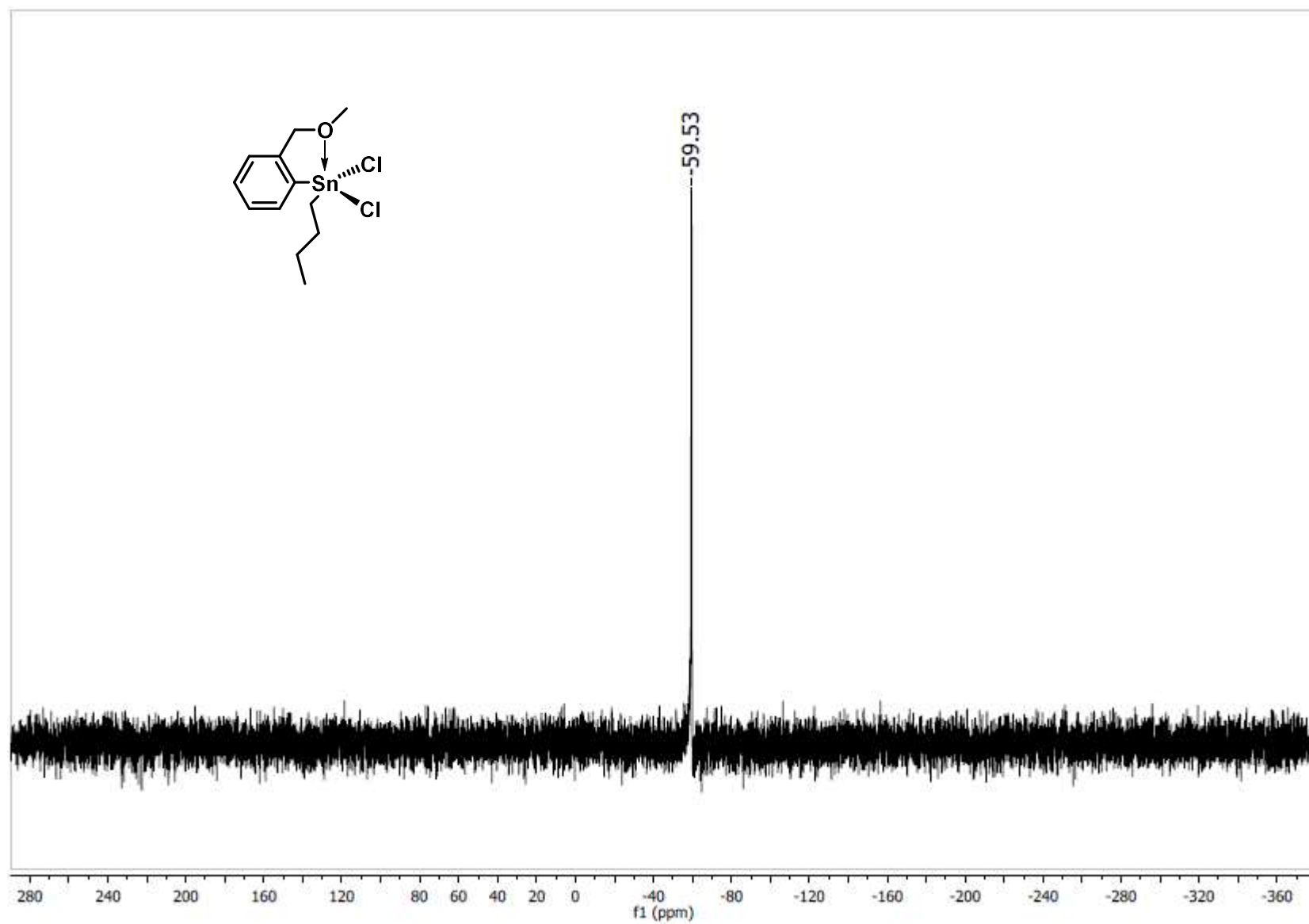
Figure A 8: ^{119}Sn NMR (CDCl$_3$) spectrum of [2-(CH$_2$OCH$_3$)C$_6$H$_4$](n-Bu)SnCl$_2$.
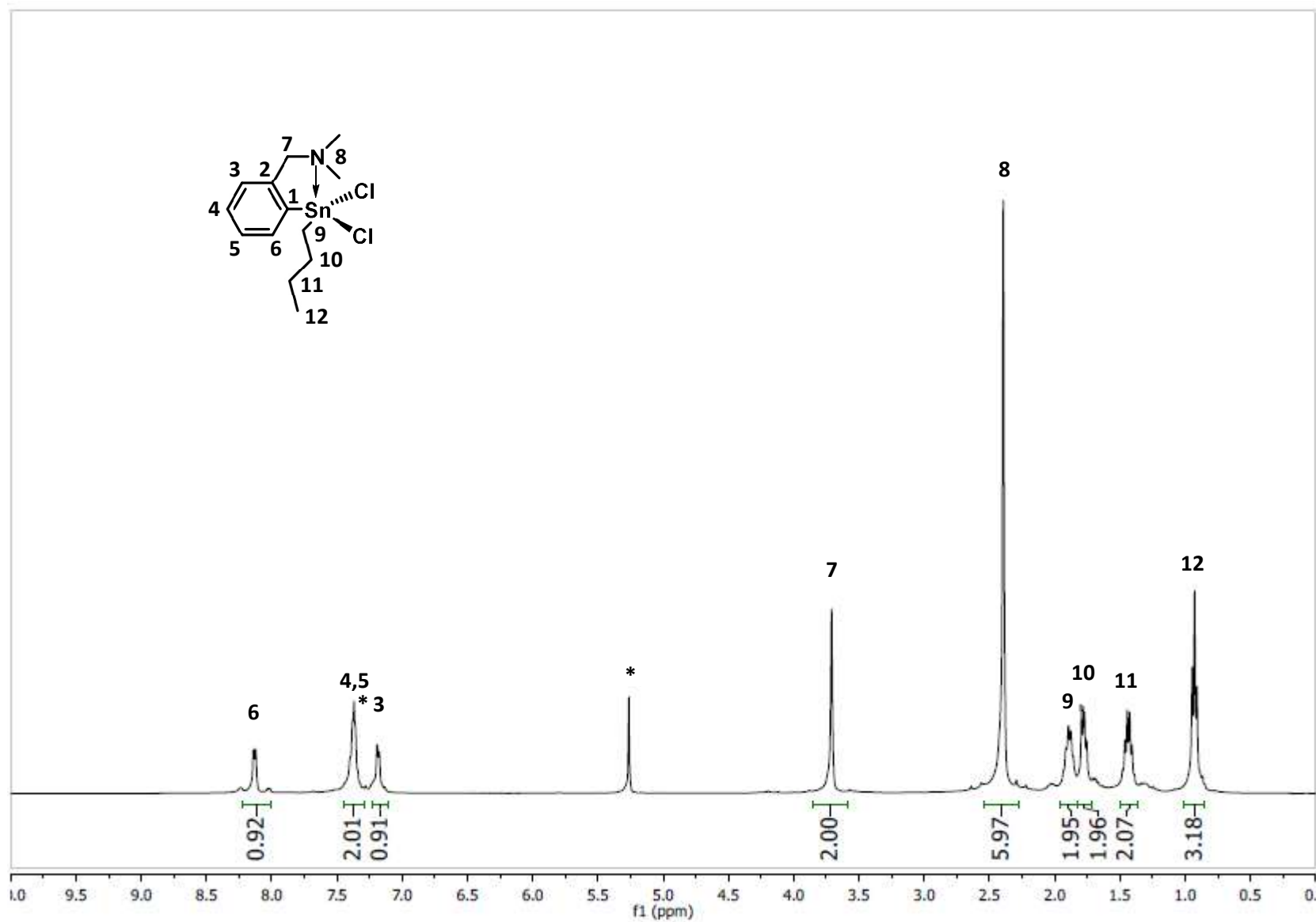
Figure A 9: ^{1}H NMR (CDCl$_3$) spectrum of [2-(CH$_2$N(CH$_3$)$_2$)C$_6$H$_4$](n-Bu)SnCl$_2$.
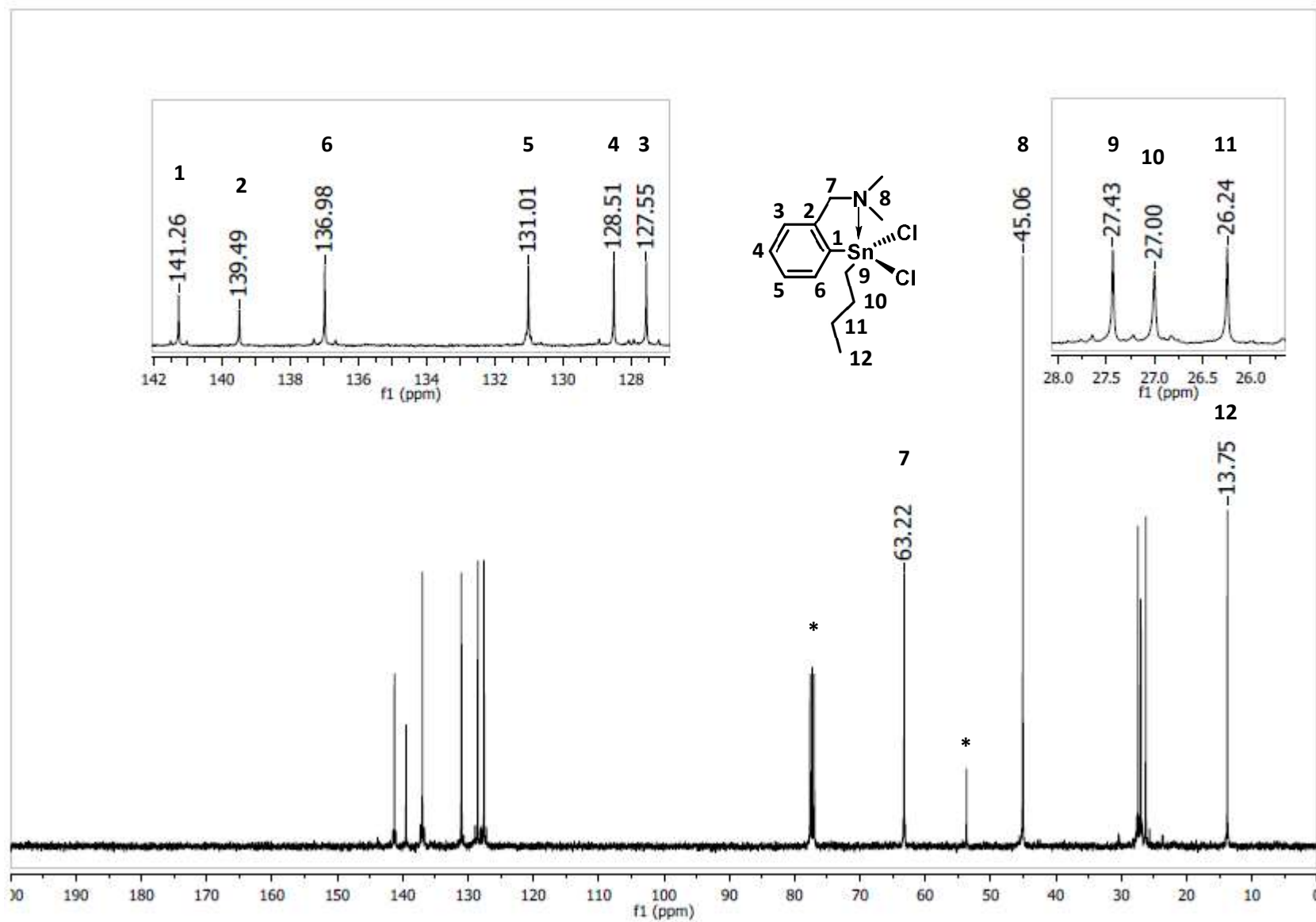
Figure A 10: ^{13}C NMR (CDCl$_3$) spectrum of [2-(CH$_2$N(CH$_3$)$_2$)C$_6$H$_4$](n-Bu)SnCl$_2$.
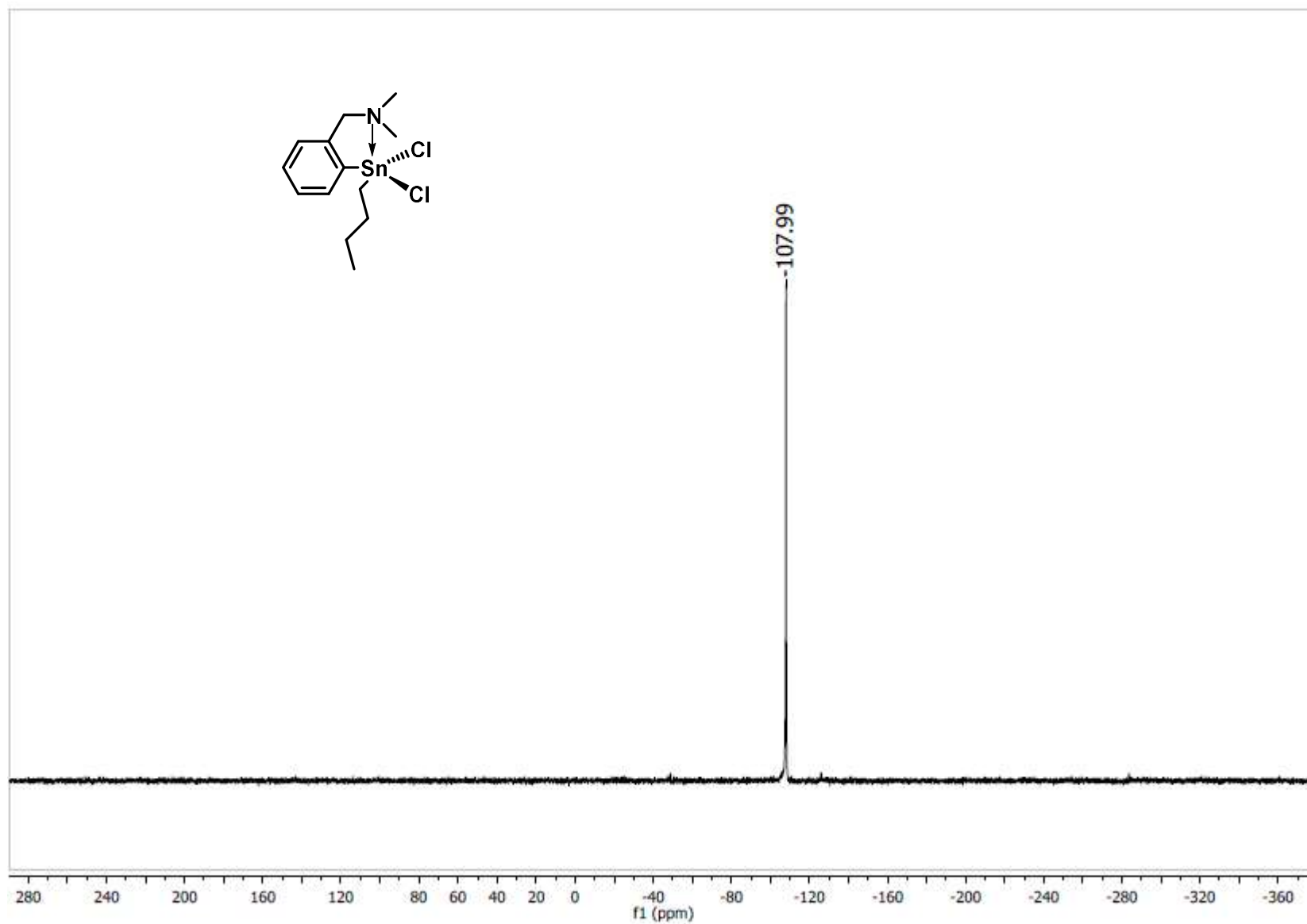
Figure A 11: ^{119}Sn NMR (CDCl$_3$) spectrum of [2-(CH$_2$N(CH$_3$)$_2$)C$_6$H$_4$](n-Bu)SnCl$_2$.
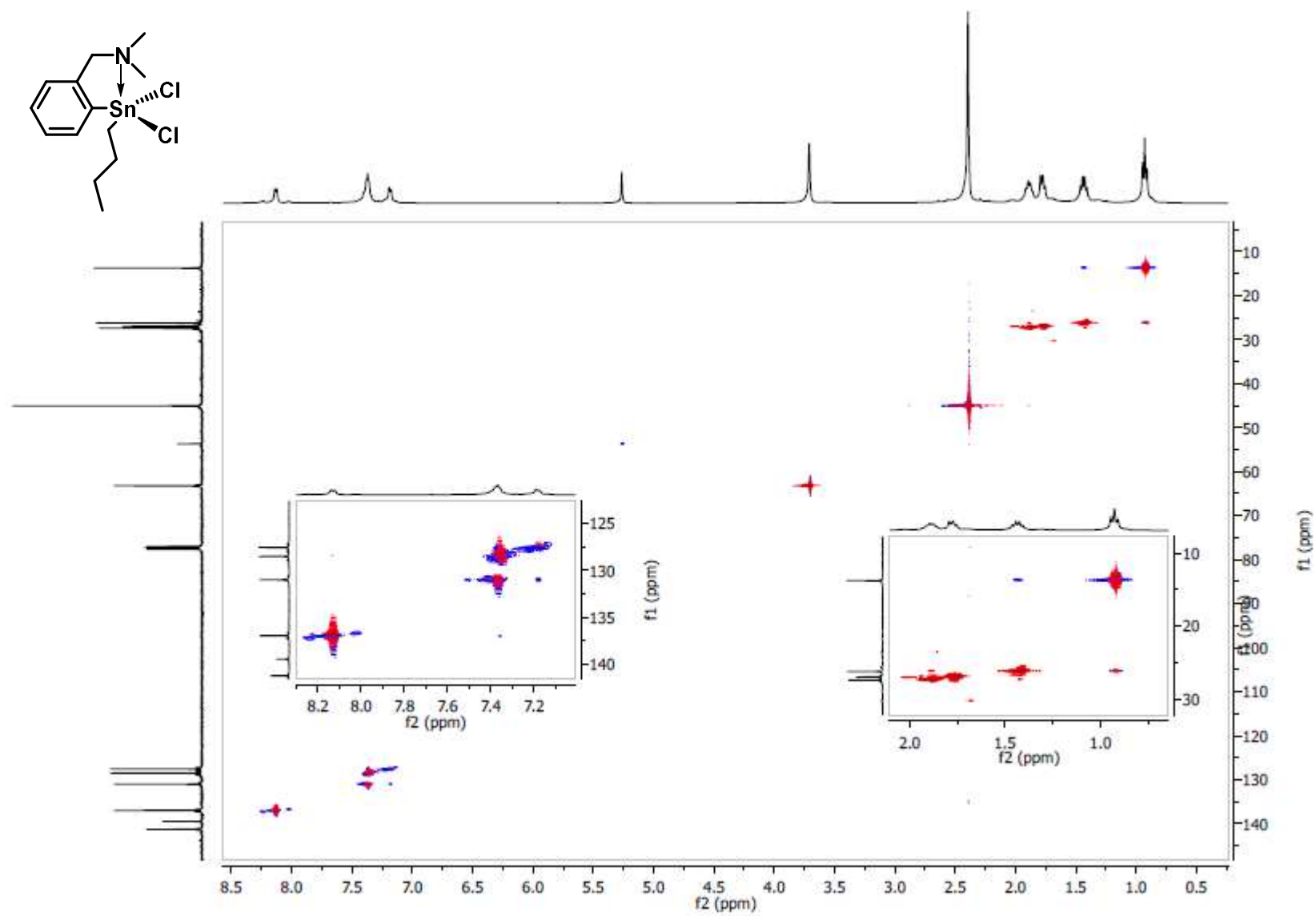
Figure A 12: 2D HSQC NMR (CDCl$_3$) spectrum of [2-(CH$_2$N(CH$_3$)$_2$)C$_6$H$_4$](*n*-Bu)SnCl$_2$.
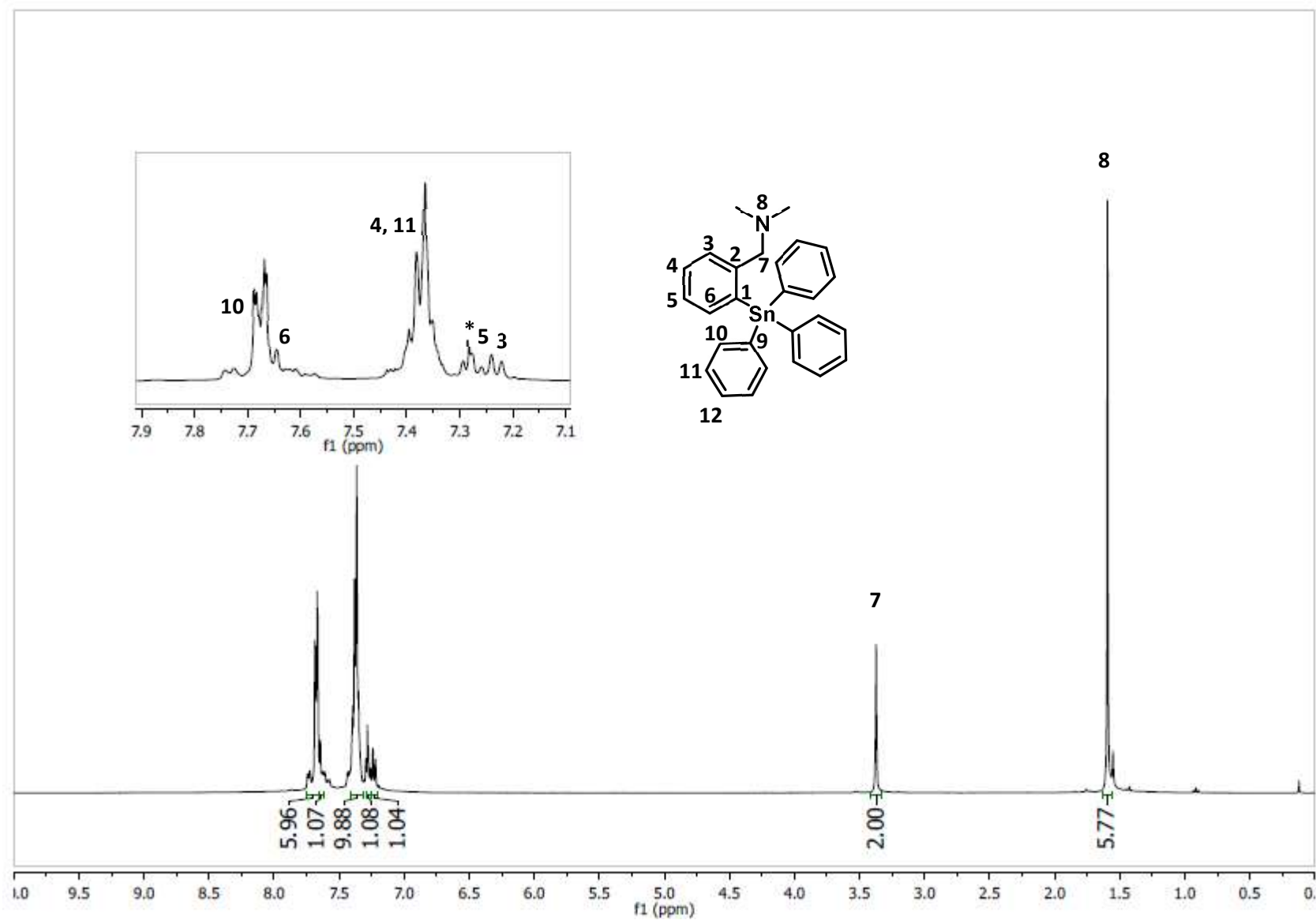
Figure A 13: ^{1}H NMR (CDCl$_3$) spectrum of [2-(CH$_2$N(CH$_3$)$_2$)C$_6$H$_4$]Ph$_3$Sn.
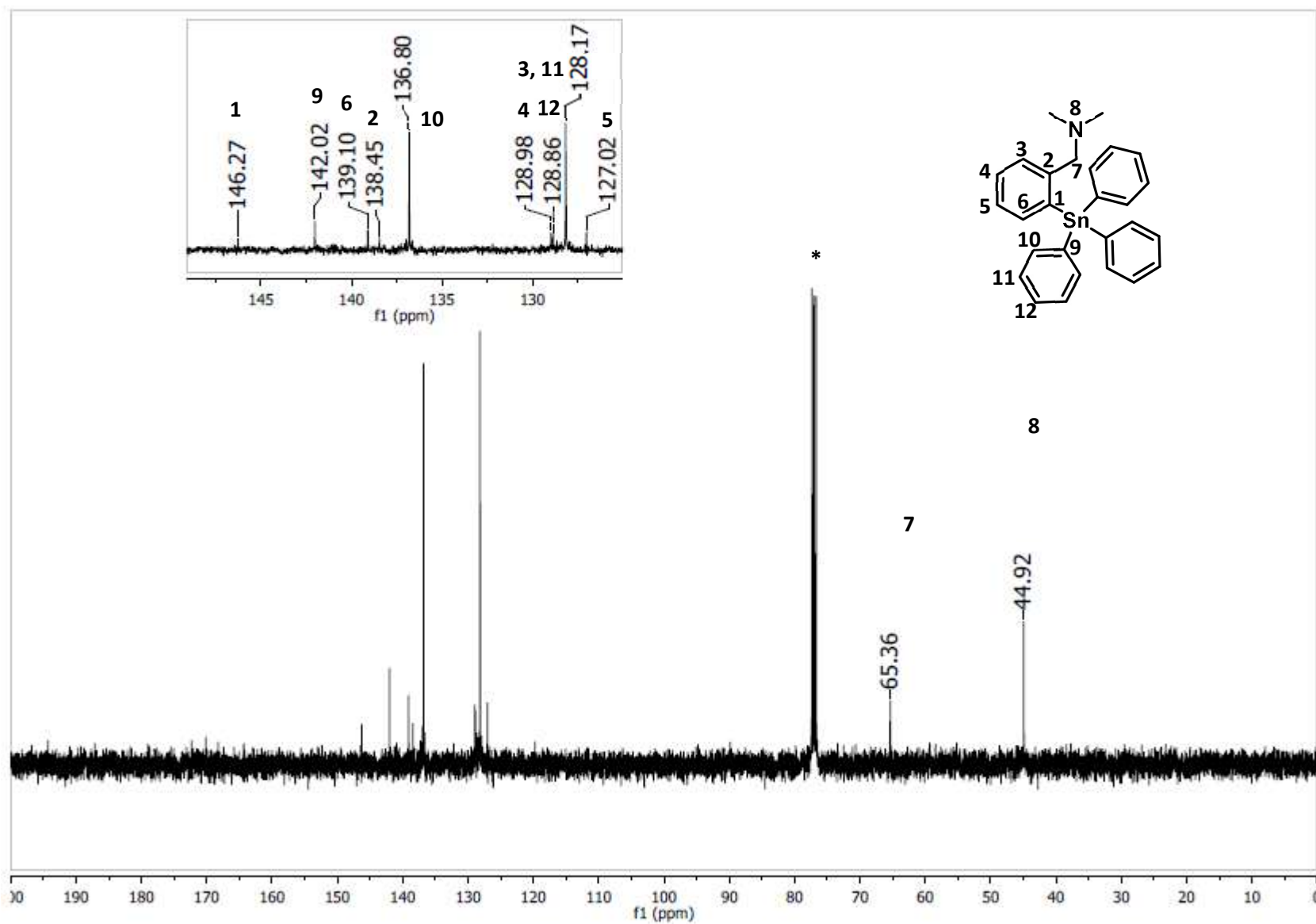
Figure A 14: ^{13}C NMR (CDCl$_3$) spectrum of [2-(CH$_2$N(CH$_3$)$_2$)C$_6$H$_4$]Ph$_3$Sn.
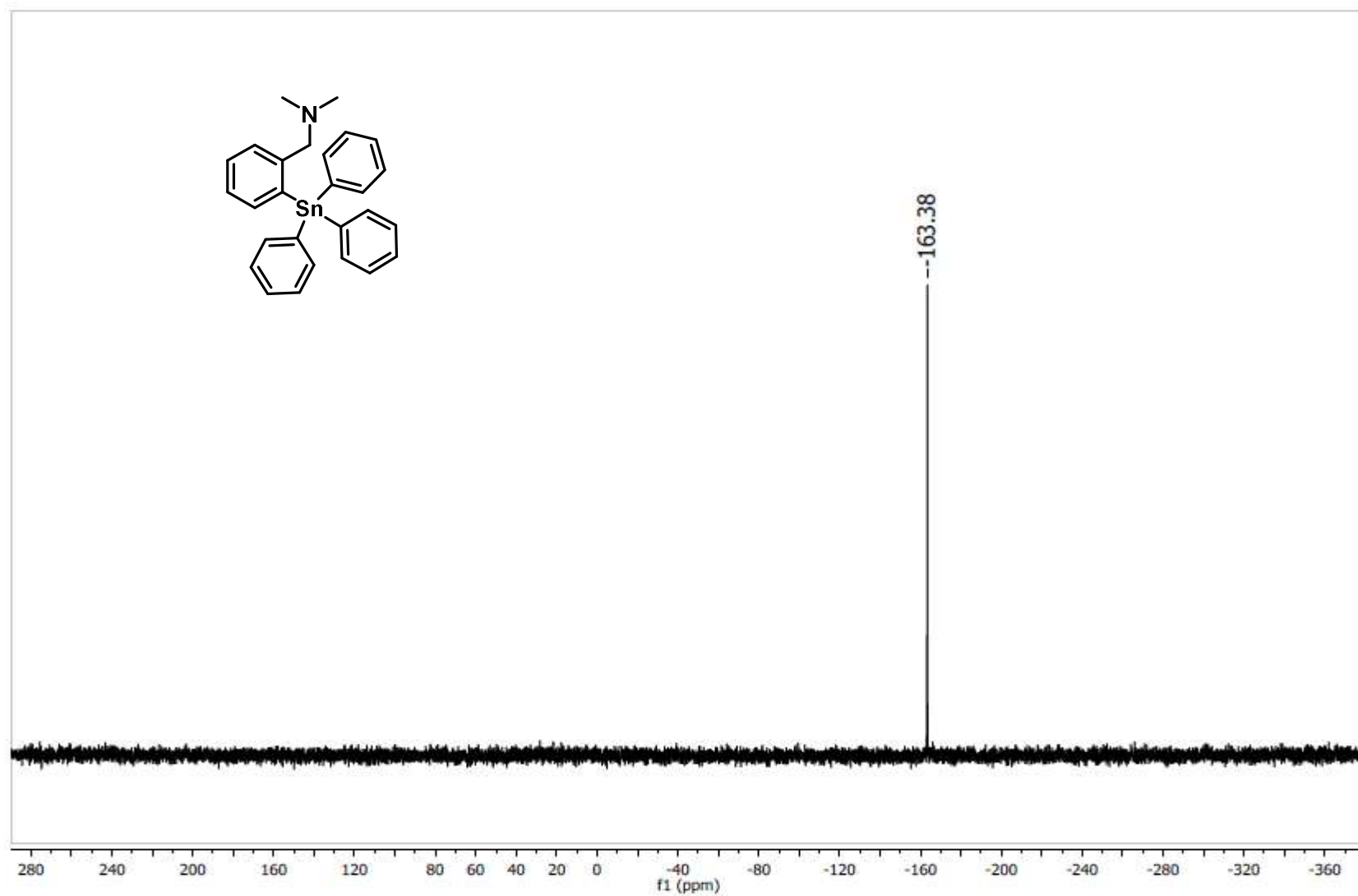
Figure A 15: ^{119}Sn NMR (CDCl$_3$) spectrum of [2-(CH$_2$N(CH$_3$)$_2$)C$_6$H$_4$]Ph$_3$Sn.
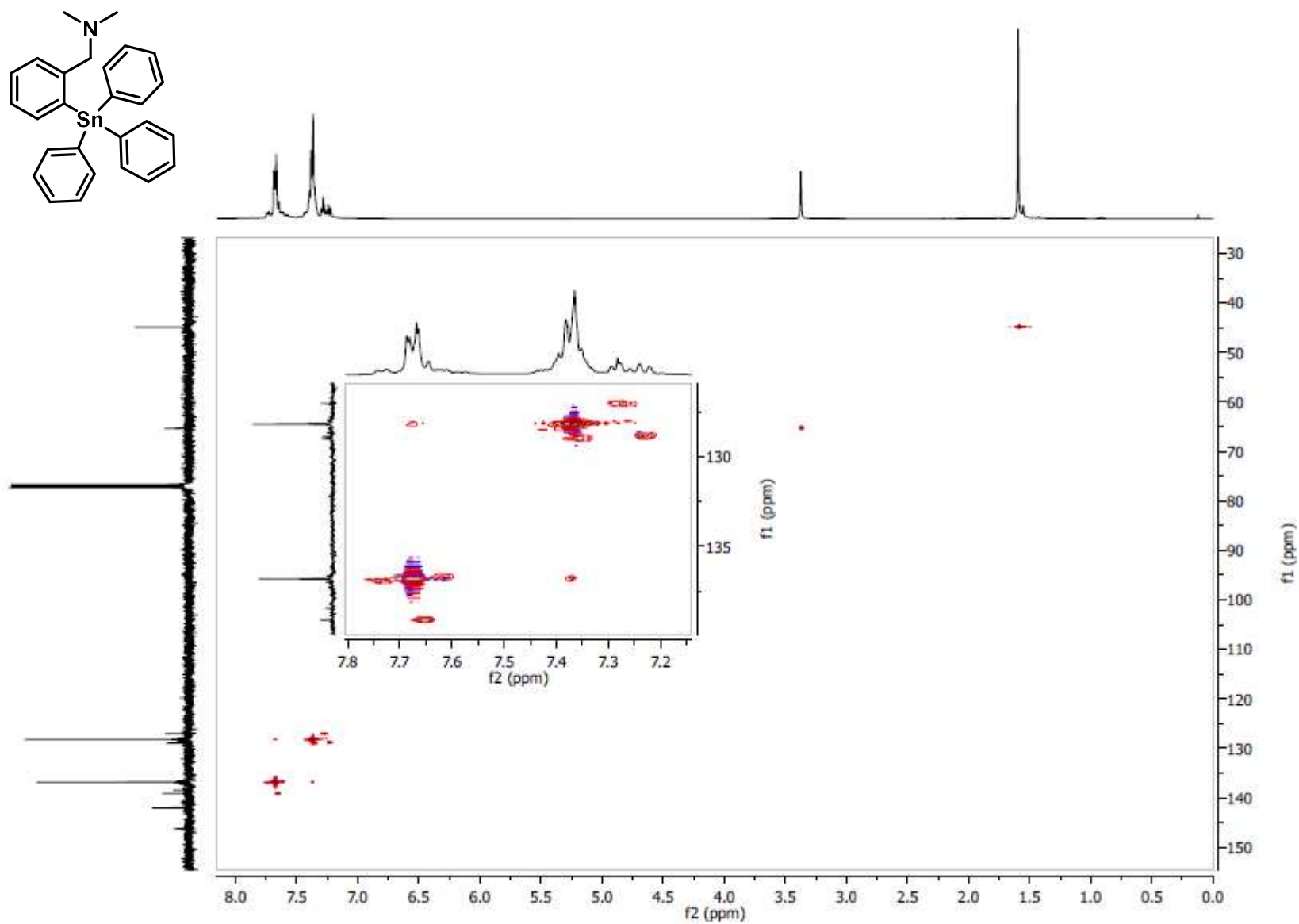
Figure A 16: 2D HSQC NMR (CDCl$_3$) spectrum of [2-(CH$_2$N(CH$_3$)$_2$)C$_6$H$_4$]Ph$_3$Sn.
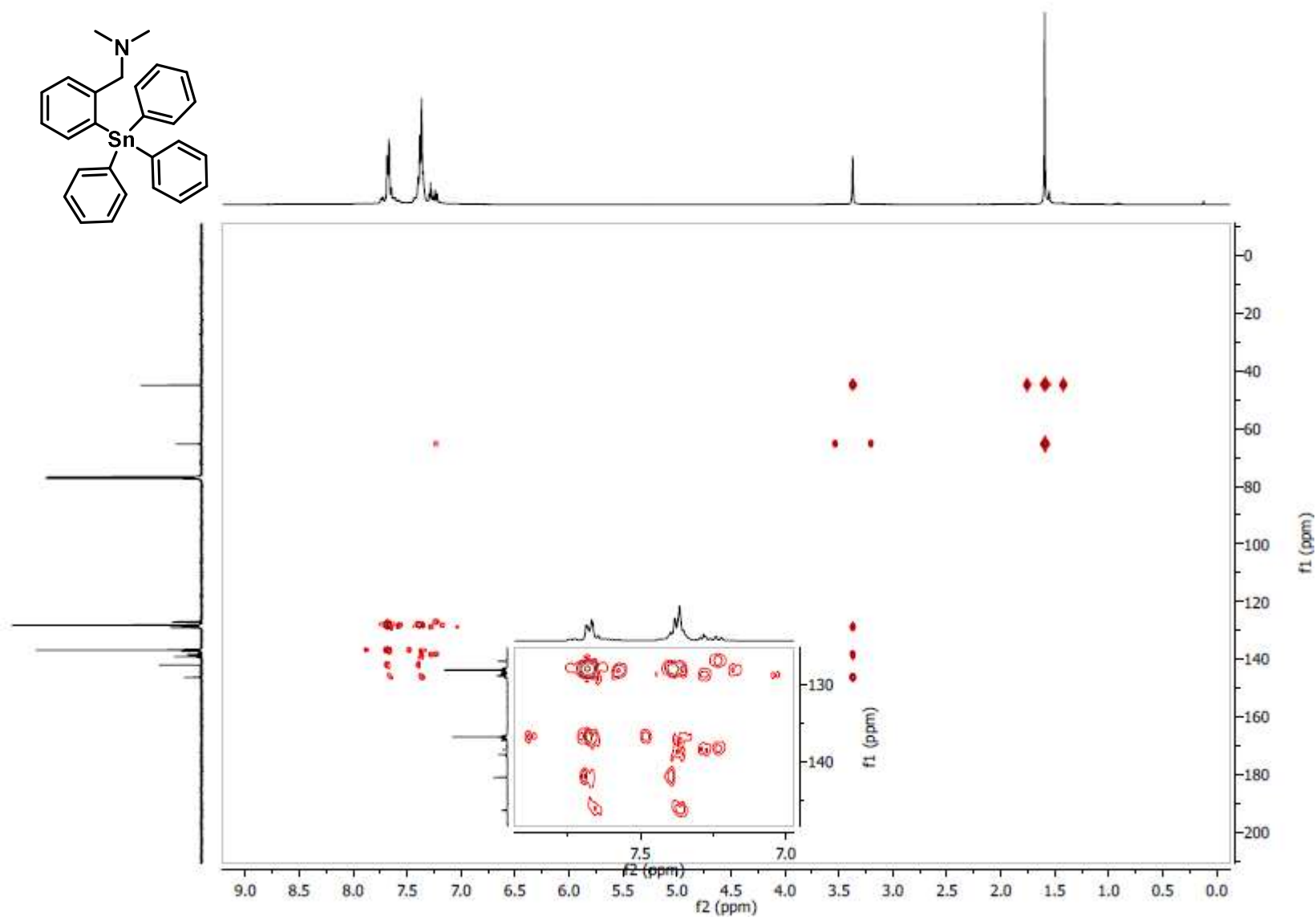
Figure A 17: 2D HMBC NMR (CDCl$_3$) spectrum of [2-(CH$_2$N(CH$_3$)$_2$)C$_6$H$_4$]Ph$_3$Sn.
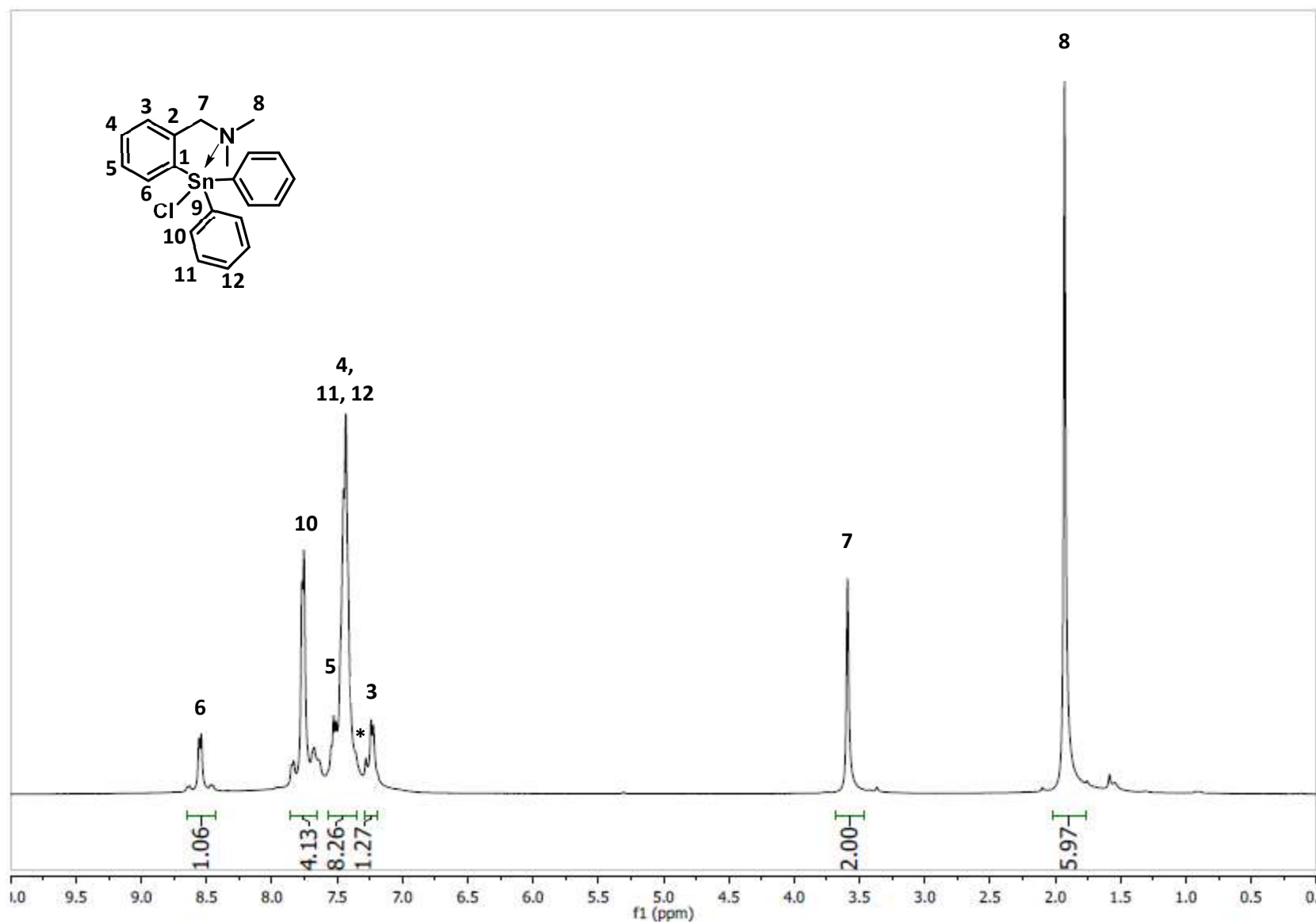
Figure A 18: ^{1}H NMR (CDCl$_3$) spectrum of [2-(CH$_2$N(CH$_3$)$_2$)C$_6$H$_4$]Ph$_2$SnCl.
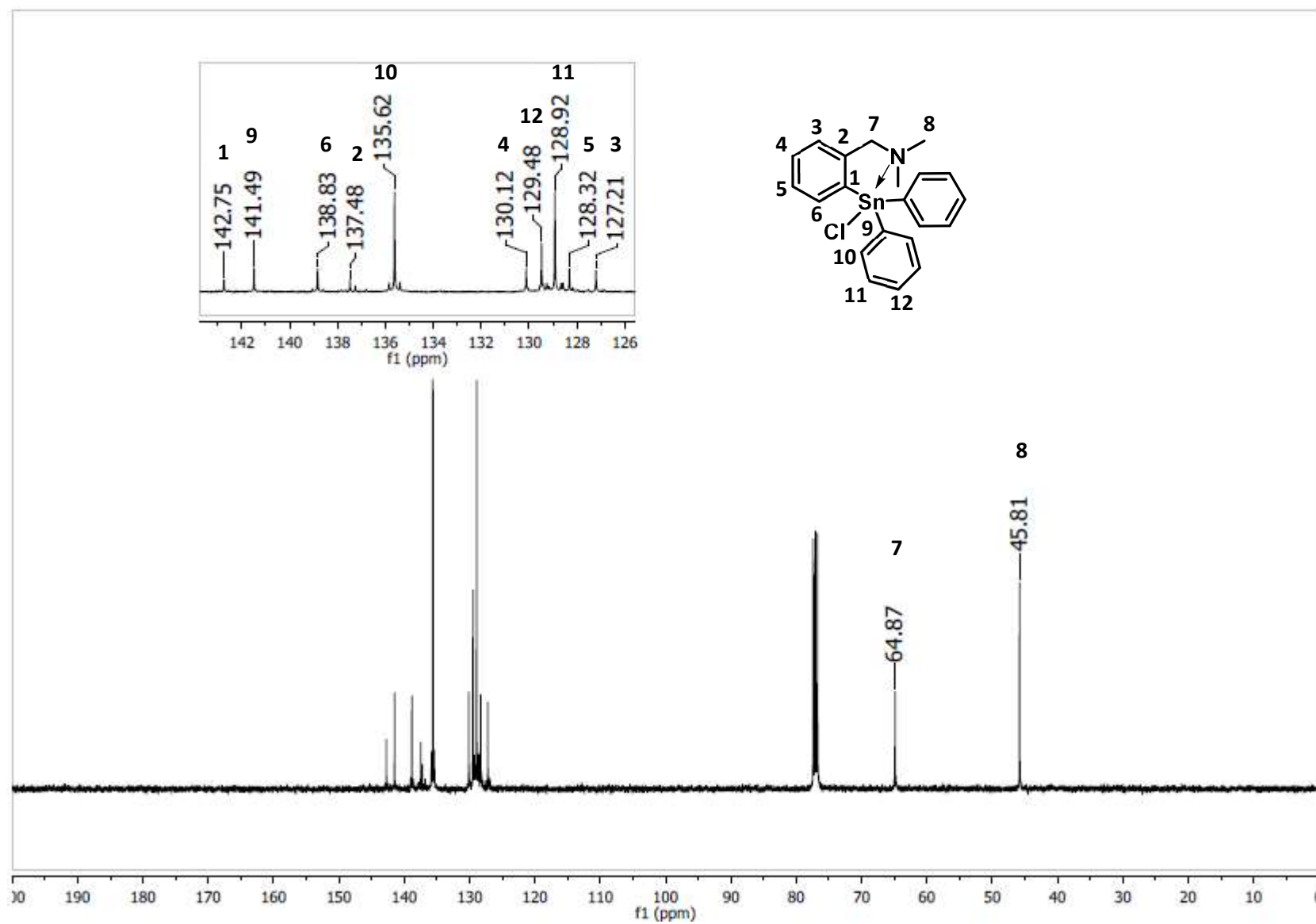
Figure A 19: ^{13}C NMR (CDCl$_3$) spectrum of [2-(CH$_2$N(CH$_3$)$_2$)C$_6$H$_4$]Ph$_2$SnCl.
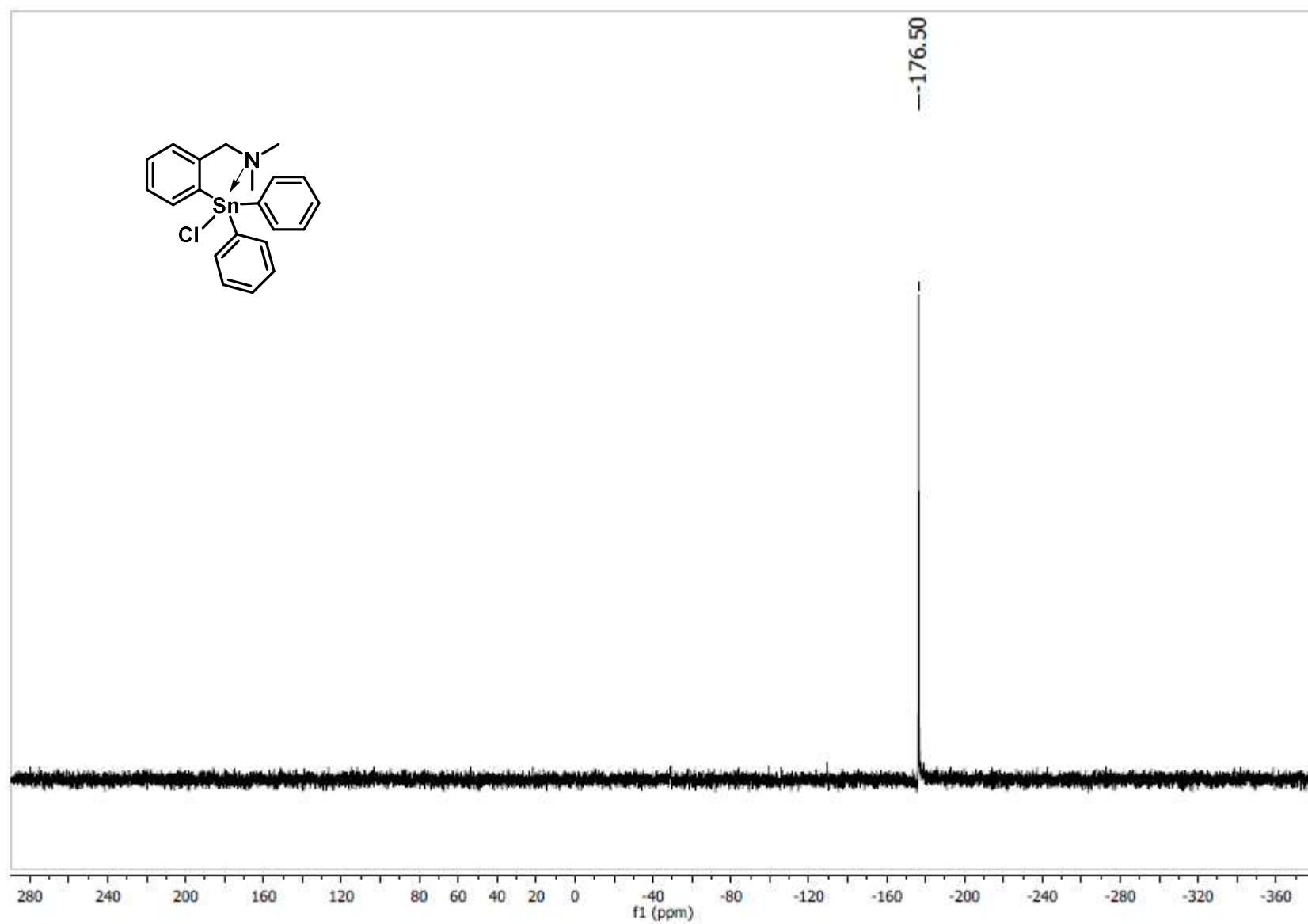
Figure A 20: ^{119}Sn NMR (CDCl$_3$) spectrum of [2-(CH$_2$N(CH$_3$)$_2$)C$_6$H$_4$]Ph$_2$SnCl.
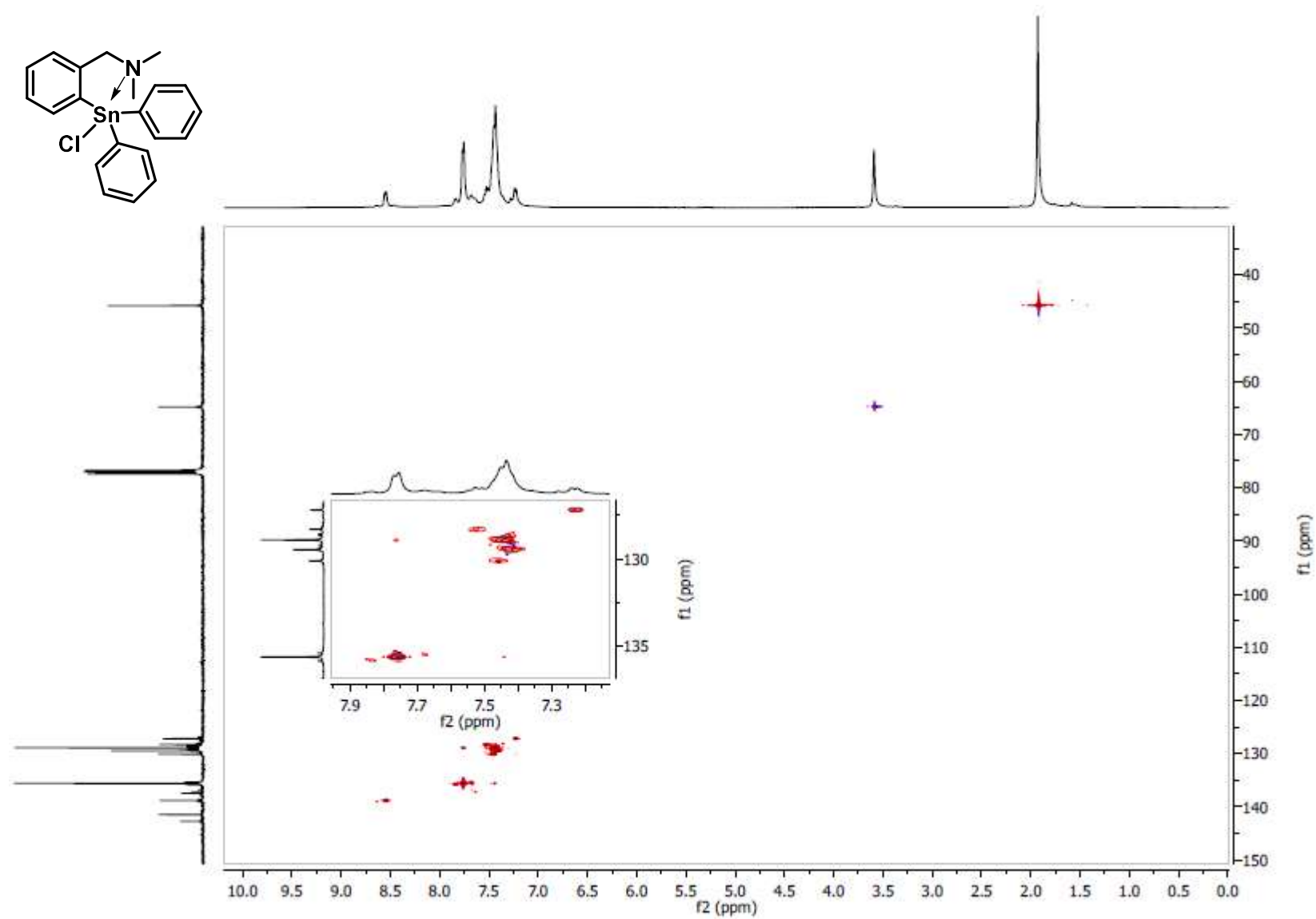
Figure A 21: 2D HQSC NMR (CDCl$_3$) spectrum of [2-(CH$_2$N(CH$_3$)$_2$)C$_6$H$_4$]Ph$_2$SnCl.
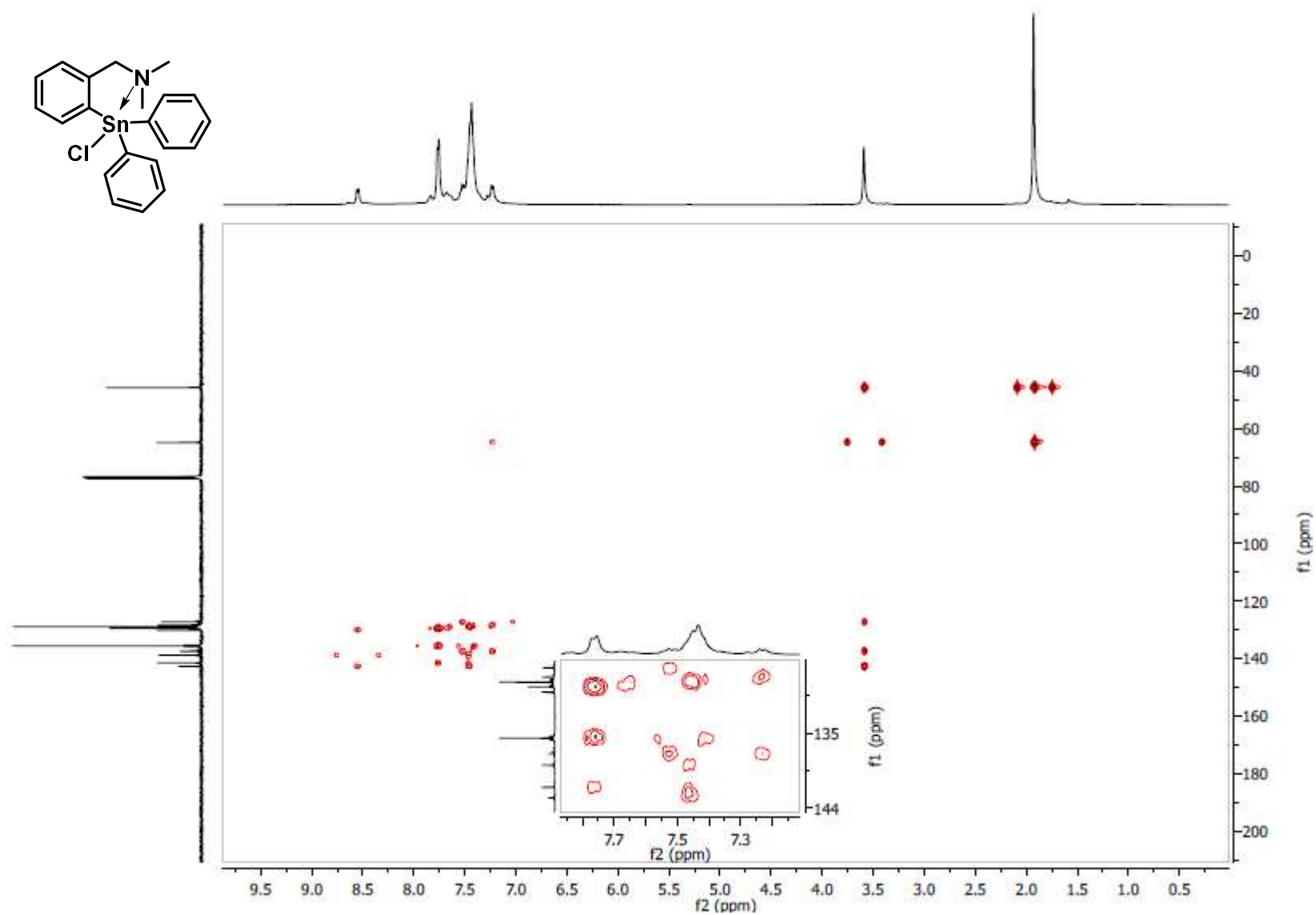
Figure A 22: 2D HMBC NMR (CDCl$_3$) spectrum of [2-(CH$_2$N(CH$_3$)$_2$)C$_6$H$_4$]Ph$_2$SnCl.
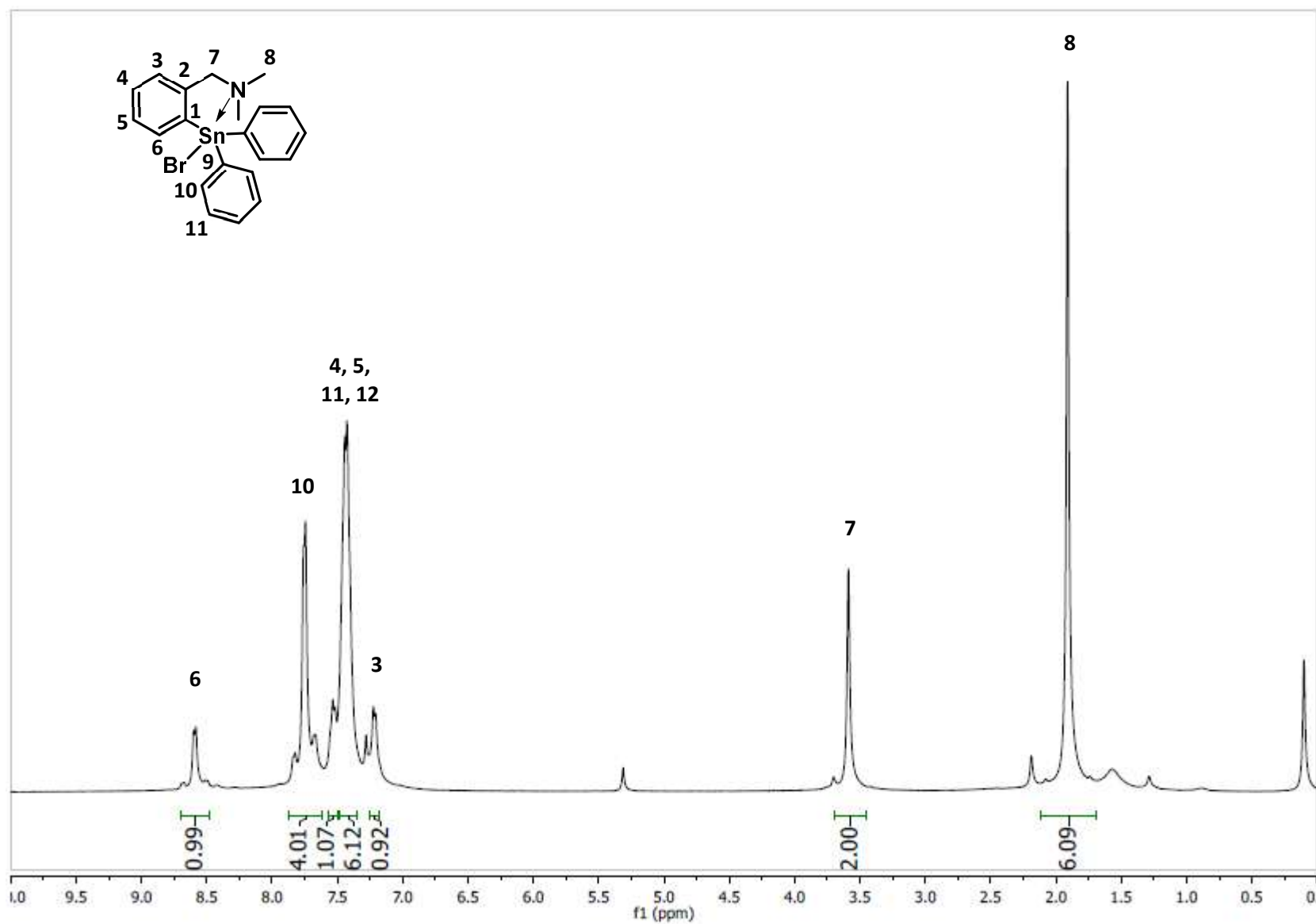
Figure A 23: ^{1}H NMR (CDCl$_3$) spectrum of [2-(CH$_2$N(CH$_3$)$_2$)C$_6$H$_4$]Ph$_2$SnBr.
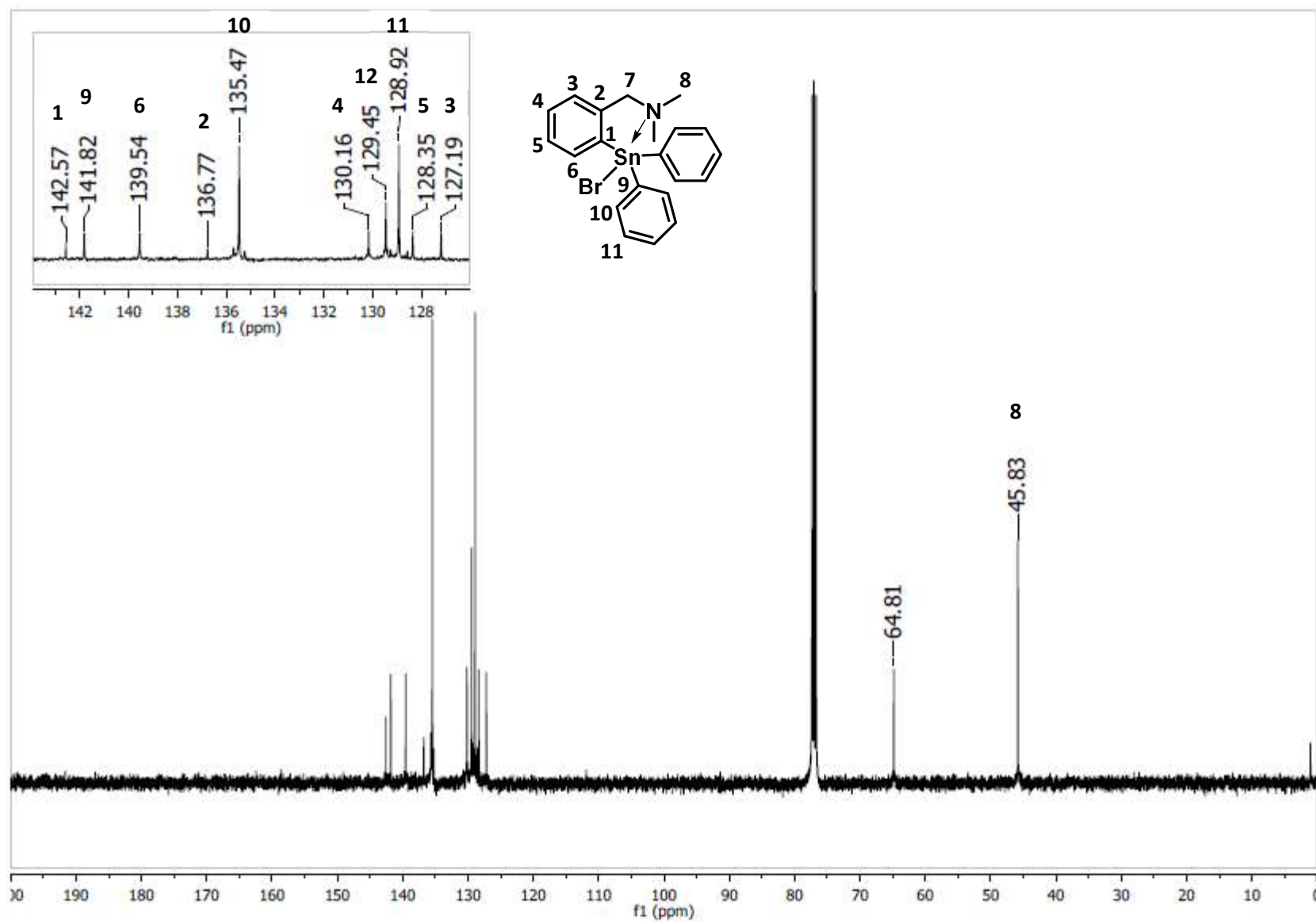
Figure A 24: ^{13}C NMR (CDCl$_3$) spectrum of [2-(CH$_2$N(CH$_3$)$_2$)C$_6$H$_4$]Ph$_2$SnBr.
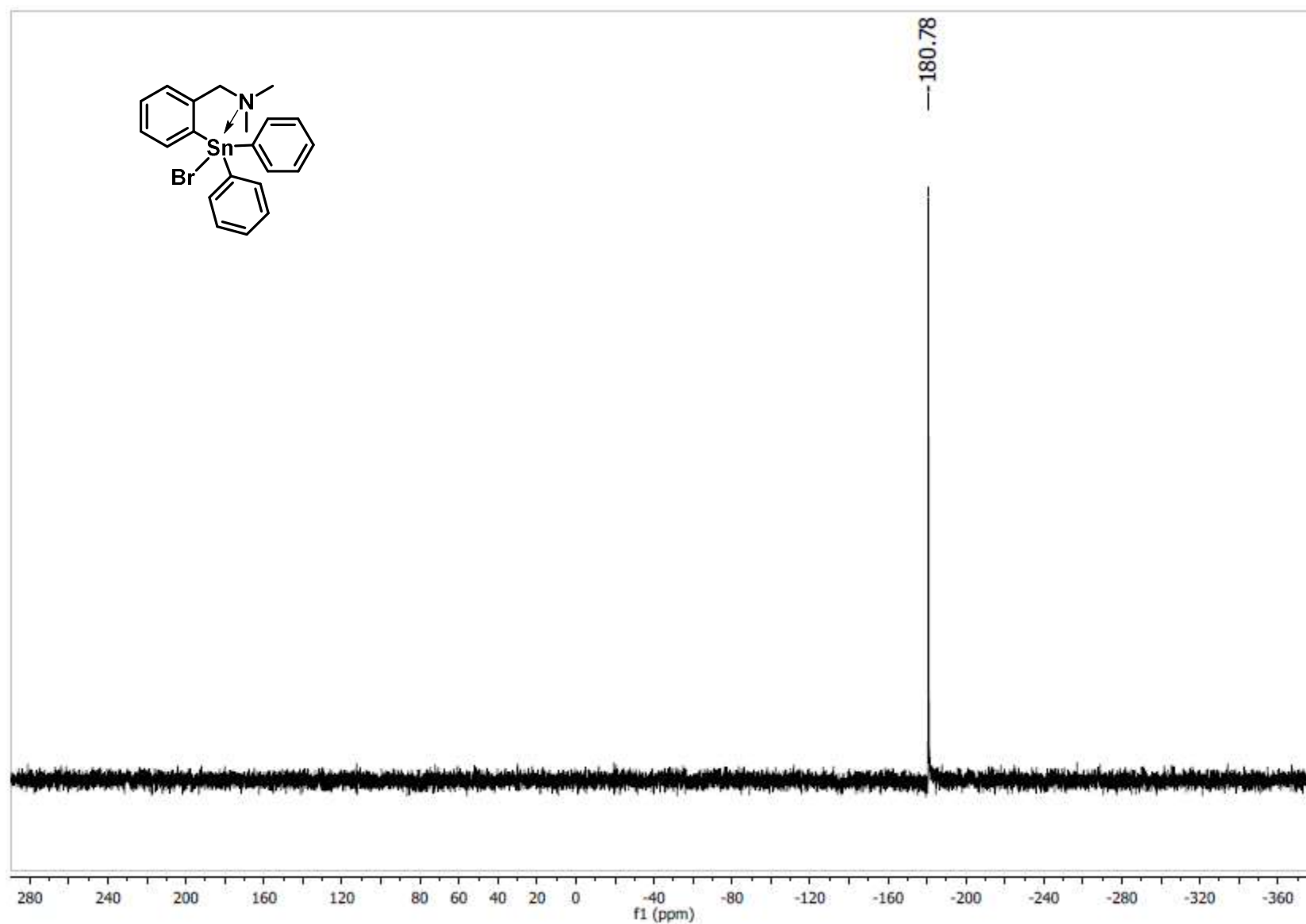
Figure A 25: ^{119}Sn NMR (CDCl$_3$) spectrum of [2-(CH$_2$N(CH$_3$)$_2$)C$_6$H$_4$]Ph$_2$SnBr.
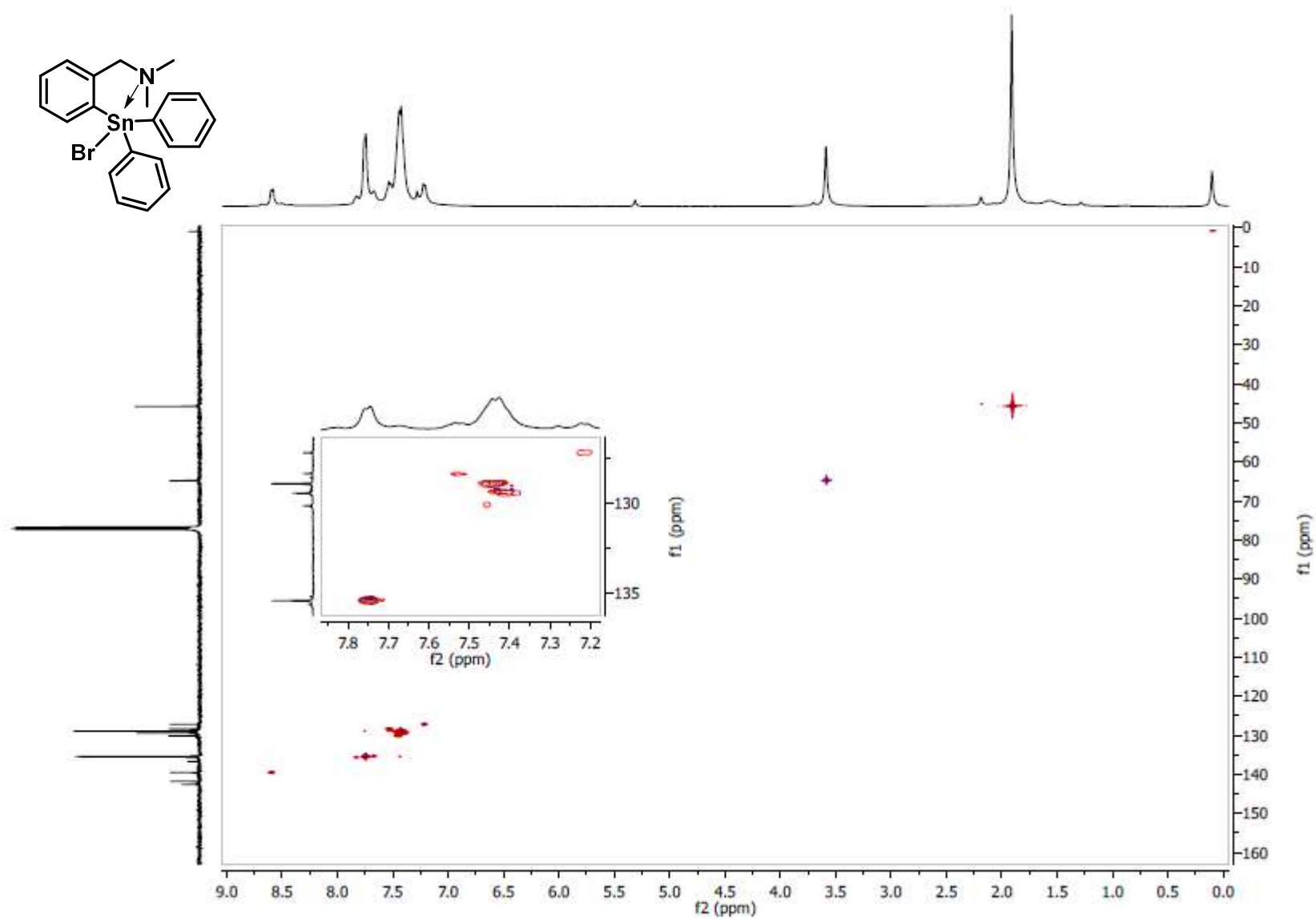
Figure A 26: 2D HSQC NMR (CDCl$_3$) spectrum of [2-(CH$_2$N(CH$_3$)$_2$)C$_6$H$_4$]Ph$_2$SnBr.
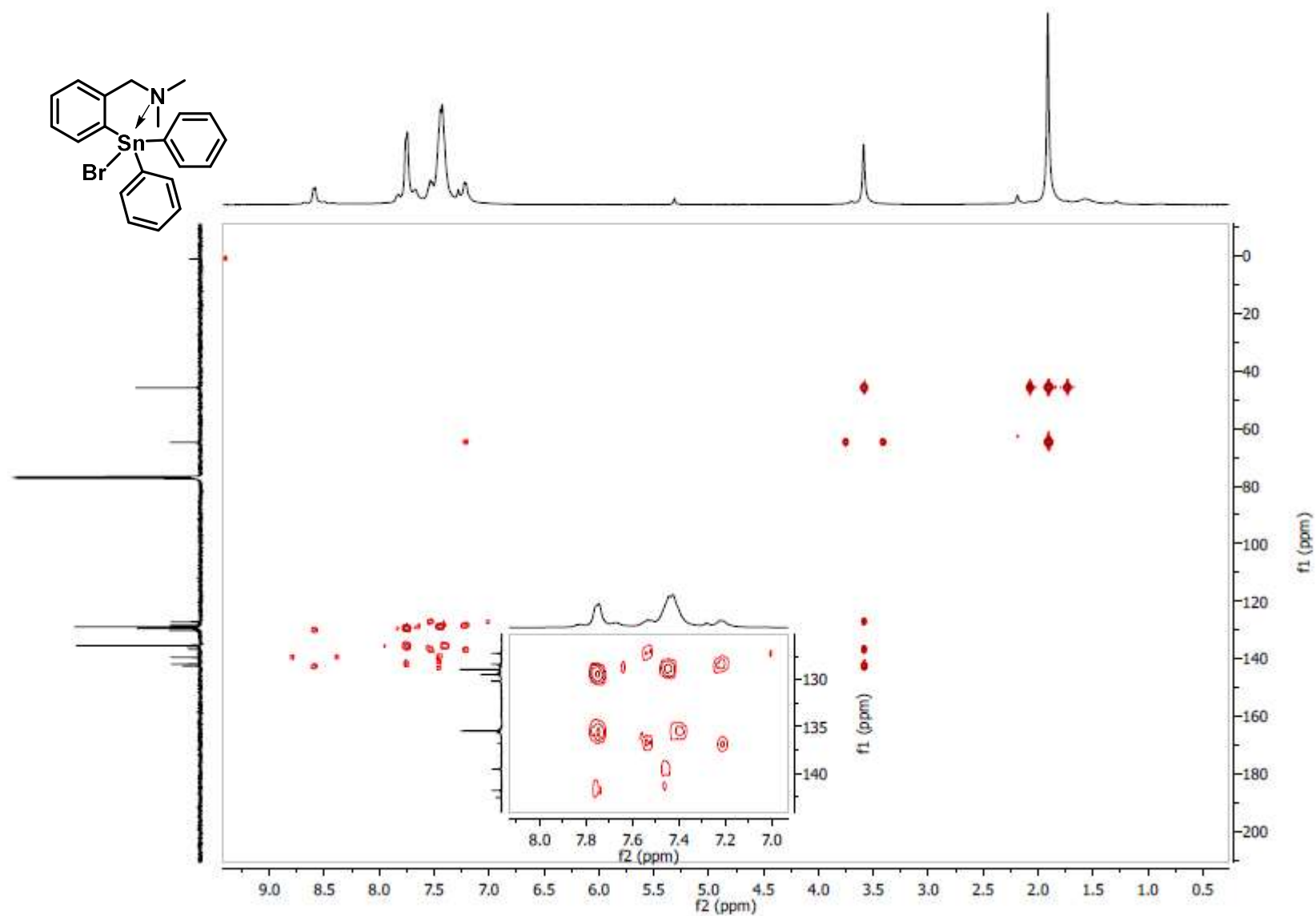
Figure A 27: 2D HMBC NMR (CDCl$_3$) spectrum of [2-(CH$_2$N(CH$_3$)$_2$)C$_6$H$_4$]Ph$_2$SnBr.
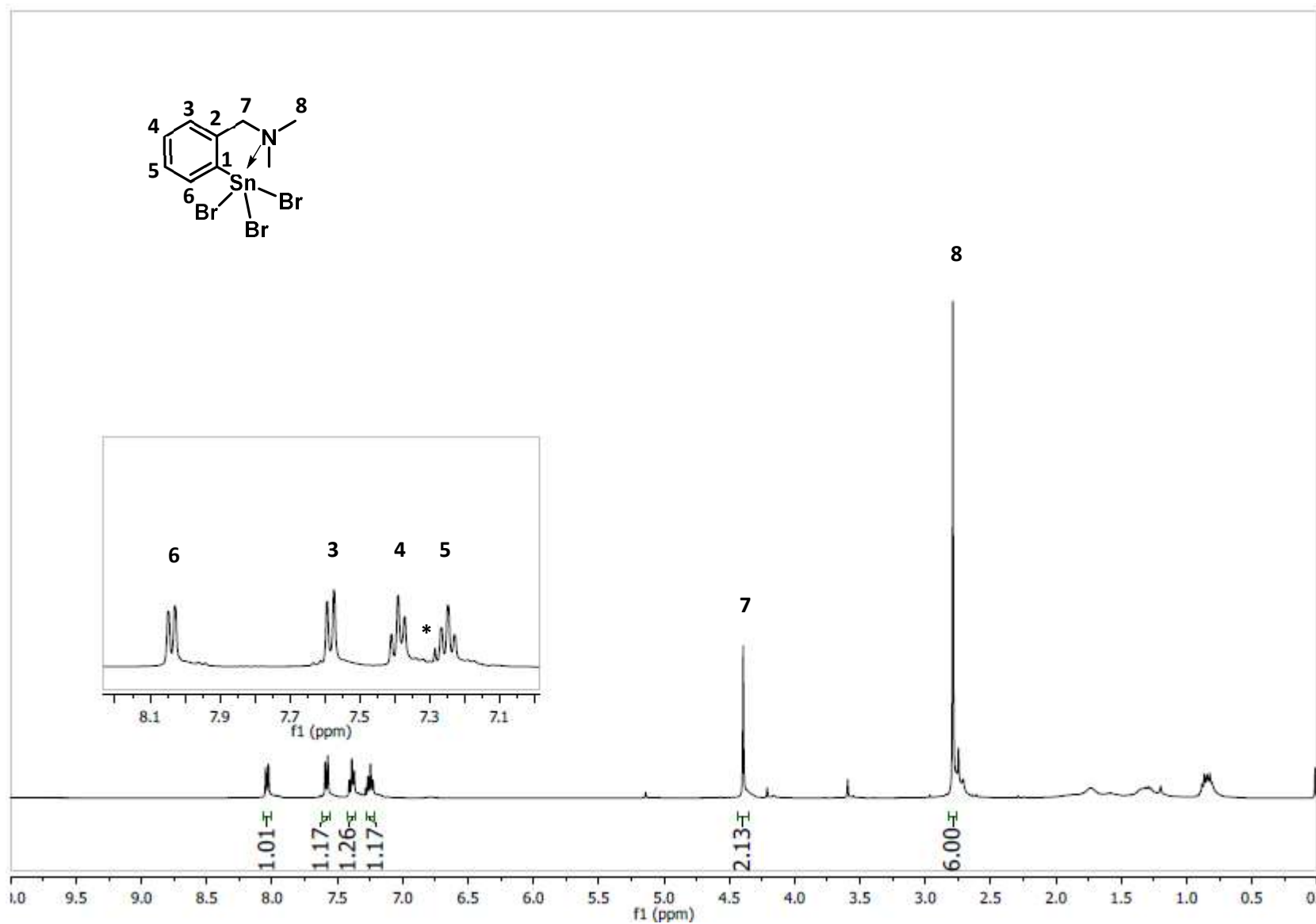
Figure A 28: ^1H NMR (CDCl$_3$) spectrum of [2-(CH$_2$N(CH$_3$)$_2$)C$_6$H$_4$]SnBr$_3$.
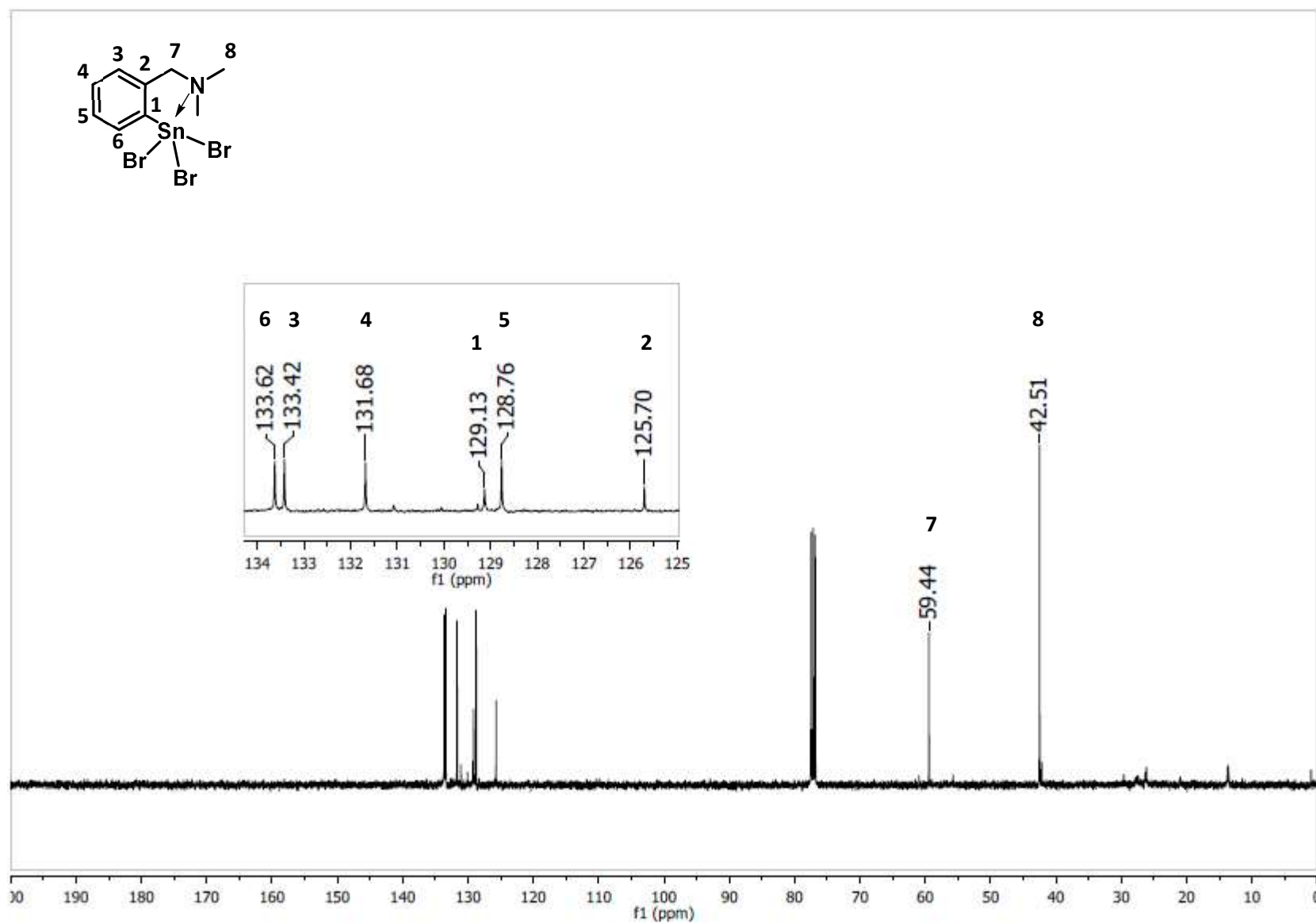
Figure A 29: ^{13}C NMR (CDCl$_3$) spectrum of [2-(CH$_2$N(CH$_3$)$_2$)C$_6$H$_4$]SnBr$_3$.
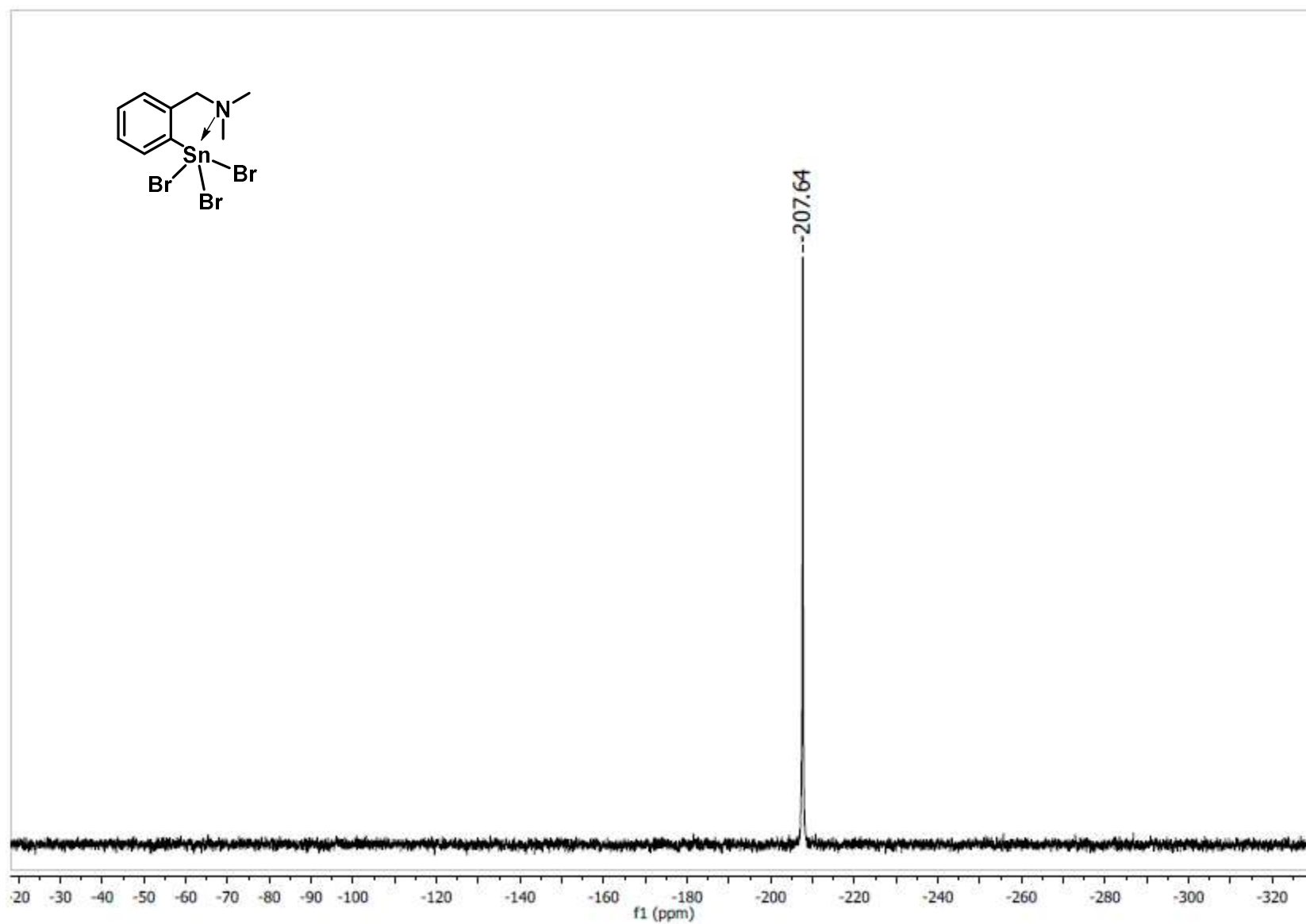
Figure A 30: ^{119}Sn NMR (CDCl$_3$) spectrum of [2-(CH$_2$N(CH$_3$)$_2$)C$_6$H$_4$]SnBr$_3$.
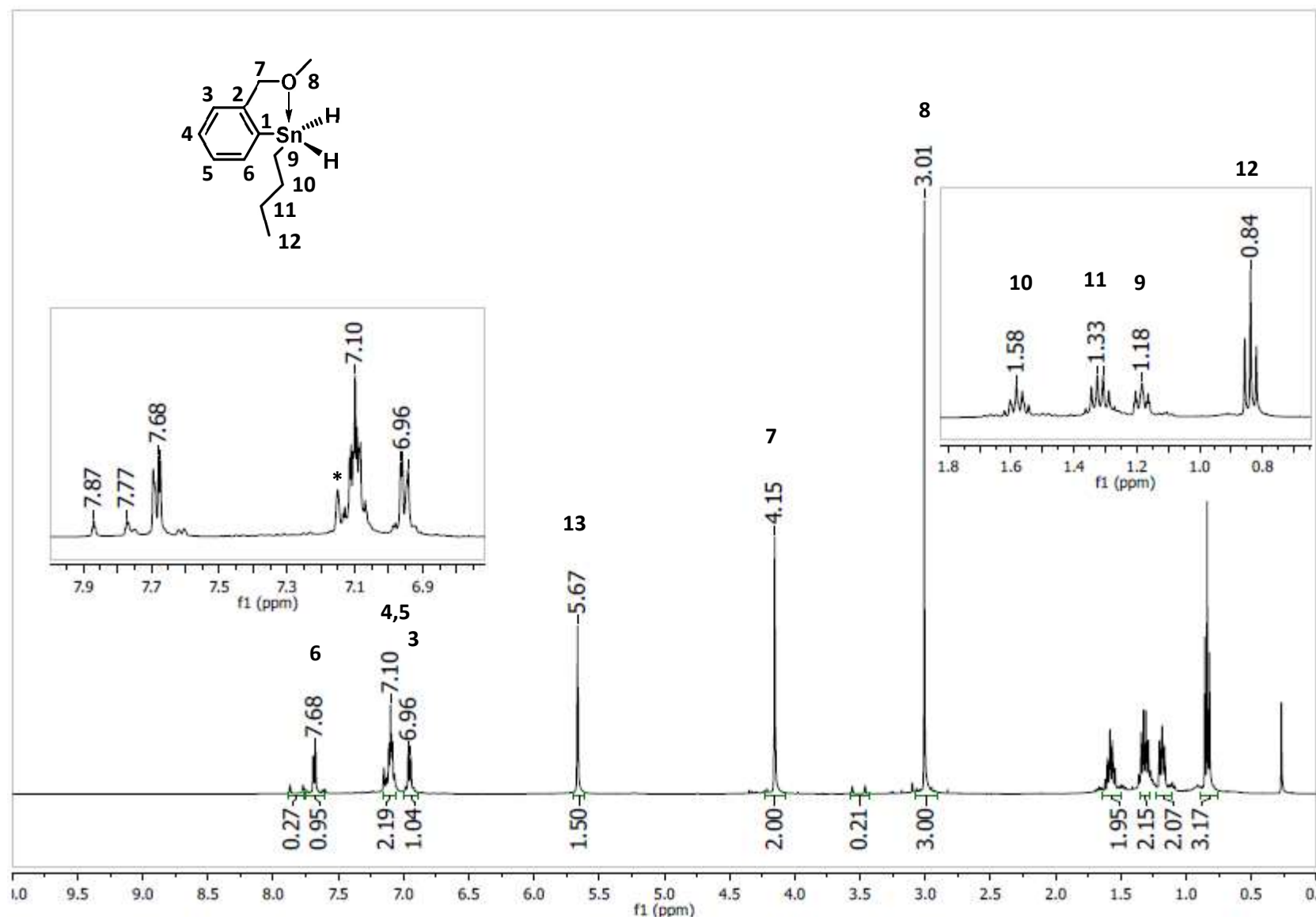
Figure A 31: ^1H NMR (C_6D_6) spectrum of [2-(CH_2OCH_3)C_6H_4](n-Bu)SnH_2.
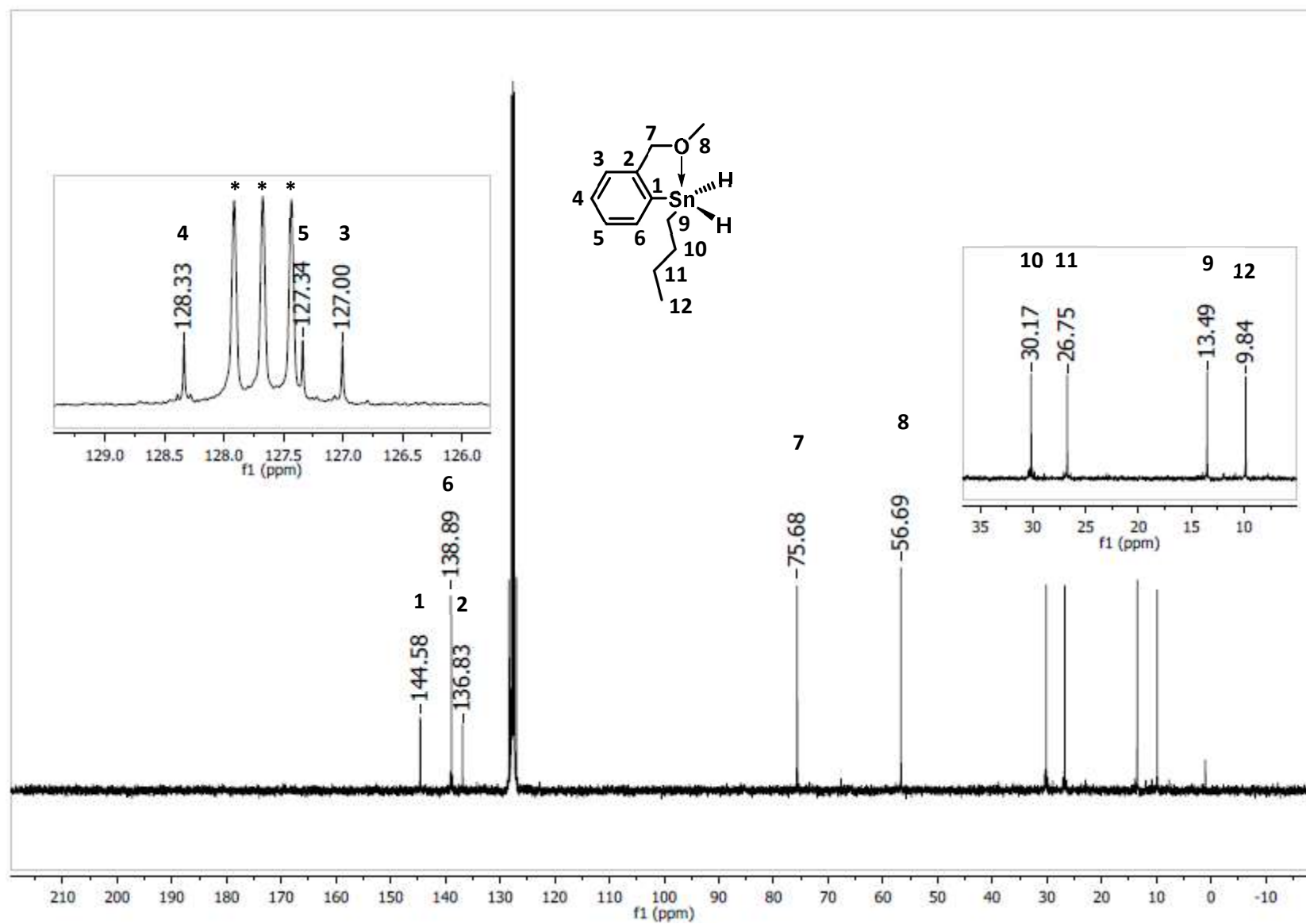
Figure A 32: ^{13}C NMR (C$_6$D$_6$) spectrum of [2-(CH$_2$OCH$_3$)C$_6$H$_4$](n-Bu)SnH$_2$.
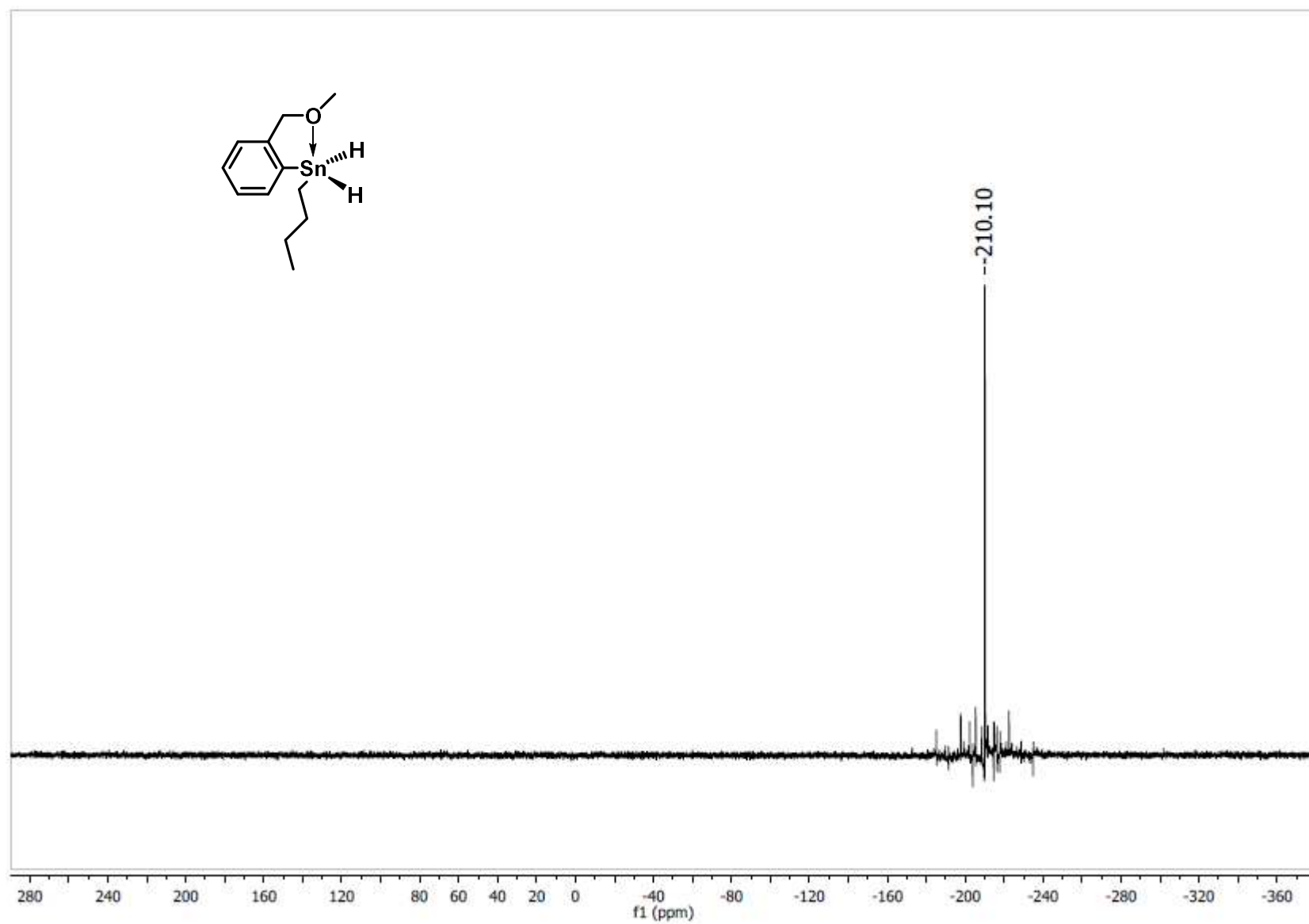
Figure A 33: ^{119}Sn NMR (C$_6$D$_6$) spectrum of [2-(CH$_2$OCH$_3$)C$_6$H$_4$](n-Bu)SnH$_2$.
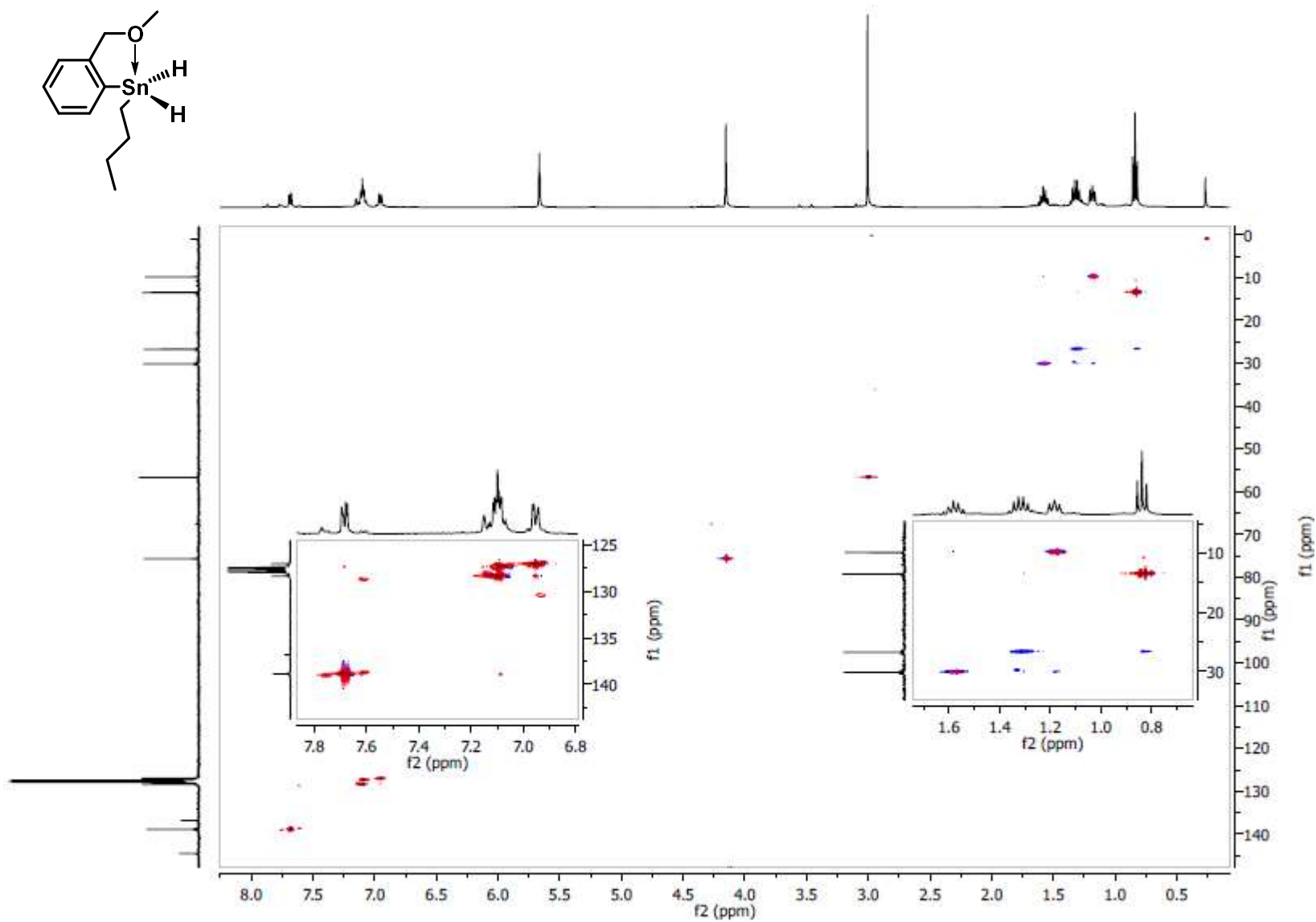
Figure A 34: 2D HSQC NMR (C_6D_6) spectrum of $[2\text{-}(CH_2OCH_3)C_6H_4](n\text{-Bu})SnH_2$.
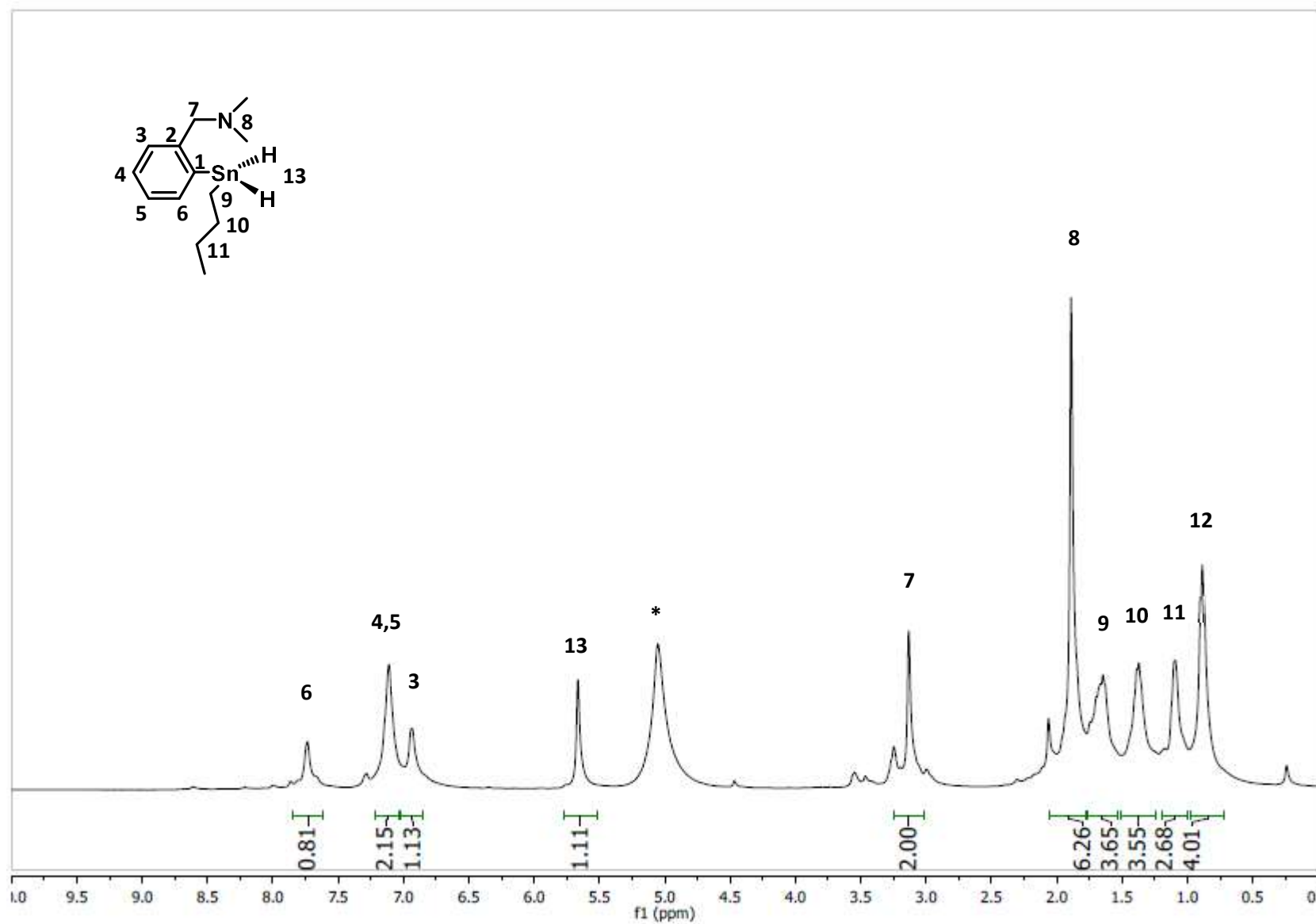
Figure A 35: ^{1}H NMR (C_6D_6) spectrum of [2-($CH_2N(CH_3)_2$)C_6H_4](n-Bu)SnH$_2$.
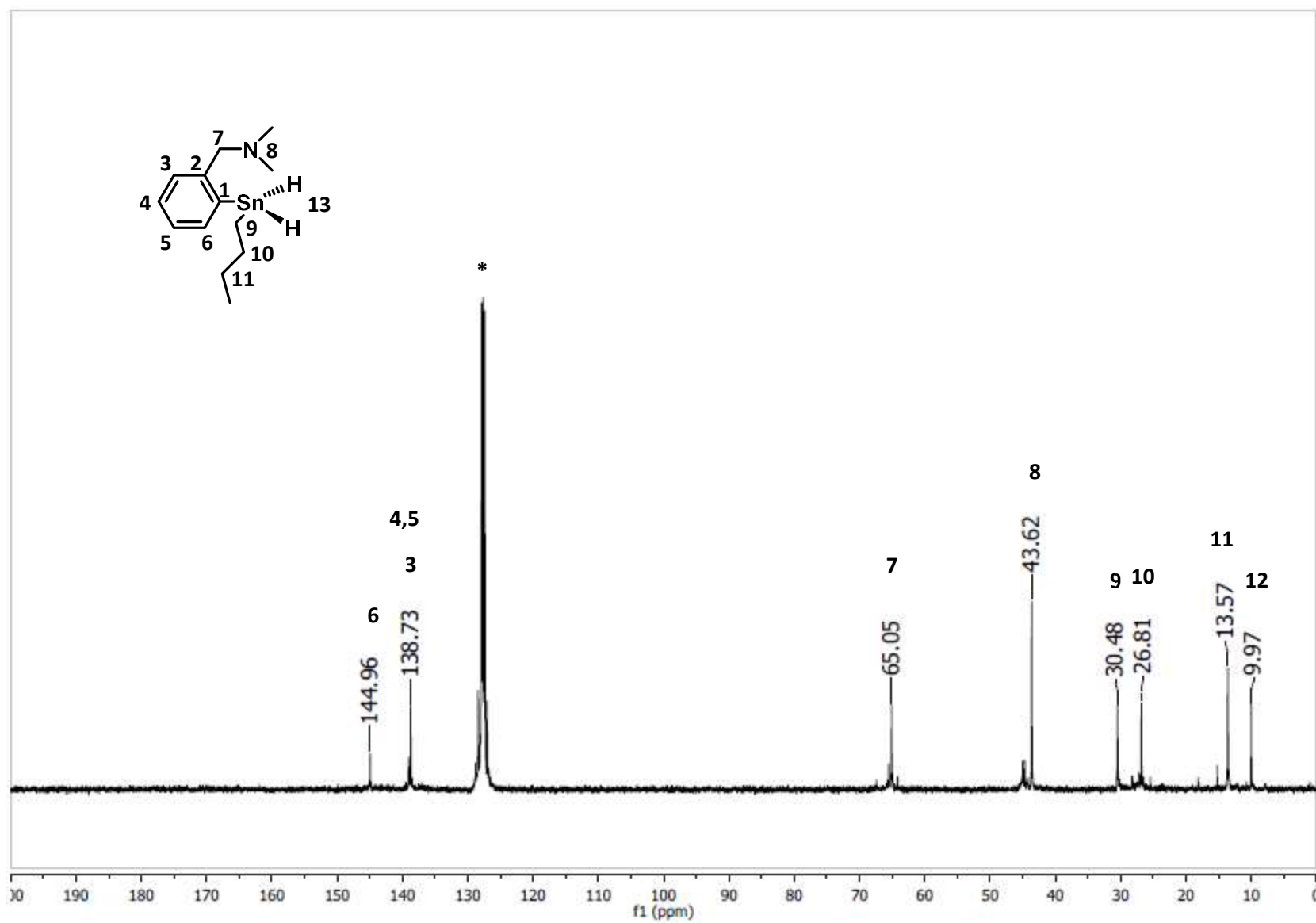
Figure A 36: ^{13}C NMR (C_6D_6) spectrum of $[2\text{-}(CH_2N(CH_3)_2)C_6H_4](n\text{-}Bu)SnH_2$.
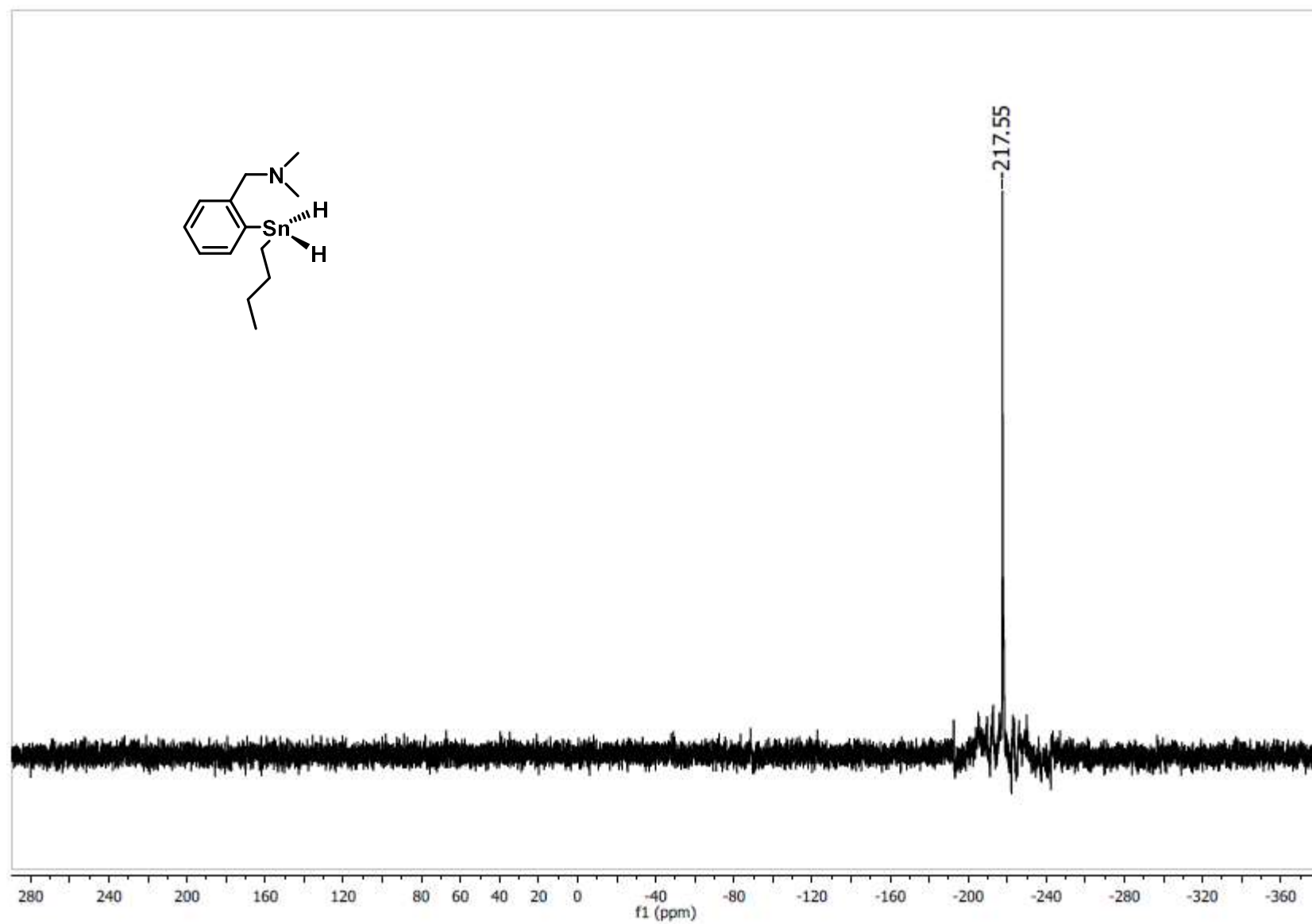
Figure A 37: ^{119}Sn NMR (C_6D_6) spectrum of [2-($CH_2N(CH_3)_2$)C_6H_4](n-Bu)SnH$_2$.
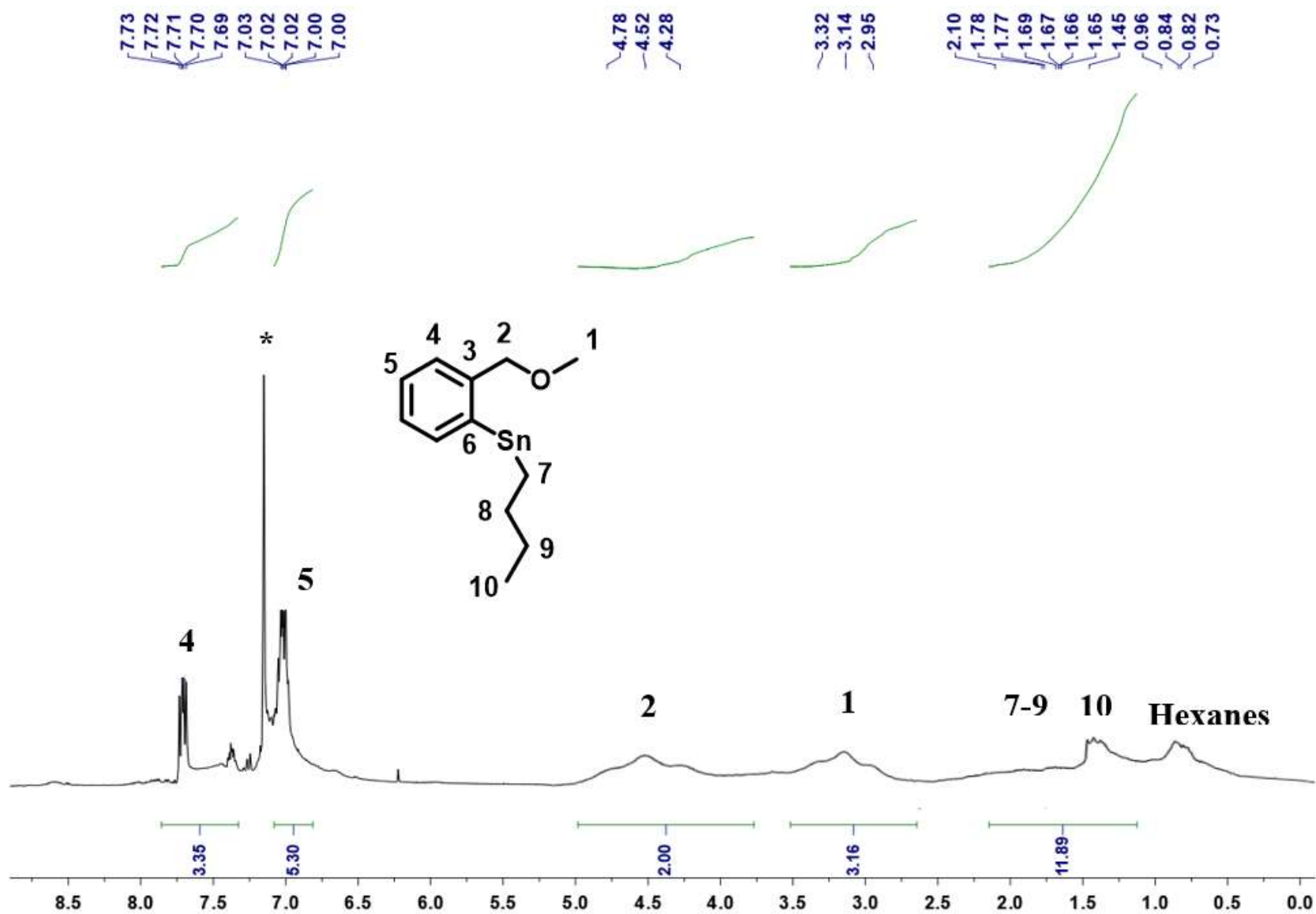
Figure A 38: ^{1}H NMR (C_6D_6) spectrum of poly([2-(CH_2OCH_3)C_6H_4](n-Bu)Sn).
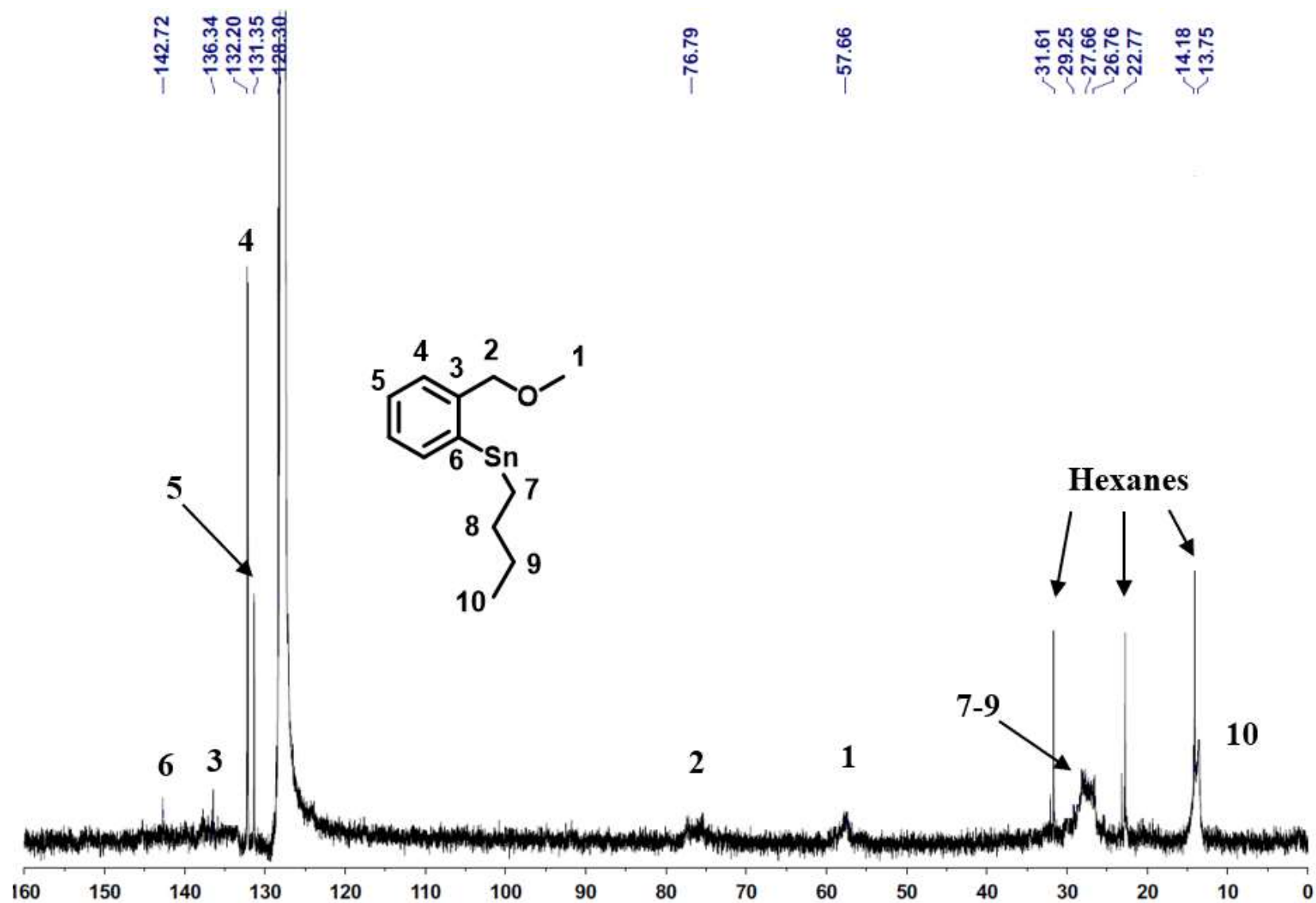
Figure A 39: ^{13}C NMR (C_6D_6) spectrum of poly([2-(CH_2OCH_3)C_6H_4](n-Bu)Sn).
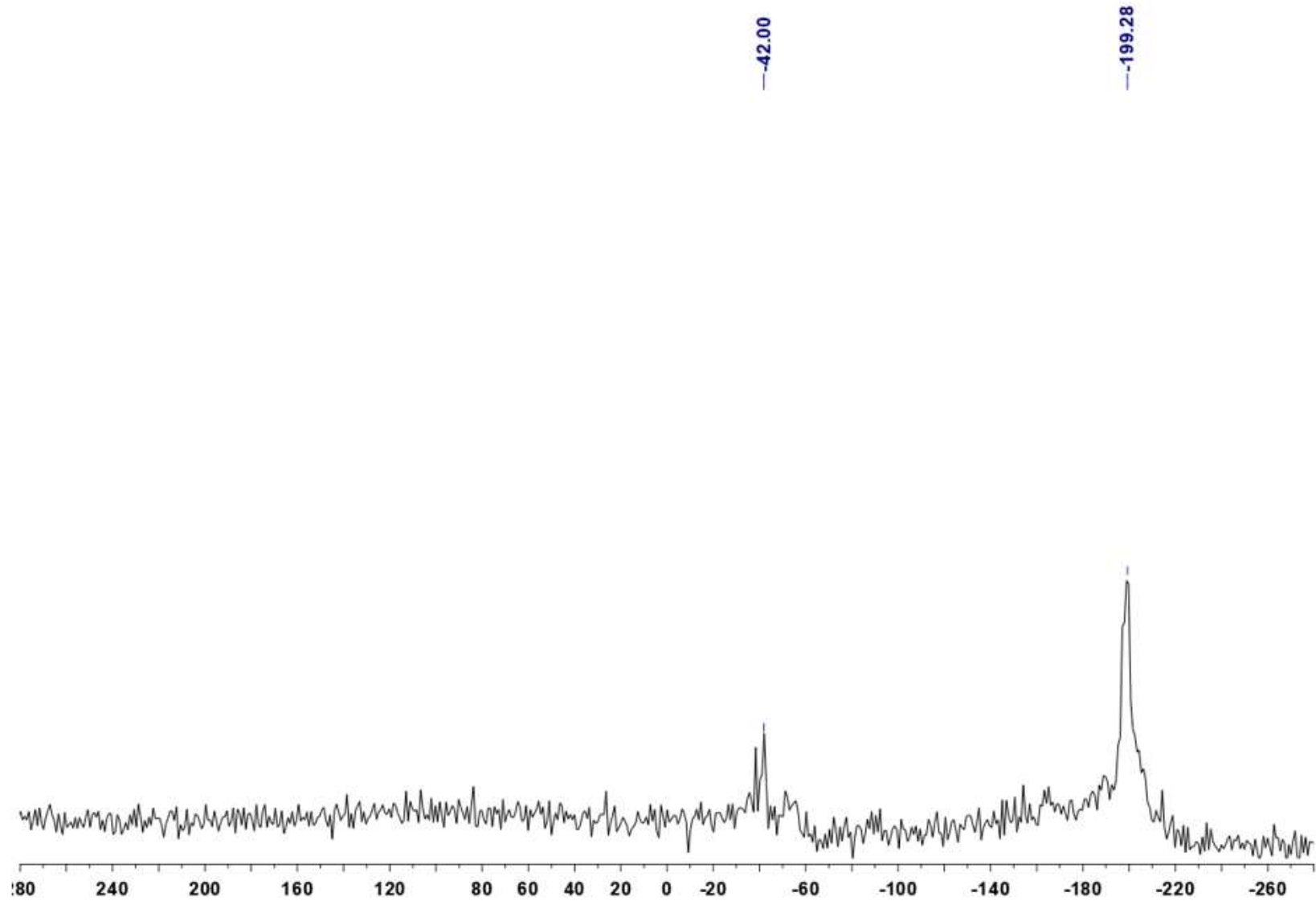
Figure A 40: ^{119}Sn NMR (C$_6$D$_6$) spectrum of poly([2-(CH$_2$OCH$_3$)C$_6$H$_4$](n-Bu)Sn).
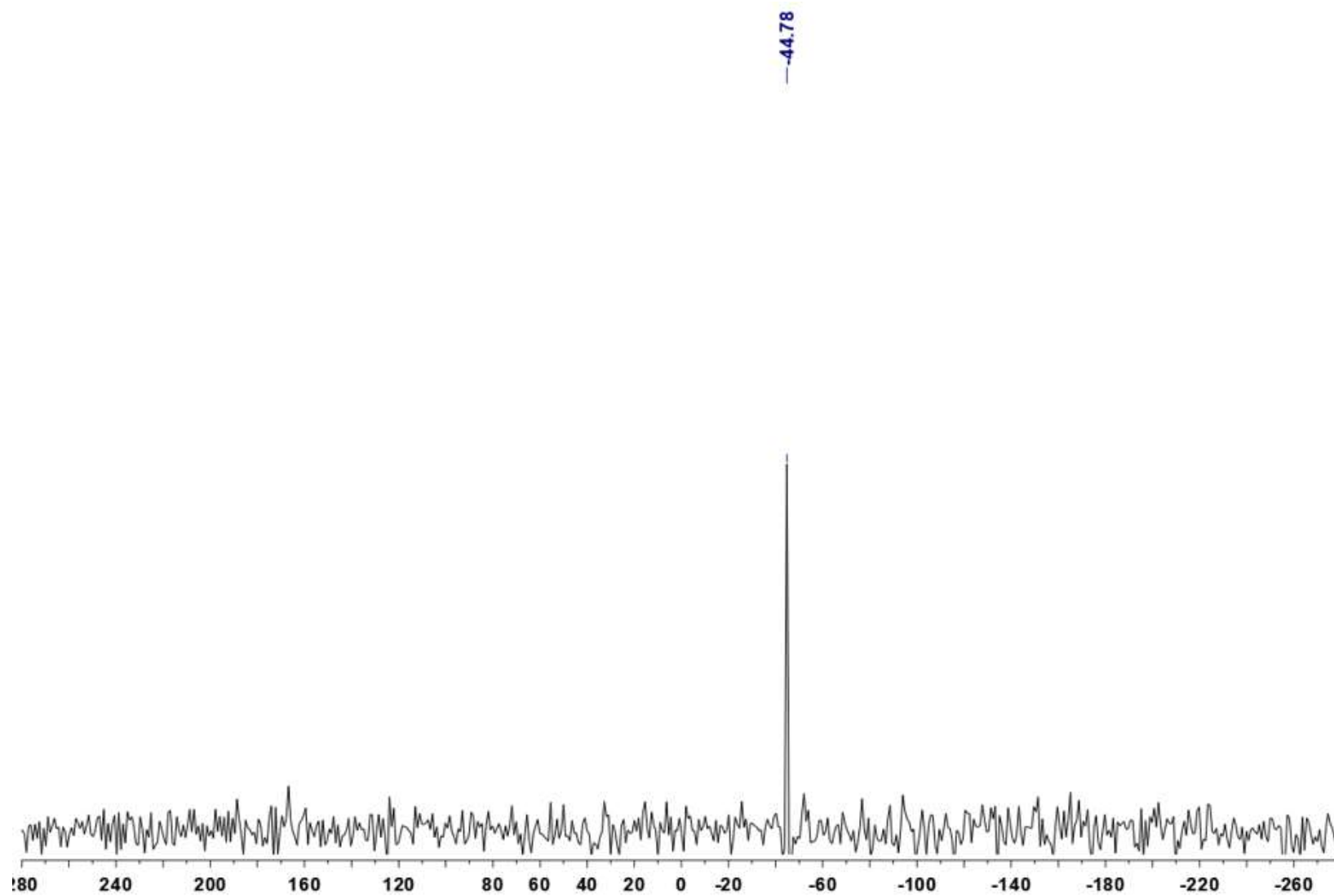
Figure A 41: ^{119}Sn NMR (THF-d$_8$) spectrum of poly([2-(CH$_2$OCH$_3$)C$_6$H$_4$](*n*-Bu)Sn).
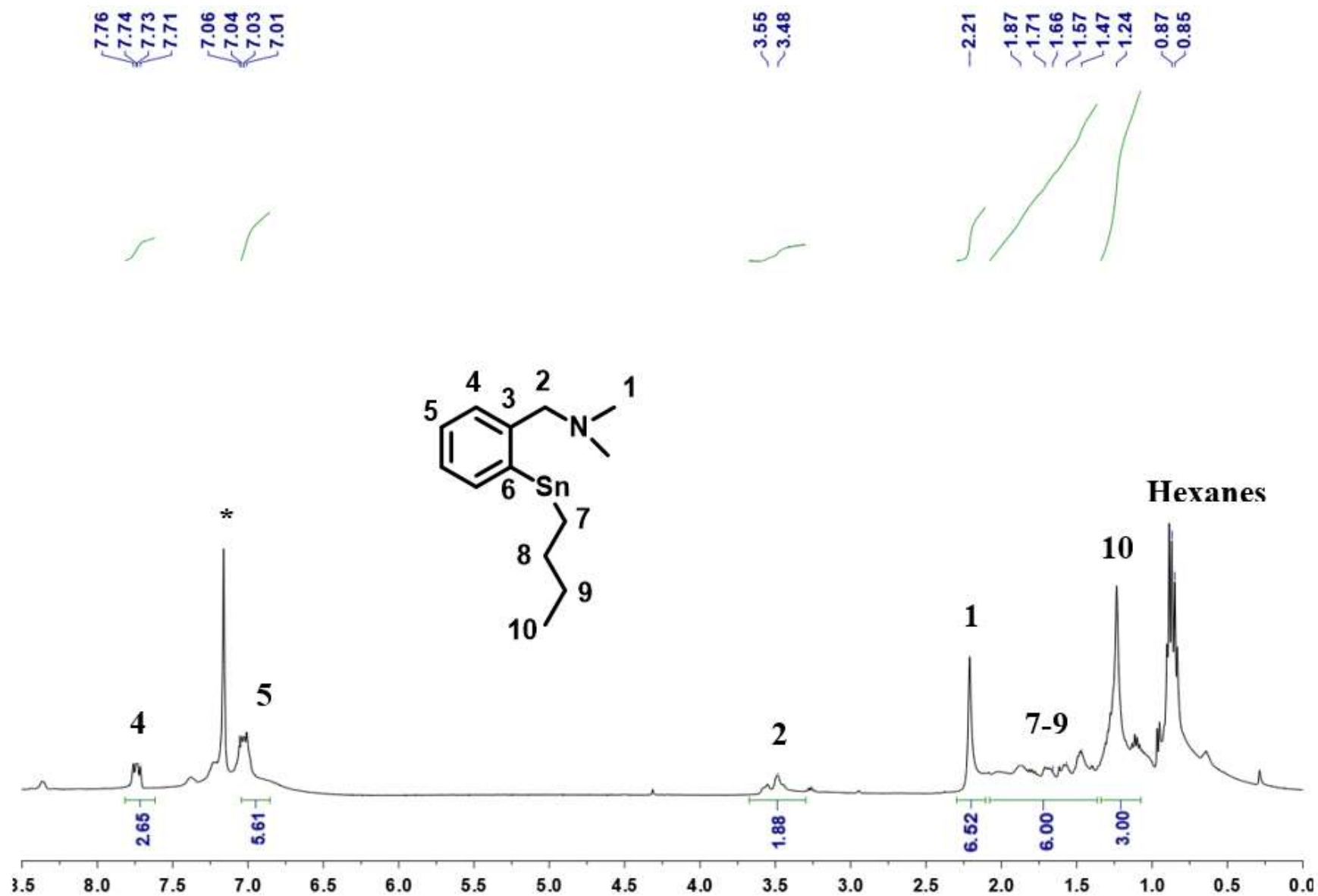
Figure A 42: ^{1}H NMR (C_6D_6) spectrum of poly([2-($CH_2N(CH_3)_2$)C_6H_4](n-Bu)Sn).
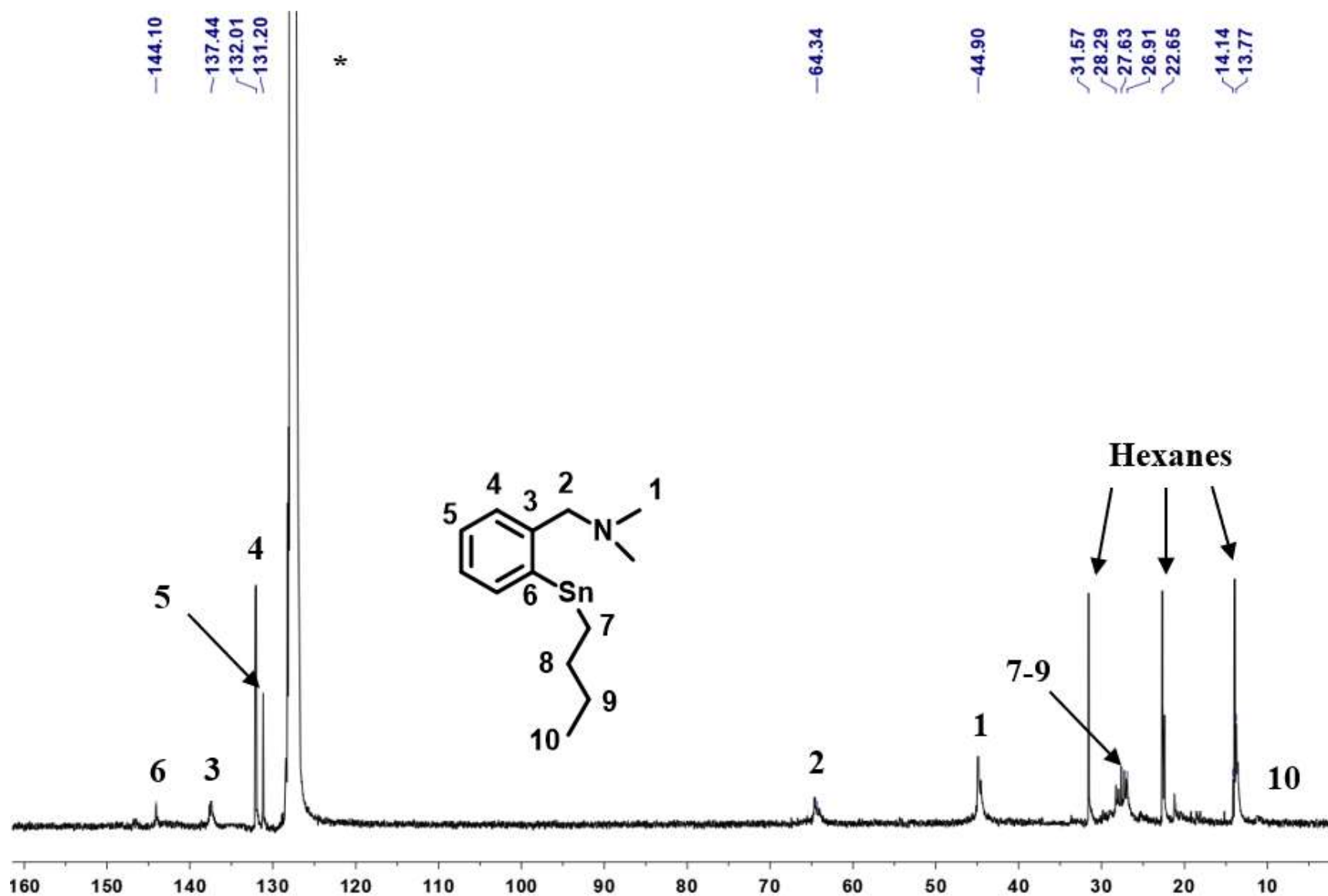
Figure A 43: ^{13}C NMR (C_6D_6) spectrum of poly([2-($CH_2N(CH_3)_2$)C_6H_4](n-Bu)Sn).
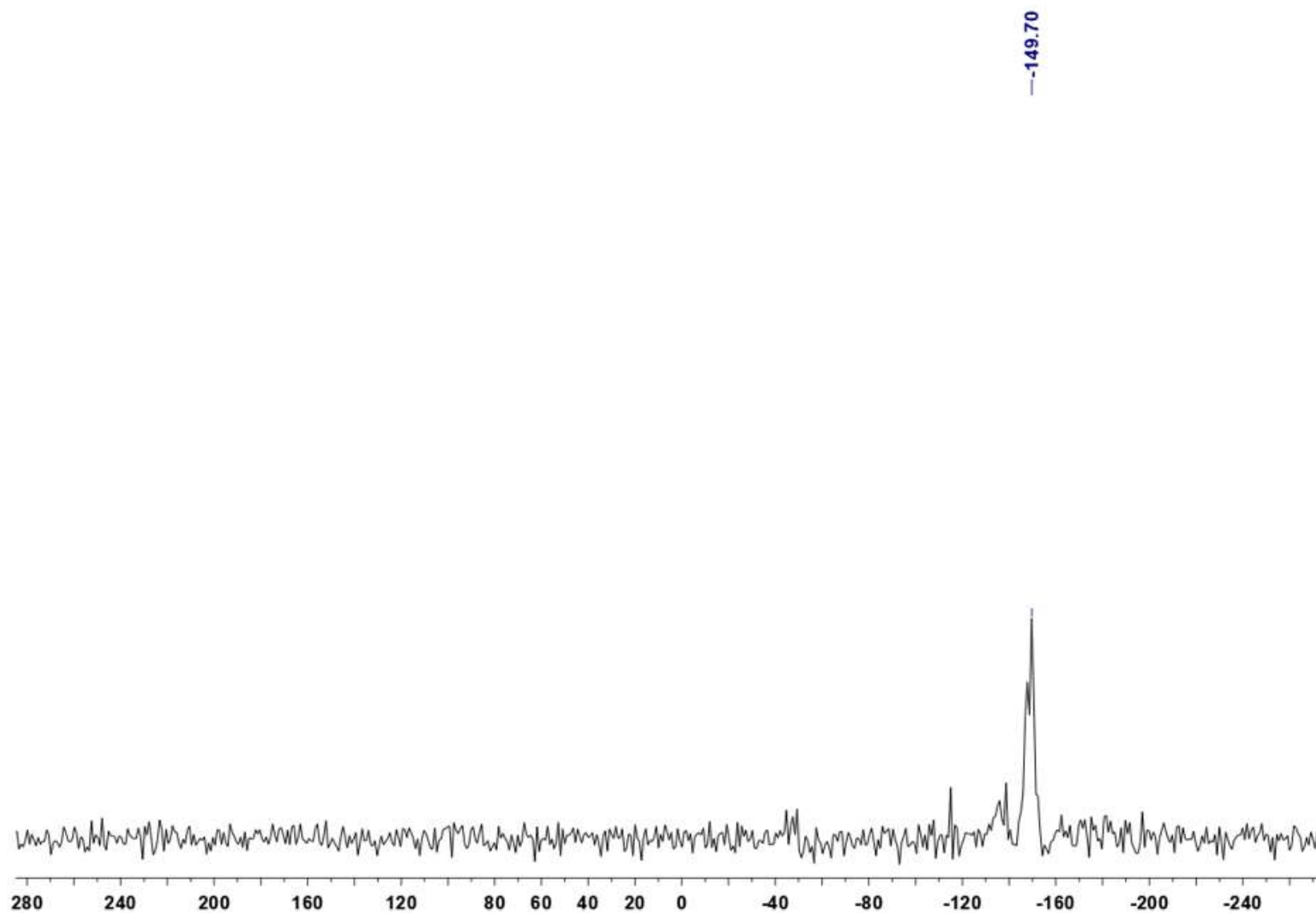
Figure A 44: ^{119}Sn NMR (C$_6$D$_6$) spectrum of poly([2-(CH$_2$N(CH$_3$)$_2$)C$_6$H$_4$](*n*-Bu)Sn).
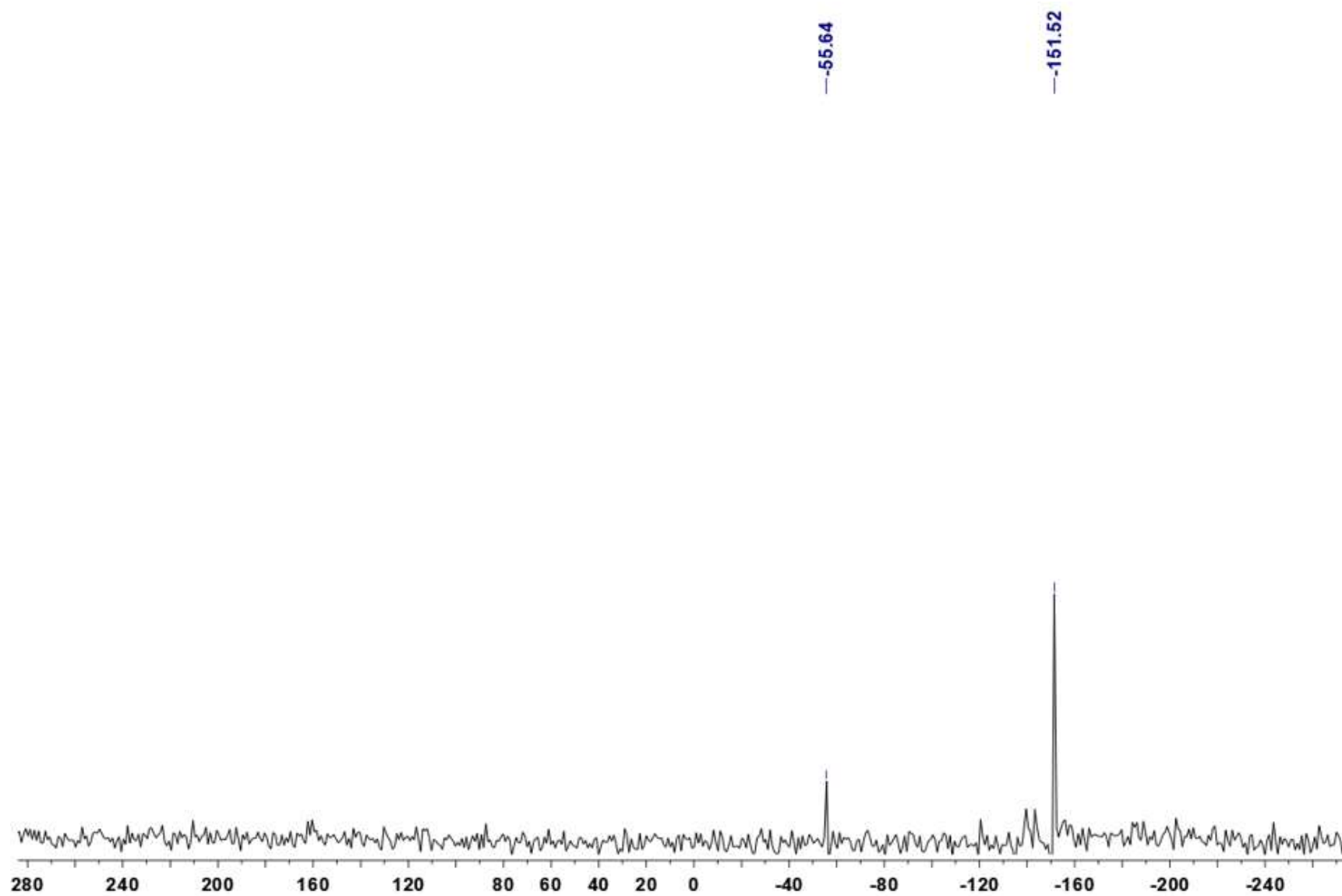
Figure A 45: ^{119}Sn NMR (THF-d$_8$) spectrum of poly([2-(CH$_2$N(CH$_3$)$_2$)C$_6$H$_4$](n-Bu)Sn).
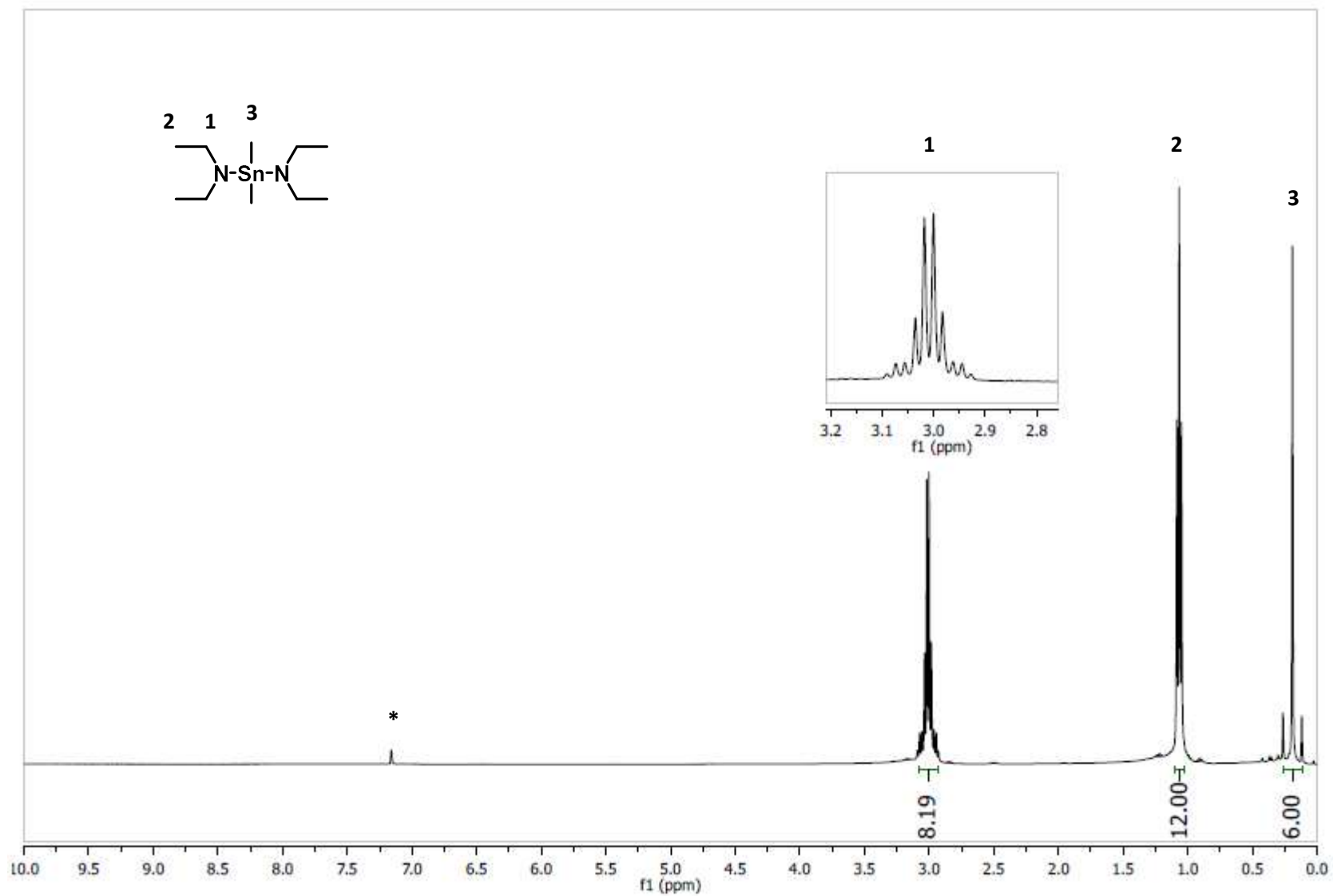
Figure A 46: ^{1}H NMR (C_6D_6) spectrum of $(CH_3)_2Sn(NEt_2)_2$.

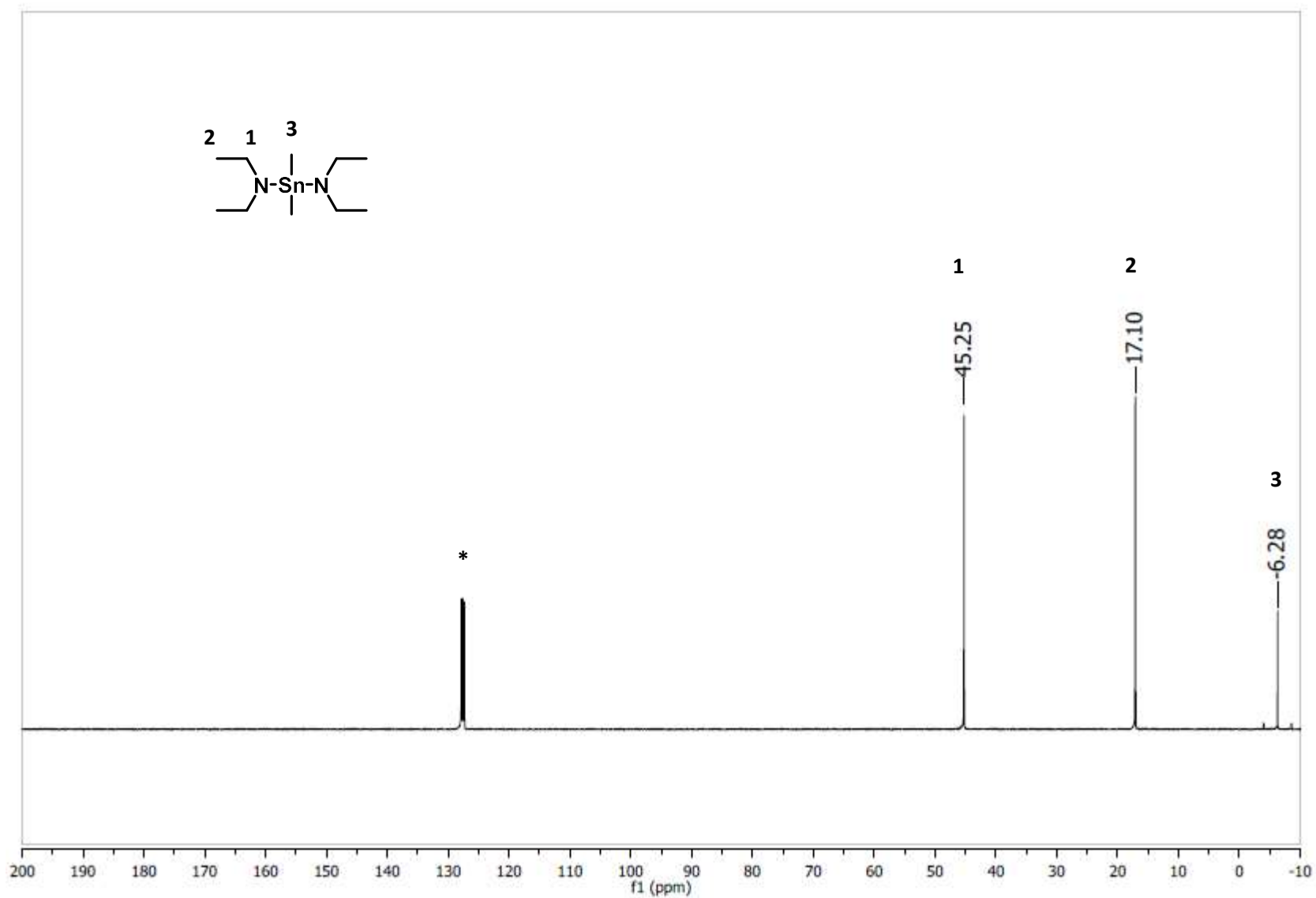**Figure A 47**: ^{13}C NMR (C_6D_6) spectrum of $(CH_3)_2Sn(NEt_2)_2$.
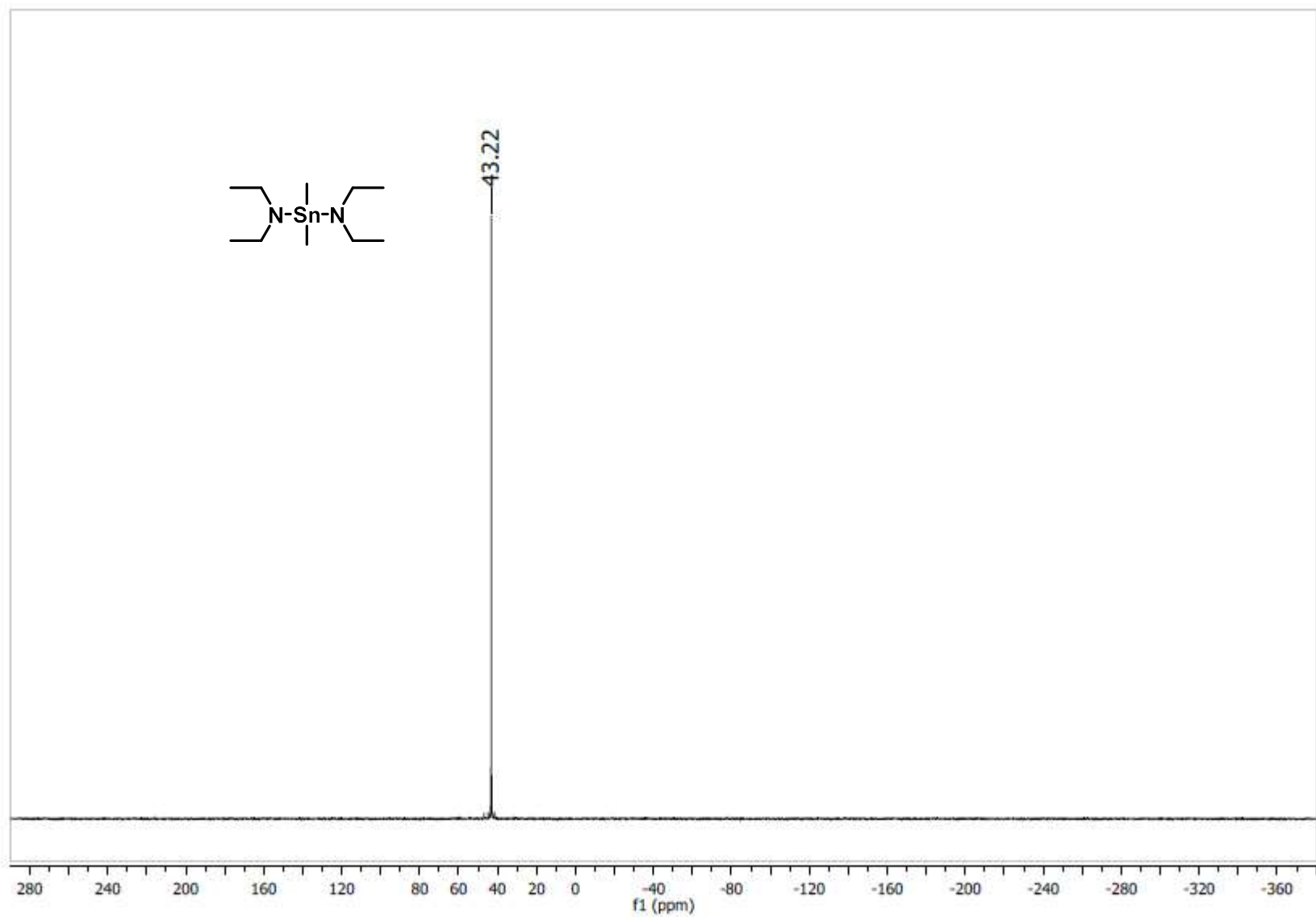
Figure A 48: ^{119}Sn NMR (C_6D_6) spectrum of $(CH_3)_2Sn(NEt_2)_2$.
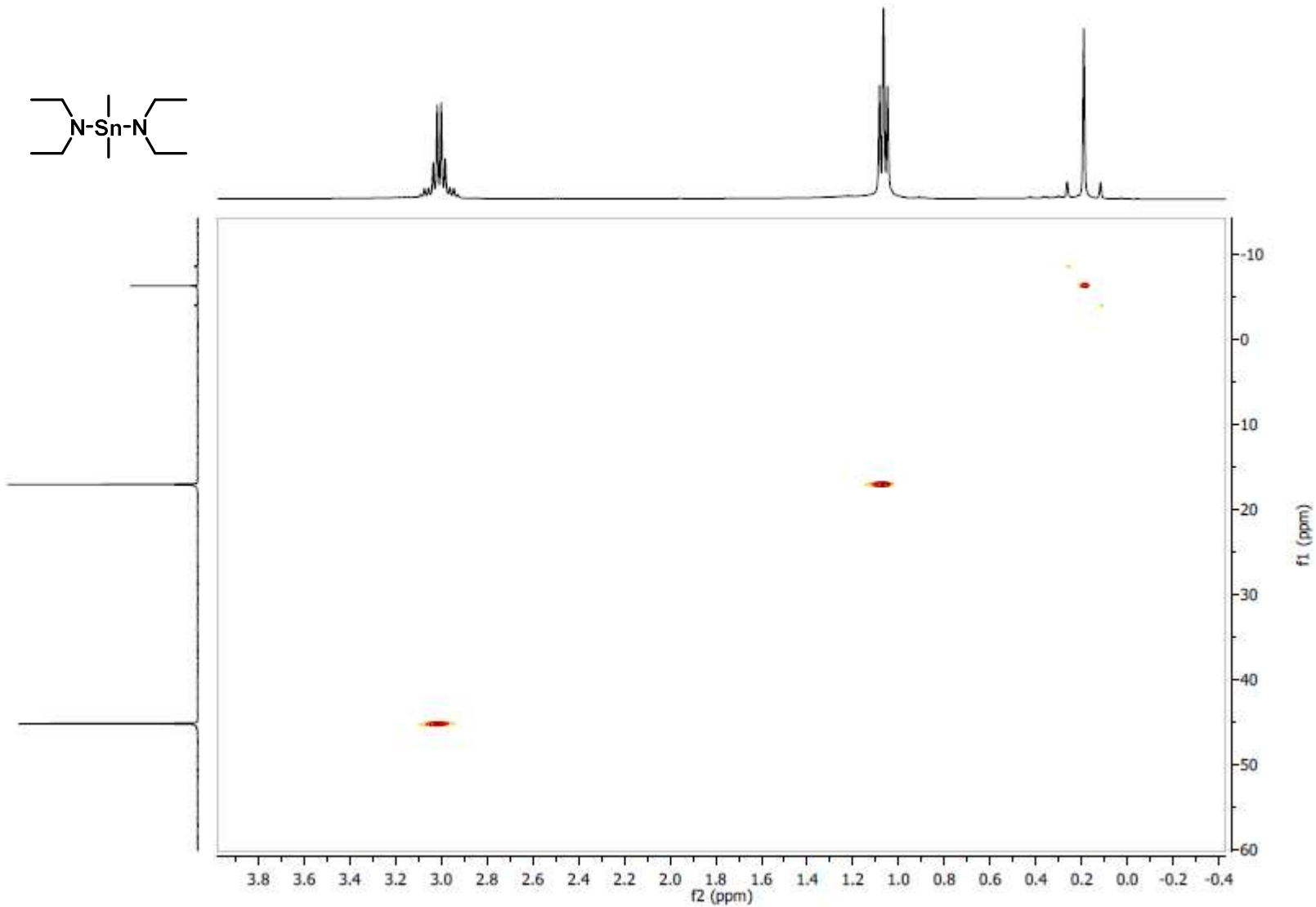
Figure A 49: 2D HSQC NMR (C$_6$D$_6$) spectrum of (CH$_3$)$_2$Sn(NEt$_2$)$_2$.
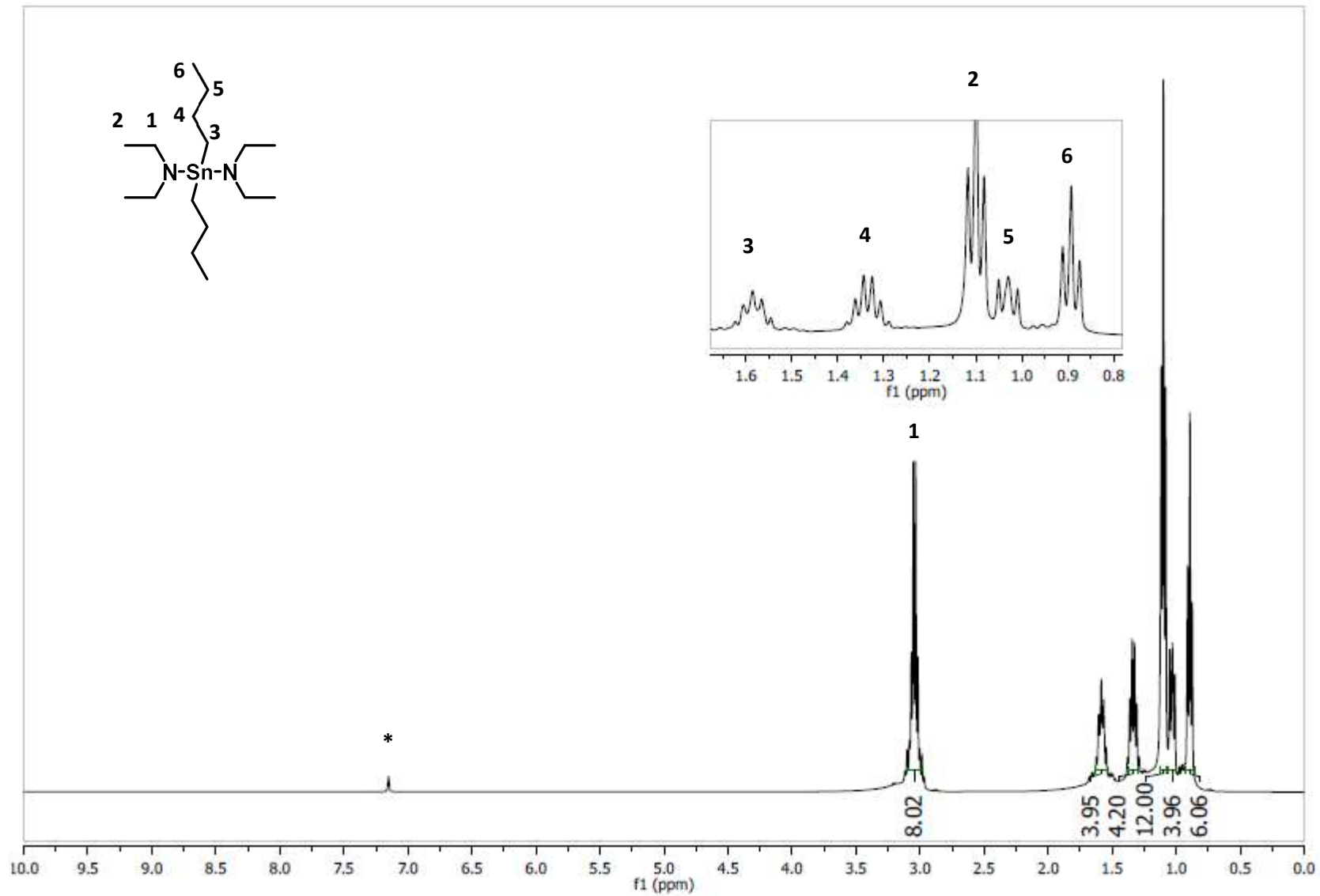
Figure A 50: ^1H NMR (C_6D_6) spectrum of (n-Bu)$_2$Sn(NEt$_2$)$_2$.
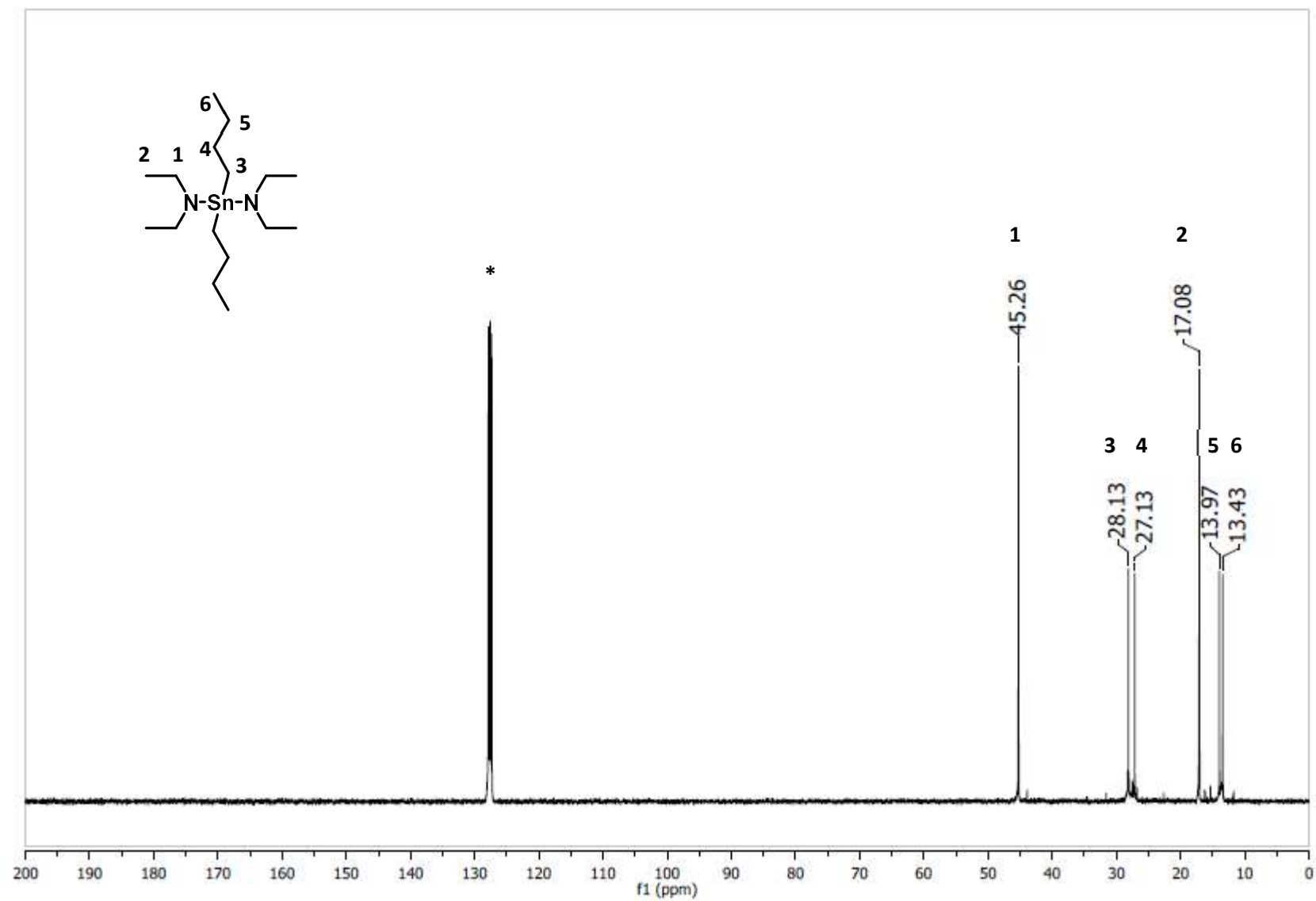
Figure A 51: ^{13}C NMR (C$_6$D$_6$) spectrum of (*n*-Bu)$_2$Sn(NEt$_2$)$_2$.
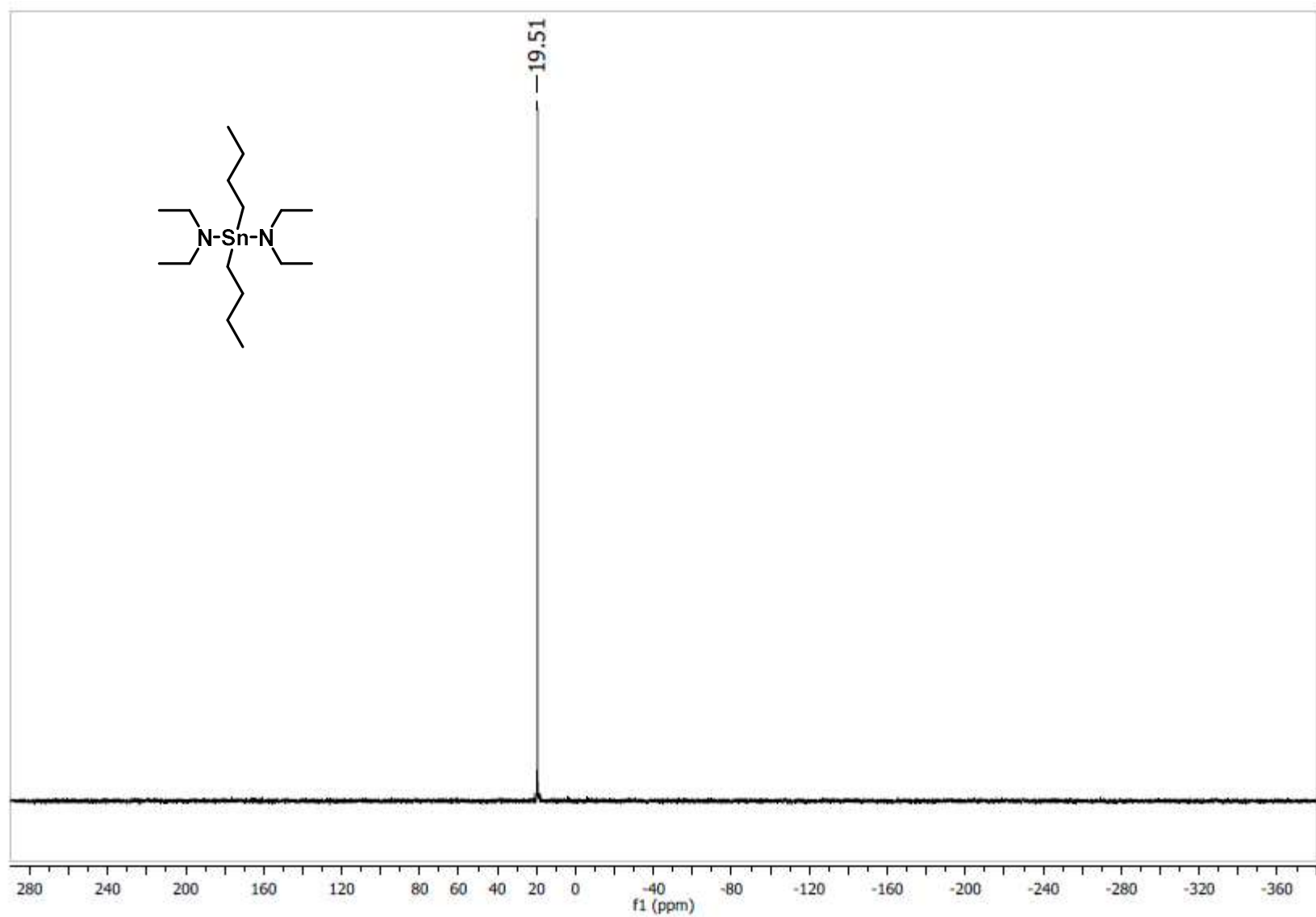
Figure A 52: ^{119}Sn NMR (C$_6$D$_6$) spectrum of (*n*-Bu)$_2$Sn(NEt$_2$)$_2$.
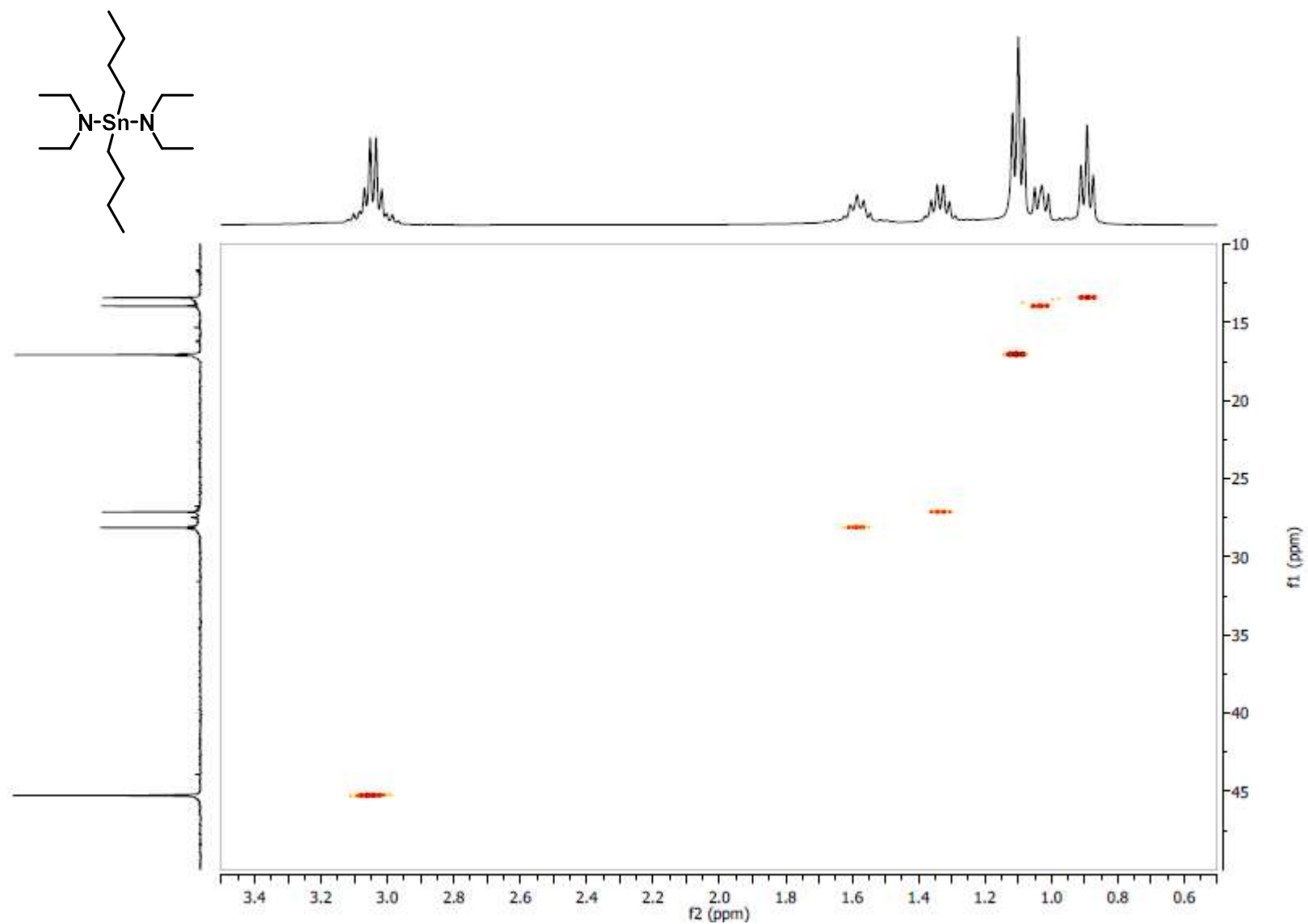
Figure A 53: 2D HSQC NMR (C_6D_6) spectrum of (n-Bu)$_2$Sn(NEt$_2$)$_2$.
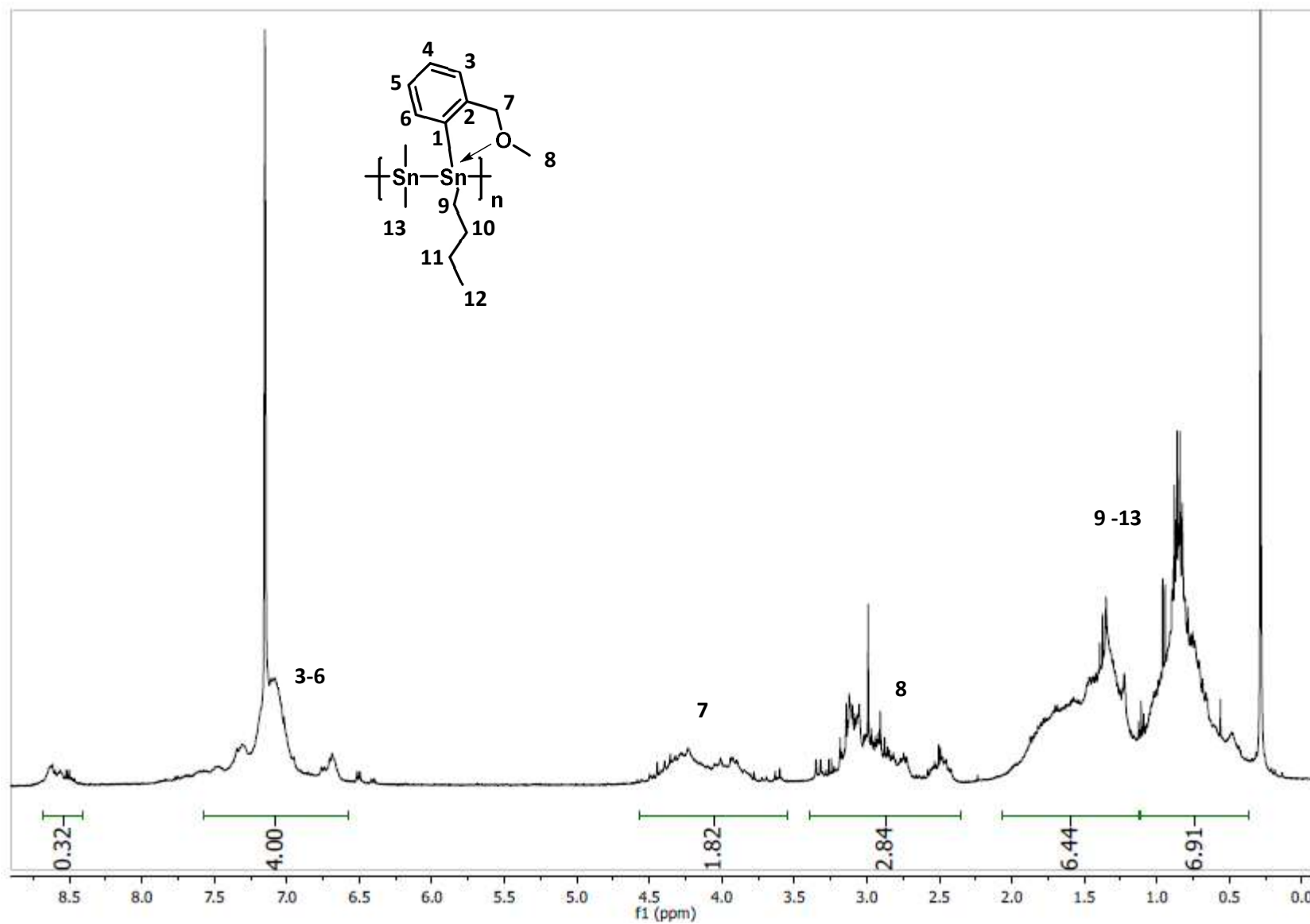
Figure A 54: ^{1}H NMR (C$_6$D$_6$) spectrum of attempted poly([2-(CH$_2$OCH$_3$)C$_6$H$_4$](*n*-Bu)]-alt-(CH$_3$)$_2$Sn).
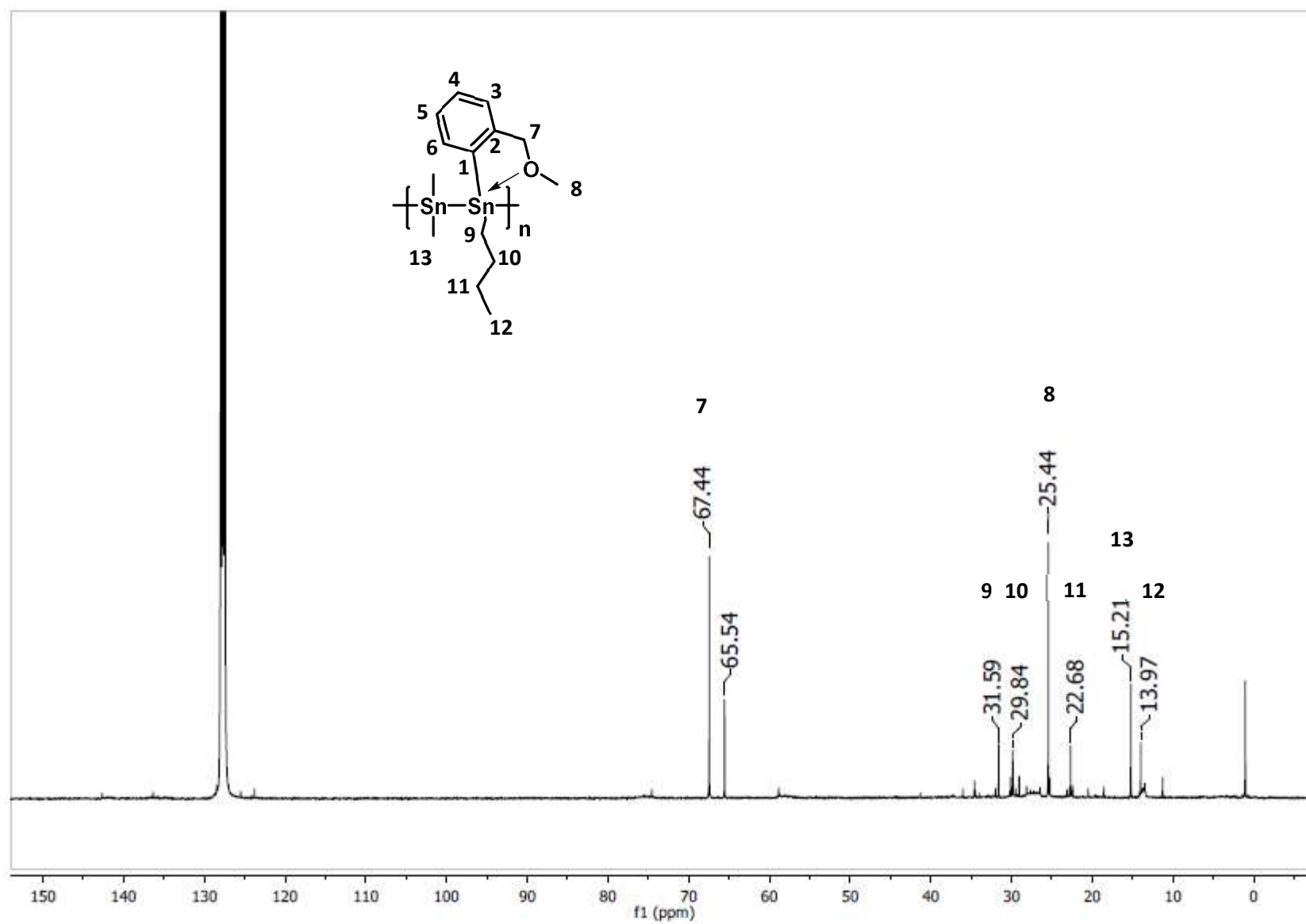
Figure A 55: ^{13}C NMR (C_6D_6) spectrum of attempted poly([2-(CH$_2$OCH$_3$)C$_6$H$_4$](*n*-Bu)]-alt-(CH$_3$)$_2$Sn).
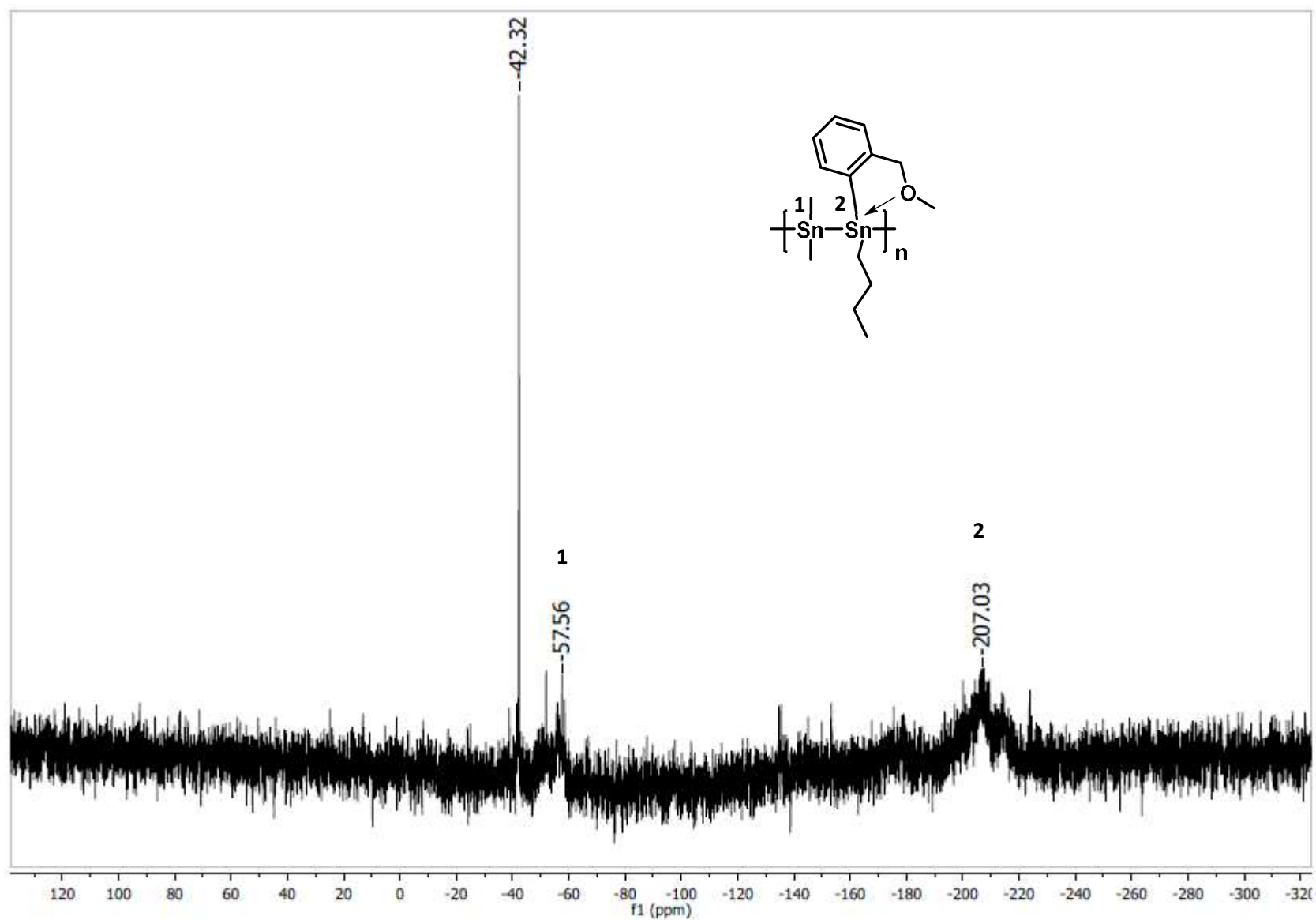
Figure A 56: ^{119}Sn NMR (C_6D_6) spectrum of attempted poly([2-(CH_2OCH_3)C_6H_4](n-Bu)]-alt-(CH_3)$_2$Sn).
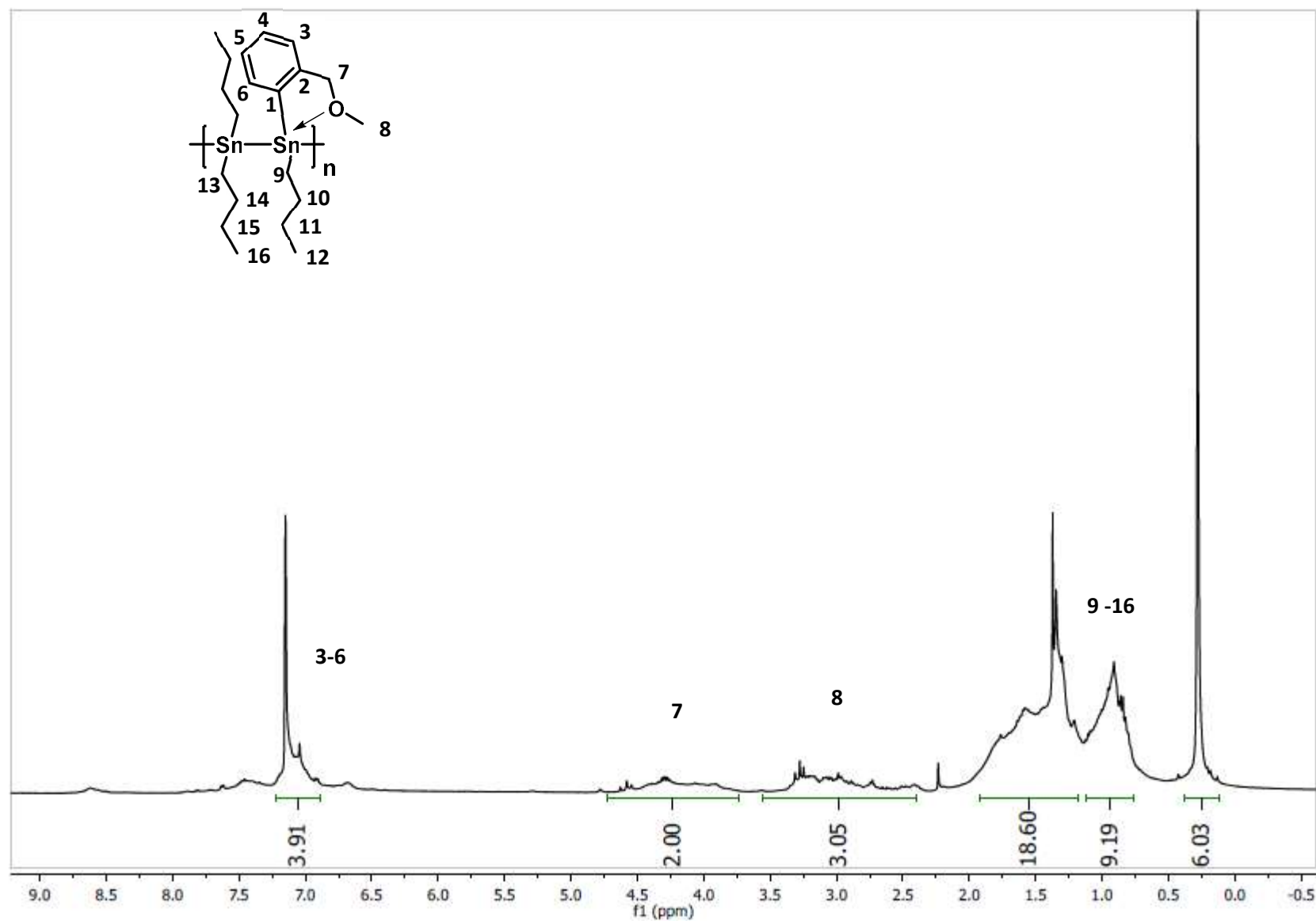
Figure A 57: ^{1}H NMR (C_6D_6) spectrum of attempted poly([2-(CH_2OCH_3)C_6H_4](n-Bu)]-alt-(n-Bu)$_2$Sn).
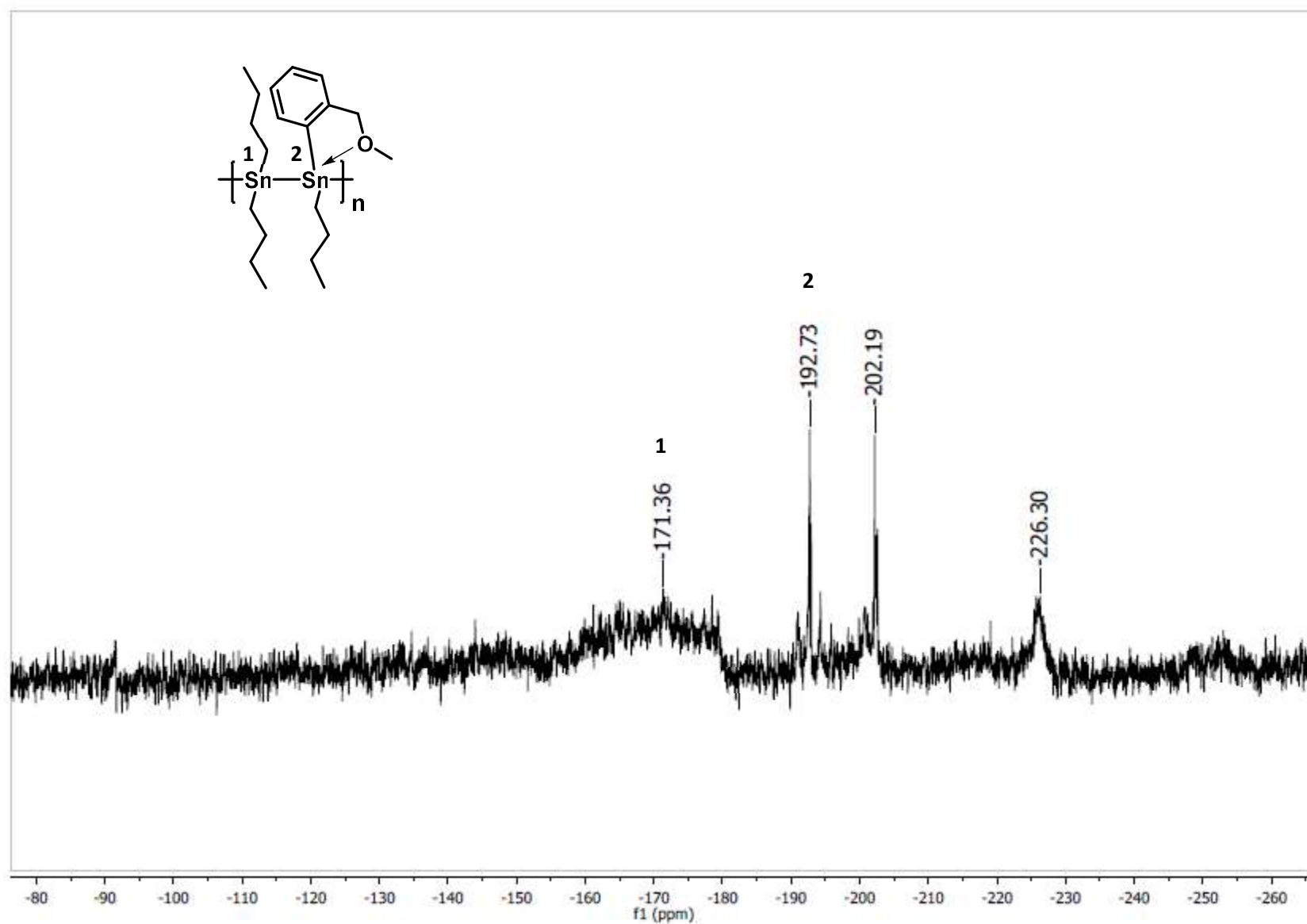
Figure A 58: ^{119}Sn NMR (C_6D_6) spectrum of attempted poly([2-(CH_2OCH_3)C_6H_4](n-Bu)]-alt-(n-Bu)$_2$Sn).

References

1) Akiba, K. Y., Chemistry of Hypervalent Compounds, John Willey & Sons, Ltd. New York, 1999.

2) Yoshimura, A.; Zhdankin, V. V., Advances in Synthetic Applications of Hypervalent Iodine Compounds. *Chem. Rev.*, **2016**, 116, 3328-3435.

3) Minyeav, R. M.; Gribanova, T. N.; Minkin, V. I., Hyperbonding and Hypercoordination in Main-Group Chemistry. Reedijk, J.; Poeppelmeier, K. R., In *Comprehensive Inorganic Chemistry II: From Elements to Application*, Elsevier, Amsterdam, 2013; 9, 109-132.

4) Baukov, Y. I.; Tandura, S. N., Hypervalent Compounds of Organic Germanium, Tin, and Lead Derivatives. Rappoport, Z., In *The Chemistry of Organic Germanium, Tin and Lead Compounds,* John Wiley & Sons, Ltd. New York, 2001; 2, 963-1239.

5) a) Van Koten, G.; Noltes, J. G., Novel chiral triorganotin halides. Stabilization of optically active tin centers by intramolecular coordination. *J. Am. Chem. Soc.*, **1976,** 98, 5393-5395.

b) Van Koten, G., Noltes, J. G.; Spek, A. L., Crystal and molecular structure of C,N-{2-[(dimethylamino)methyl]phenyl} diphenyltinbromide. *J. Organomet. Chem.*, **1976**, 118, 183.

c) Van Koten, G.; Jastrzebski, J. T. B. H.; Noltes, J. G.; Pontenagel, W. M. G. F.; Kroon, J.; Spek, A. L., Synthesis of C,Sn-chiral triorganotin halides via C-chiral arylcopper and arylgoldlithium intermediates. Crystal and molecular structure of one {2-[1-(S)-(dimethylamino)ethyl]phenyl}methylphenyltinbromide diastereomer. *J. Am. Chem. Soc.*, **1978**, 100, 5021.

d) Jastrzebski, J. T. B. H.; Knaap, C. T.; Van Koten, G., Pentacoordinate [8-dimethylamino)naphthyl]diorganotin halides containing a rigid, flat NCCCSn chelate rings.

An unexpected redistribution reaction between [8-dimethylamino)naphthyl]trimethyltin and trimethyltin halide. *J. Organomet. Chem.,* **1983**, 255, 287-293.

6) Jastrzebski, J. T. B. H.; Grove, D. M.; Boersma, J.; Van Koten, G., ^{119}Sn NMR study of organotin compounds havingintramolecular Sn-N coordination. *Magn. Reson. Chem.*, **1991**, 29, 25-30.

7) Wrackmeyer, B., Fundamentals in Tin Chemistry. Davies, A. G.; Gielen, M.; Pannell, K. H.; Tiekink, E. R. T., In *Tin Chemistry: Fundamentals, Frontiers, and Applications,* John Wiley & Sons, Ltd. New York, 2008; 17-283.

8) a) Ruzicka, A.; Pejchal, V.; Holecek, J.; Lycka, A.; Jacob, K., ^{119}Sn, ^{15}N, ^{13}C, and ^{1}H NMR study of the intramolecular Sn-N donor-acceptor interaction in [2-(dimethylaminomethyl)-phenyl]stannanes, *Collect. Czech. Chem. Commun.*, **1998**, 63, 977-989.

b) Ruzicka, A.; Jambor, R.; Brus, J.; Cisarova, I.; Holecek, J., Solution and cross-polarization/magic angle spinning NMR investigation of intramolecular coordination Sn-N in some organotin(IV) C,N-chelates, *Inorg. Chim. Acta.*, **2001**, 323, 163-170.

c) Bisesmans, M.; Martins, J. C.; Willem, R.; Lycka, A.; Ruzicka, A.; Holecek, J., ^{1}H,[117]Sn J-HMBC spectroscopy as a tool for the determination of long-range $^nJ(^1H,^{117}Sn)$ coupling constants in the investigation of intramolecular donor–acceptor interaction in [2-(N,N-dimethylaminomethyl)phenyl]stannanes, *Magn. Reson. Chem.,* **2002**, 40, 65-69.

d) Novak, P.; Padelkova, Z.; Kolarova, L; Cisarova, I.; Ruzicka, A.; Holecek, J., Structure and properties of double-C,N-chelated tri- and diorganotin(IV) halides, *Appl. Organometal. Chem.* **2005**, 19, 1101-1108.

e) Novak, P.; Padelkova, Z.; Cisarova, I.; Kolarova, L; Ruzicka, A.; Holecek, J., Structural study of C,N-chelated monoorganotin(IV) halides, *Appl. Organometal. Chem.* **2006**, 20, 226-232.

f) Svec, P.; Padelkova, Z.; Cisarova, I.; Ruzicka, A.; Holecek, J., Structure of C,N-chelated n-butyltin(IV) chlorides, *Main Group Met. Chem.,* **2008**, 31, 305-309.

9) Svec, P.; Ruzickova, Z.; Vlasak, P.; Turek, J.; De Proft, F.; Ruzicka, A., Expanding the family of C,N-chelated organotin(IV) pseudohalides: Synthesis and structural characterization, *j. Organomet. Chem.*, **2016**, 801, 14-23.

10) Wrackmeyer, B.; ^{119}Sn-NMR parameters; *Annu. Rep. NMR Spectrosc*. **1985**; 16, 73-186.

11) Munguia, T.; Lopez-Cardoso, M.; Cervantes-Lee, F.; Pannell, K. H., Intramolecular Chalcogen-Tin Interactions in (o-MeE-C_6H_4)$CH_2SnPh_{3-n}Cl_n$ (E) S, O; n = 0, 1, 2), Characterized by X-ray Diffraction and ^{119}Sn Solution and Solid-State NMR, *Inorg. Chem.*, **2007**, 46, 1305-1314.

12) Deacon, P. R.; Devylder, N.; Hill, M. S.; Mahon, M. F.; Molloy, K. C.; Price, G. J., Organotin compounds bearing mesogenic sidechains: synthesis, X-ray structures and polymerisation chemistry, *J. Organomet. Chem.*, **2003**, 687, 46-56.

13) Caseri, W.; Polystannanes: processible molecular metals with defined chemical structures, *Chem. Soc. Rev.,* **2016**, 45, 5187-5199.

14) Takeda, K.; Shiraishi, K., Electronic structure of chain-like polystannanes, *Chem. Phys. Lett..*, **1992**, 195, 121-126.

15) Harrypersad, S.; Liao, L.; Khan, A.; Wylie, S. R.; Foucher, D. A., Linear Oligostannanes: A Synthetic and TD-DFT Study, *J. Inorg. Organomet. Polym. Mater*., **2015**, 25, 515–528.

16) Reich, H. J.; Goldenberg, W. S.; Sanders, A. W.; Jantzi, K. L.; Tzschucke, C. C., Amine- and Ether-Chelated Aryllithium Reagents – Structure and Dynamics, *J. Amer. Chem. Soc.*, **2003**, 125, 3509-3521.

17) Mahmud, T.; Iqbal, J.; Imran, M.; Mckee, V., Synthesis and Spectroscopic Studies of 2-Bromo *N,N*-Dimethylbenzylamine and Its Complexes with $Mo(CO)_6$ and $W(CO)_6$, *J. Applied Sci.*, **2007**, 7, 1347-1350.

18) Khan, A.; Pau, J.; Loungxay, J.; Magobenny, T.; Wylie, R. S.; Lough, A. J.; Foucher, D. A., Hypercoordinated Organotin (IV) compounds containing *C,O*- and *C,N*- chelating ligands: Synthesis, Characterization, DFT-Studies and Polymerization Behaviour. *J. Organomet. Chem.* **2019**. Manuscript submitted for publication.

19) Lycka, A.; Snobl, D.; Handlir, K.; Holecek, J.; Nadvornik, M. J., *Collect. Czech. Chem. Commun.*, **1981**, 46, 1383–1388.

20) Jastrzebski, J. T. B. H.; Grove, D. M.; Boersma, J.; Van Koten, G.; Ernsting, J, ^{119}Sn NMR Study of Organotin Compounds having Intramolecular Sn-N Coordination, *Organomet. Coordin. Chem.*, **1991**, 29, S25-S30.

21) Ruzicka, A.; Pejchal, V.; Holecek, J.; Lycka, A.; Jacob, K., ^{119}Sn, 15N, 13C, and 1H NMR Study of the Intramolecular Sn-N Donor-Acceptor Interaction in [2-(Dimethylaminomethyl)phenyl]stannanes, *Collect. Czech. Chem. Commun.*, **1998**, 63, 977-989.

22) Khan, A., The preparation and characterization of structurally stable 5-coordinate polystannanes. Ph.D. Thesis, Ryerson University, Toronto, ON, 2014.

23) Zeppek, C.; Johann, P.; Torvisco, A.; Flock, M.; Uhlig, F., Aryltin chlorides and hydrides: Preparation, detailed NMR studies and DFT calculations, J. Organomet. Chem.¸ **2013**, 740, 41-49.

24) Mahon, M. F.; Molloy, K. C.; Waterfield, P. C., Synthesis, Characterization, and Reaction Chemistry of [2-(2-Pyridyl)ethyl]-,[2-(4-Pyridyl)ethyl]-, and [2-(2-Oxo-N-pyrrolidinyl)ethyl]triphenyltin(IV), *Organometallics*, **1993**, 12, 769-774.

25) Bender, D., Hypercoordinated Oxazoline and Ethyl Pyridyl Organotin Compounds: Potential Routes to Stable Polystannanes. MSc. Thesis, Ryerson University, Toronto, ON, 2018.

26) Van Koten, G.; Noltes, J. G., Crystal and Molecular Structure of *C,N*-{2-[(Dimethylamino)methyl]phenyl}diphenyltin bromide, *J. Organomet. Chem.*, **1976**, 118, 183-189.

27) Turek, J.; Padelková, Z.; Cernošek, Z.; Erben, M.; Lycka, A.; Nechaev, M.S.; Císarová, I.;, Ruzicka A., C,N-chelated hexaorganodistannanes, and triorganotin(IV) hydrides and cyclopentadienides, J. Organomet. Chem., **2009**, 694, 3000-3007.

28) Khan, A.; Komejan, S.; Patel, A.; Lombardi, C.; Lough, A. J.; Foucher, D. A., *J. Organomet. Chem.*, **2015**, 776, 180–191.